Doctoral thesis

Dynamics of Electronically Excited States of Lead Phthalocyanine Thin Films Studied with Two-Photon Photoemission Spectroscopy

by
Masahiro Shibuta

Osaka University

February 2010

Doctoral thesis

Dynamics of Electronically Excited States of Lead Phthalocyanine Thin Films Studied with Two-Photon Photoemission Spectroscopy

２光子光電子分光法による鉛フタロシアニン薄膜の電子励起状態ダイナミクス

by

Masahiro Shibuta

渋田　昌弘

Department of Chemistry, Graduate School of Science,

Osaka University

大阪大学大学院理学研究科化学専攻

2010 年 2 月提出

Abstract

Recently, organic thin film devices and molecular electronics are rapidly developing. Understanding of electric conduction at the interface between substrate and molecule is indispensable to solve the origin of such functionalities. The electric conduction at the interface occurs through occupied and unoccupied levels in the vicinity of the Fermi level (E_F). However, the information on the unoccupied states and their dynamics are scarce so far compared to the occupied level. I have employed two-photon photoemission (2PPE) spectroscopy to probe the unoccupied state. In 2PPE, a first light pumps electron in an occupied states to an unoccupied level then the excited electron is probed by the second light as a photoelectron.

I have measured occupied an unoccupied levels of lead phthalocyanine (PbPc) thin films on graphite (HOPG) with high signal-to-noise ratio. All energy levels around the E_F due to adsorbed molecule were detected: The second highest molecular orbital (HOMO-1), HOMO, the lowest unoccupied molecular orbital (LUMO), LUMO+1, and LUMO+2 in addition to the first image potential unoccupied level (IPS) formed on the films. The 2PPE line shape analysis revealed excitation dynamics in 2PPE process as follows:

(1) Vibrationally resolved 2PPE spectroscopy for PbPc film on graphite

Nuclear motion in the excited state plays key role in the electric conduction between electrode and molecule. But it is hardly resolved for the first adsorbed layer because lifetime of the excited state becomes too short by interaction with the substrate. Here, vibronic fine structure of HOMO-derived ionic state of the PbPc film was identified. I found that the vibrational component decreased only when the photon energy slightly exceeded the resonance energy with LUMO+2 level. The decrease was attributed to the nuclear motion of molecule in the intermediate state associated with LUMO+2 occured in a few fs.

(2) Resonant effects on 2PPE spectroscopy: Line widths and intensities of occupied and unoccupied features for PbPc films on graphite

In order to expand the 2PPE spectroscopy as a versatile method for investigating unoccupied levels, the basic understanding of 2PPE process should be clarified. Particularly,

understanding of the resonance process is still not sufficient. The present work of line shape analysis around the resonance directly pointed out that refinement of 2PPE theory is required. In addition, by detecting the resonance with relevant unoccupied levels, the 2PPE spectroscopy can resolve occupied levels, which are not well resolved in one-photon photoemission.

Contents

Abbreviations

BBO Beta barium borate (β-barium borate, BBO or β-BaB_2O_4)

CW Continuous wave

DFT Density functional theory

E_F Fermi level

FW Fundamental wave

FWHM Full width at half maximum

HOMO The highest occupied molecular orbital

HOPG Highly oriented pyrolytic graphite

IPES Inverse photoemission spectroscopy

IPS Image potential state

LUMO The lowest unoccupied molecular orbital

ML Monolayer

Nd:YVO_4 Neodymium Yttrium Vanadate

OFHC Oxygen-free high thermal conductivity

PbPc Lead phthalocyanine

PES Photoemission spectroscopy

RT Room temperature

SH Second harmonic

SHG Second harmonic generation

TH Third harmonic

THG Third harmonic generation

Ti: Sa Titanium sapphire

TOF Time of flight

TP Time plate

UHV Ultra high vacuum

UPS Ultraviolet photoemission spectroscopy

XPS X-ray photoemission spectroscopy

1PPE One- photon photoemission spectroscopy

2PPE Two-photon photoemission spectroscopy

1. General introduction

Surface chemical reaction and functionalities is used in all over human life. Recently, new electronic devices and surface photochemistry have been extensively developed by using organic thin films which has the attracting function such as electro luminescence, rectifying action, photovoltaic effects [1-4]. Moreover, actual development of "molecular electronics" has been started from 21th century [5]. Understanding of electric conduction at the interface between a solid substrate and adsorbed molecule is a crucial to elucidate the fundamental mechanism of the functionalities. Since the electron or hole transports through the electronic state at the interface, information on occupied and unoccupied electronic structure in the vicinity of the Fermi level (E_F) as well as their dynamics are indispensable to reach the final goal [6,7]. In particular, the electron excitation to the unoccupied state plays an especially important role for the surface phenomena.

Photoemission spectroscopy (PES) have been widely used for a long time as a method to know the information on the occupied state such as the highest occupied molecular orbital (HOMO)-derived level at the adsorbed interface [8,9] and the results have been successfully discussed together with the theoretical calculations [10,11]. On the other hand, investigation for the unoccupied levels are still challenging [12].

Two-photon photoemission (2PPE) spectroscopy based on ultrafast laser pulses is one of the powerful methods to probe the unoccupied levels and its dynamics [12,13]. In 2PPE, a first light pulse excites electron from an occupied level to an unoccupied level. The excited electron is probed by photoemission with the second pulse. Therefore, occupied and unoccupied states can be detected at the same time. Moreover, the 2PPE signal is resonantly enhanced when photon energy corresponds to the energy difference between the relevant occupied and unoccupied levels.

The image potential unoccupied states (IPS's) formed on metal and semiconductor surfaces have been reported most successfully, as well as its dynamics by 2PPE spectroscopy, since it was performed firstly by Steinmann at 1985 [14,15]. Harris, Höfer and Wolf have been extended IPS works to simple adsorption systems such as rare gases or alkane molecules adsorbed on noble metal surface to understand the effect of dielectric isolation layer and the interaction between IPS and electron affinity [16-19].

However, only several examples of the unoccupied states for functional organic thin films have been reported by 2PPE so far, e. g. for C_{60}, PTCDA on noble metals [20,21]. One can consider two main reasons for the problem.

Firstly, the observed energy levels are typically broadened due to the lateral inhomogeneity of substrate and various growth processes of organic molecules [8,22]. Thus, intrinsic information of properties in the system are buried in the complicated energy levels.

Secondary, the understanding of 2PPE process is not sufficient. While 2PPE provides rich information for the IPS, whether other unoccupied levels are observed or not is strongly dependent on the system and photon energy. That is a crucial unresolved problem among the 2PPE scientists and any convincing explanation has not been indicated so far. May be, the 2PPE process and its line shape should include the unknown information at the surface within the periods of femto seconds (10^{-15} s) such as a dynamics of electron-hole excitation or that of adsorbed molecules. The frontier also restricts 2PPE spectroscopy to be a versatile methods for investigating unoccupied levels.

For the first issue, lateral inhomogeneity of electronic state, can be fairly solved by our unique system of microspot 2PPE system in which the laser light is focused with diffraction limited diameter [22]. The microspot method was effective to selectively observe laterally homogeneous surface areas, while the number of photoelectrons from the small probe areas was limited to suppress the space charge effect [22].

This thesis is focused on the second issue. We chose the system of 1 monolayer (ML) lead phthalocyanine (PbPc) films on graphite (highly oriented pyrolytic graphite: HOPG) substrate [23]. PbPc was used as a model of functional organic semiconductor which is applied as field-effect transistors or memory diode [24,25]. Graphite substrate was chosen because its weak chemical interaction with adsorbate to avoid the complication of observed energy levels. In previous work on microspot-2PPE for PbPc/HOPG, we have reported the occupied and unoccupied energy levels around E_F; molecule- derived second-HOMO (HOMO-1), HOMO, the lowest unoccupied molecular orbital (LUMO), LUMO+1, and LUMO+2 (in the order of energy), as well as the IPS [23]. Moreover, resonant excitation from the HOMO level to the LUMO+2 level and the HOMO to IPS were observed in our capable photon energy.

Here, the PbPc/HOPG work was extended to the 2PPE line shape and intensity analysis by taking 2PPE spectra with high resolution. In cost of the spatial resolution, signal to noise

ratio of 2PPE spectra were fairly higher than the microspot configuration. Surface inhomogeneity was negligible by making well ordered 1 ML films through suitable sample annealing. The PbPc/HOPG system for which we have detected "all" energy levels below and above E_F and resonances between the energy levels, is an excellent example to investigate what we see in the 2PPE spectroscopy.

The two main bodies of this thesis are as follows:

(1) Vibrationally resolved 2PPE spectroscopy for PbPc film on graphite

Vibronic structure has been resolved in 2PPE from HOMO-derived level of PbPc film formed on graphite. The 2PPE from the HOMO-derived level was enhanced by the resonance with LUMO+2 derived level. At photon energies below and well-above the resonance, the intensity of the vibronic structure was similar to that of one-photon photoemission. On the other hand, the vibronic structure was significantly weak at photon energies slightly above (< 0.4 eV) the resonance. The decrease of the vibronic structure was attributed to the nuclear motion of molecule in the intermediate state associated with LUMO+2.

(2) Resonant effects on 2PPE spectroscopy: Line widths and intensities of occupied and unoccupied features for PbPc films on graphite

Highly resolved energy levels of the 1 ML PbPc film on HOPG and three resonances between the levels (HOMO-1 to π^*-band of graphite substrate, HOMO to LUMO+2, and HOMO to IPS) were observed. The variations of intensities and widths of the 2PPE features at around the resonances revealed the excitation processes of the intermediate states. The photon energy dependence of the LUMO and LUMO+1 derived features demonstrated that the deeper occupied levels, which are not well resolved in one-photon photoemission, can be resolved by resonant 2PPE spectroscopy.

This thesis is composed by seven chapters as follows.

In Chapter 2, I address the some general methods to probe the occupied and unoccupied electronic state including 2PPE spectroscopy.

Chapter 3 describes the experimental set up for 2PPE spectroscopy; ultra high vacuum system, principles of electron energy analyzer and femto second laser pulse as a right source.

General properties of graphite substrate and PbPc molecule were also shown in the chapter.

In Chapter 4, brief summary of our previous microspot 2PPE results for PbPc on HOPG were introduced. Then, a facing problem for understanding 2PPE process is discussed with some characteristic examples.

In Chapter 5, I present the first main body, (1) vibrationally resolved 2PPE spectroscopy for PbPc film on graphite.

Second one, (2) resonant effects on 2PPE spectroscopy: Line widths and intensities of occupied and unoccupied features for PbPc films on graphite, shows in chapter 6.

Chapter 7 concludes the present work and gives future prospects.

Many references, examples and additional experiments to verify some discussions are summarized in Appendix.

References

[1] S. R. Forrest, Chem. Rev. **97**, 1793(1997).

[2] M. Ibn-Elhaj and M. Schadt, Nature **410**, 796 (2001).

[3] S. Miyata, Y. Sakuratani and X. T. Tao, Optical Materials **21**, 99 (2003).

[4] M. Hiramoto, K. Nakayama, I. Sato, H. Kumaoka and M. Yokoyama, Thin Solid Films **331**, 71 (1998).

[5] C. Joachim, J. K. Gimzewski, and A. Aviram, Nature **408**, 541 (2000).

[6] H. Ishii, K. Sugiyama, E. Ito and K. Seki, Advanced Materials **11**, 1 (1999).

[7] W. R Salanek, K. Seki, A. Kahn, and J. J. Pireaux, *Conjugated Polymer and Molecular Interfaces* (Marcel Dekker, New York, 2002).

[8] S. Kera, H. Yamane, and N. Ueno, Prog. Surf. Sci. **84**, 135 (2009).

[9] N. Ueno and S. Kera, Prog. Surf. Sci. **83**, 490 (2008).

[10] J.-L. Brédas, D. Biljonne, V. Coropceanu, and J. Cornil, Chem. Rev. **104**, 4971 (2004).

[11] V. Coropceanu, J. Cornil, D. A. da S. Filho, Y. Olivier, R. Silbey, and J.-L.Brédas, Chem.

Rev. **107**, 926 (2007).

[12] X.-Y. Zhu, Surf. Sci. Rep. **56**, 1 (2004).

[13] H. Petek and S. Ogawa, Prog. Surf. Sci. **56**, 239 (1997).

[14] K. Giesen, F. Hage, F. J. Himpsel, H. J. Riess, and W. Steinmann, Phys. Rev. Lett. **55** 300 (1985).

[15] H. L. Dai, W. Ho, *Laser Spectroscopy and Photochemistry on metal Surfaces Part 1* (World scientific, Singapore, 1995).

[16] C. B. Harris, N. –H. Ge, R. L. Lingle, Jr., J. D. McNeill, Annu. Rev. Phys. Chem. **48**, 711 (1997).

[17] A. Hotzel, G. Moos, K. Ishioka, M. Wolf, G. Ertl, Appl. Phys. B **68**, 615 (1999).

[18] W. Berthold, F. Rebentrost, P. Feulner, U. Höfer, Appl. Phys. A **78**, 131 (2004).

[19] J. Güdde, U. Höfer, Prog. Surf. Sci. **80**, 49 (2005).

[20] G. Dutton and X.-Y. Zhu, J. Phys. Chem. B **108**, 7788 (2004).

[21] C. H. Schwalb, S. Sachs, M. Marks, A. Schöll, F. Reinert, E. Umbach, and U. Höfer, Phys. Rev. Lett. **101**, 146801 (2008).

[22] T. Munakata, M. Shibuta, M. Mikamori, T. Yamada, K. Miyakubo, T. Sugiyama, and Y. Sonoda, Proc. SPIE **6325**, 63250M (2006).

[23] I. Yamamoto, M. Mikamori, R. Yamamoto, T. Yamada, K. Miyakubo, N. Ueno, and T. Munakata, Phys. Rev. B **77**, 115404 (2008).

[24] T. Yasuda, T. Thuthui, Jpn. J. Appli. Phys. **45**, L595 (2006)

[25] B. Mukherjee, A. K. Ray, A. K. Sharma, M. J. Cook, and I. Chambrier, J. Appl. Phys. **103**, 074507 (2008).

2. Techniques for studying surface electronic states

2. 1. Photoelectron Emission Spectroscopy: PES

PES is one of the most versatile techniques for analyzing the occupied electronic structure. The basis of the technique lies in Einstein's explanation of the photoelectronic effect [1,2]. Photons can induce photoemission from a solid when the photon energy ($h\nu$) is greater than the work function (Φ). Φ is defined as a minimum energy for removing an electron from solid. The photoelectron kinetic energy E_k is given by

$$E_k = h\nu - (\Phi - E_i) \quad (E_i < 0) \tag{2. 1}$$

where E_i is the initial energy with respect to the Fermi level. When ultraviolet (UV) ray such as the He I resonance line (21.22 eV) is used, the spectra are called ultraviolet photoemission spectra (UPS). The UPS is frequently applied to probe the density of state of electron-filled occupied band which has important information for chemical bonding and reactivity. On the other hands, X-ray (XPS) is sufficient to induce the photoemission from core level which does not participate in chemical bonding. Because the core levels of an atom or molecule are strongly depend on the species, XPS will give the information on sample compositions, thickness of adsorbate, surface impurity and so on [1]. The energetics of UPS and XPS experiments are shown schematically in Fig. 2- 1. Recently, energy resolution of PES is drastically increased by improving the resolution of photoelectron analyzer. Moreover, the field is extensively expanded by new light source such as lasers or synchrotron radiations.

To avoid confusion with two-photon photoemission spectroscopy which has been performed in our experiment, here the PES is called "one-photon photoemission (1PPE)". Note that the PES spectrum always gives us the information of the electronic structure of final state, that is, ionic state.

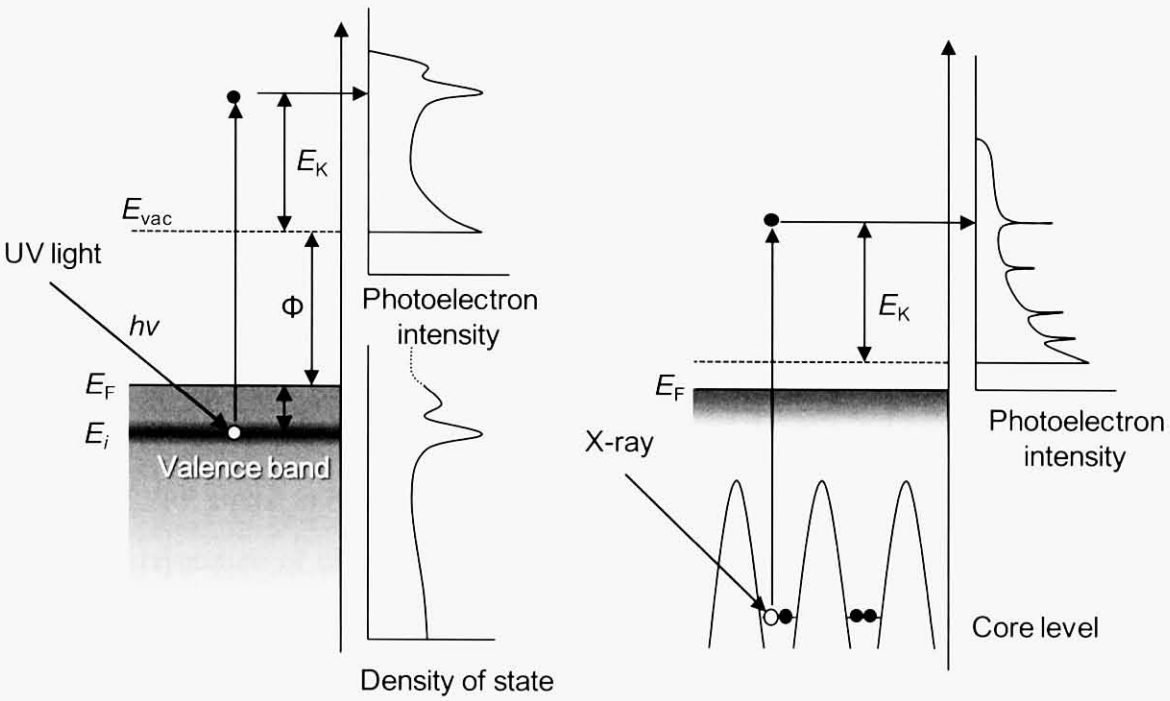

Fig. 2- 1. Schematic drawings of the energetics of the PES, (left) UPS and (right) XPS experiment. UPS is frequently used to prove weakly bounded valence band which participates in the chemical bonding. On the other hand, XPS is used for assignment of atom species; X-ray is sufficient to excite electron from atom-characteristic core levels.

2. 2. Inverse Photoemission Spectroscopy: IPES

Inverse photoemission spectroscopy (IPES) experiments have been done to probe the unoccupied levels. When low energy electron incident onto the surface, the radiation is observed by energetical relaxation to an unoccupied level [3]. The energy diagram of the process is shown in Fig. 2- 2. The energy of the unoccupied level, E_m with respect to E_F is given by (2. 2)

$$E_m = E_p - h\nu$$

where E_p is the primary electron energy, and $h\nu$ is photon energy of the radiation.

However, the tradition probability of inverse photoemission is extremely lower than PES. And the flux of the incident electron is limited to avoid the sample destruction. This problem is especially serious in the adsorbed surface. The energy resolution which mainly depends on the monochromization of incident electron beam is generally larger than 0.1 eV. Note that the IPES gives an anionic state as a final state.

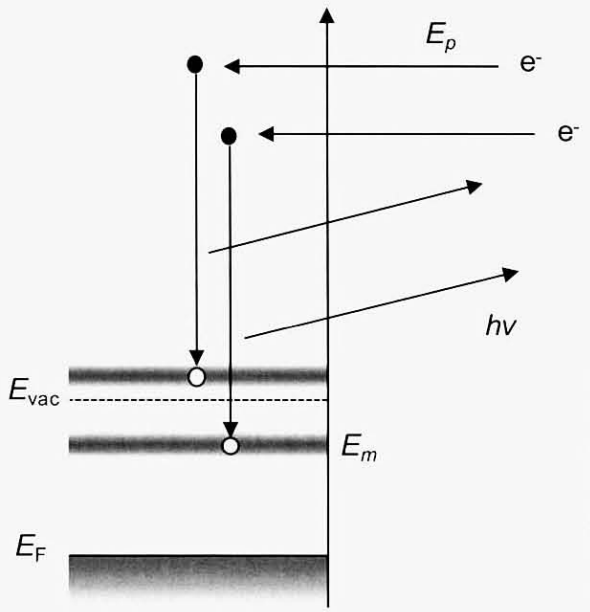

Fig. 2- 2. The principle of IPES. Actually in IPES measurement, the same *hv* is detected with tuning E_p. In contrast to PES, the transition probability of the process is very low and electron flax of E_p is limited to avoid the surface destruction.

2. 3. Two-Photon Photoemission spectroscopy: 2PPE

Two-photon photoemission (2PPE) spectroscopy was applied in this work to know the electronic states and its dynamics. 2PPE spectroscopy based on ultrafast laser pulses is a powerful method to probe unoccupied levels and electron dynamics in the levels [4,5]. In 2PPE, a first light pulse excites electron from an occupied level to an unoccupied level. The excited electron is probed by photoemission with the second pulse. When photon energies of pump and probe pulse are the same, the kinetic energy of photoelectron E_K from this two-step process (1ω) is written as

$$E_k = h\nu + E_m \tag{2. 3}$$

where $h\nu$ is the photon energy and E_m (> 0) is the energy of the unoccupied level with respect to the E_F. The two-step process (1) competes with the coherent two-photon process (2ω) which results in the photoelectron of

$$E_k = 2h\nu + E_i \tag{2. 4}$$

where E_i (< 0) is the initial energy of the occupied level. One of the key points of 2PPE spectroscopy is this competition of two processes. The energy diagrams of these two 2PPE processes are shown in Fig. 2- 3(a). By plotting E_k against $h\nu$, photoelectrons from 1ω process lie on a line with slope one, and those from 2ω process, on a line with slope two as shown in Fig. 2- 3(b). We can thus assign occupied and unoccupied states from 2PPE measurements by using different photon energies. Moreover, when photon energy corresponds to E_m - E_i, 2PPE signal is resonantly enhanced confirming the initial and intermediate states. The energy resolution of the measurement is better than 30 meV, as discussed in Chapter 3. The resolution is better than IPES by one order of magnitude. We can also perform the time resolved measurement by pump probe method [4,5].

2PPE has been applied effectively to probe image potential states and its dynamics on metal or semiconductor surfaces [6], while only several examples of the unoccupied states for functional organic thin films have not been reported so frequently. One of the reasons is that the understanding of 2PPE process is not sufficient from theoretical point of view. This is discussed as one of the main subjects of this thesis. The facing problem of 2PPE is briefly mentioned in Chapter 4. 2. By clear understanding of 2PPE process, 2PPE spectroscopy will be widely applied for many materials and adsorbed systems to investigate their unoccupied

state and dynamics.

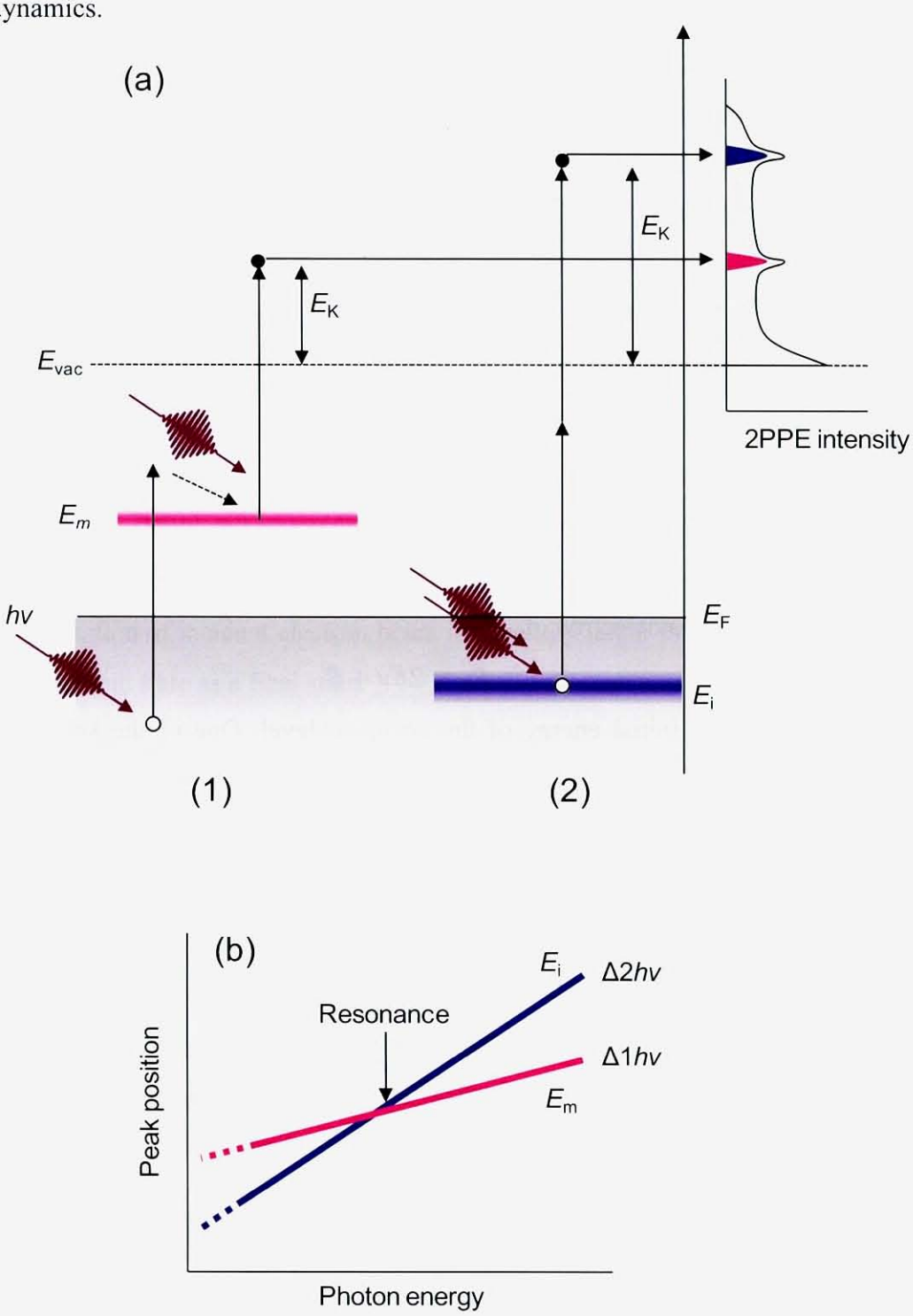

Fig. 2- 3. (a) two processes of 2PPE which are (1) 2PPE from unoccupied level E_m after some relaxation and (2) coherent 2PPE from occupied level. (c) Photon energy dependence of observed level. When the energy positions of observed peaks were plotted against the photon energy, the structure of occupied and unoccupied levels are aligned the slope of 2 and 1, respectively, related with the photon energy. Another remarkable is the resonance at $hv = E_m - E_i$. At the resonance, 2PPE signal is resonantly enhanced.

References

[1] G. Ertl, L. Küppers, *Low Energy Electron and Surface Chemistry* (VCH Publishers, New York, 1985).

[2] Gary Atterd and Colin Banes, *Surfaces* (Oxford University press, New York, 1998).

[3] N. V. Smith, Rep. Prog. Phys. **51**, 1227 (1988).

[4] H. Petek and S. Ogawa, Prog. Surf. Sci. **56**, 239 (1997).

[5] X. Y. Zhu, Surf. Sci. Rep. **56**, 1 (2004).

[6] H. L. Dai, W. Ho, *Laser Spectroscopy and Photochemistry on metal Surfaces Part 1* (World scientific, Singapore, 1995).

3. Experimental system and sample

3. 1. Brief description of 2PPE measurement

All 2PPE measurements were performed in an ultra high vacuum (UHV) chamber. The overview of the experimental set up including light source was shown in Fig. 3- 1.

The light source was *p*-polarized frequency tripled of tunable titanium sapphire (Ti: Sa) laser output pumped by Neodymium Yttrium Vanadate (Nd: YVO_4) laser. The repetition rate and pulse duration of the TH were 76 MHz and 100 fs, respectively. The photon energy region of the TH was 4.04~4.77 eV. The power of the incident light was controlled to be less than 0.19 nJ/pulse in order to avoid surface destruction. The light focused onto the sample in UHV through quartz window by an r = 70 cm concave mirror at the incident angle of 60°. The spot size was about 80 μm.

Photoelectrons emitted to the surface normal were detected with a hemispherical energy analyzer which has nine channeltrons. Photoelectrons emitted to the surface normal were detected with a hemispherical energy analyzer of 20 meV resolution. The total energy resolution of the 2PPE system including laser band width was ~30 meV. The analyzer was modified to limit the electron acceptance angle to be ± 1°. Well ordered 1 ML PbPc on graphite was prepared in a preparation chamber separated by gate valve. The details and principles of each part were addressed after this section.

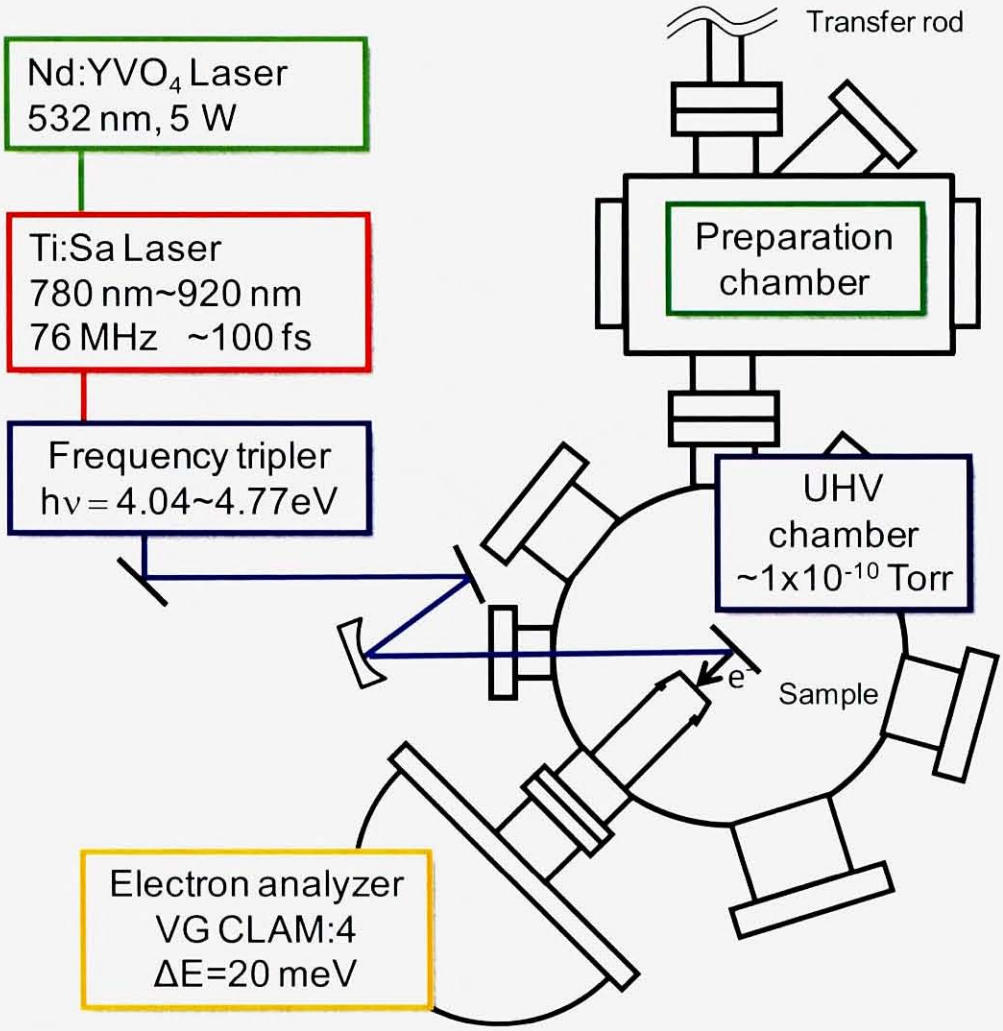

Fig. 3- 1. Experimental set up of 2PPE spectroscopy

3. 2. Environment

3. 2. 1. Ultrahigh vacuum chamber system

The UHV and shielding from external magnetic field are indispensable to perform 2PPE experiment. The main UHV chamber is systematically shown in Fig. 3- 2. The chamber was shielded from external magnetic field by inner μ-metal shield. An electron energy analyzer (Vacuum Generator: CLAM-4) was equipped at the chamber. Additionally, the main chamber also consists of quadrupole-mass spectrometer to confirm the impurity of UHV. The UHV window for introducing UV laser pulse as a 2PPE light source was made from 1 mm thick quartz plate. Helium discharge lamp for generating He resonance line was equipped at a neighboring laser-in port to perform conventional 1PPE measurement. Those systems were pumped by turbo molecular pumps combined with rotary pumps and a titanium sublimation pump. Base pressure of the main chamber was generally achieved less than 1×10^{-10} Torr.

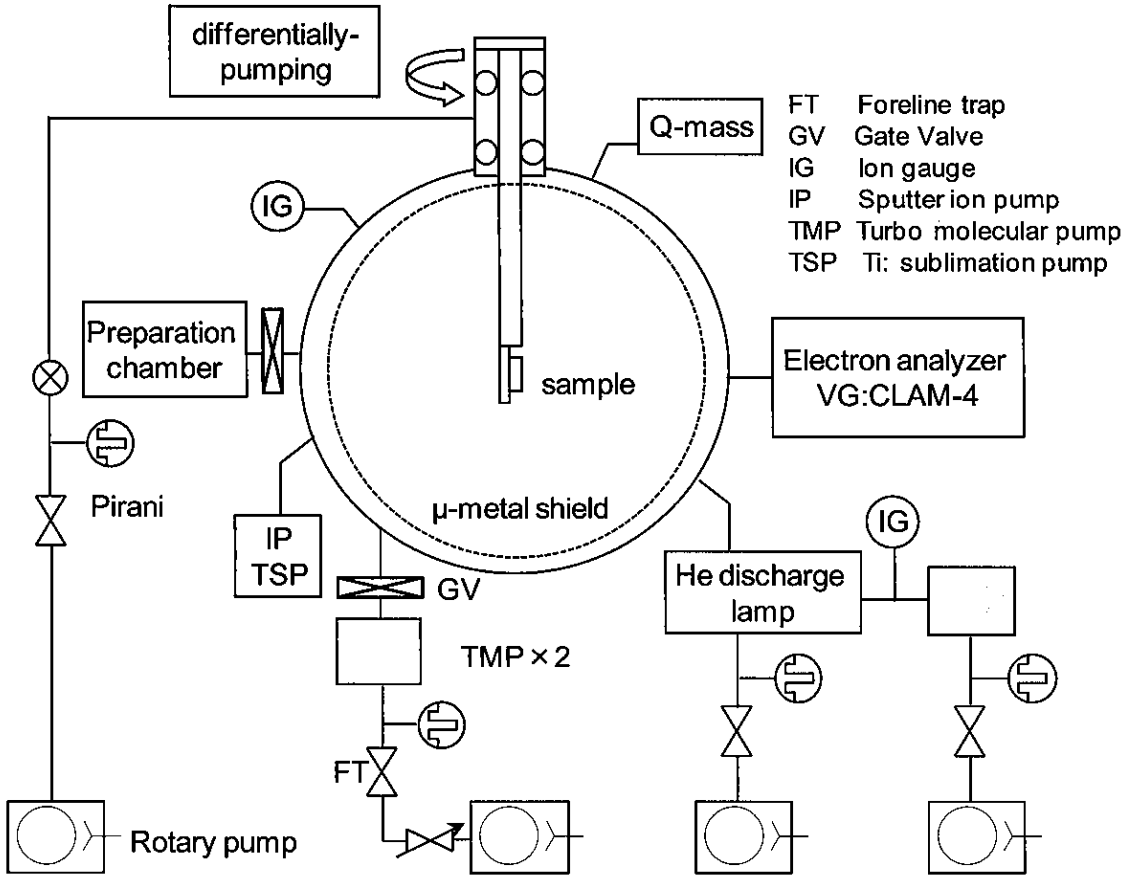

Fig. 3-2 UHV system for main chamber

3. 2. 2. Preparation chamber

Sample cleaning and evaporation of PbPc molecule were performed at a preparation chamber separated by gate valve from the main chamber. The preparation chamber which consists of the quartz-cell evaporator and quartz microbalance thickness mater (INFICON, IC/5) was pumped by a set of rotary and turbo molecular pumps. The configuration for PbPc evaporation is displayed in Fig. 3- 3. PbPc in the quartz cell was resistitively-heated and sublimated by electric current. Deposition amount of PbPc molecule was controlled by rotating a shutter in front of the sample made of oxygen free high conductivity copper (OFHC).

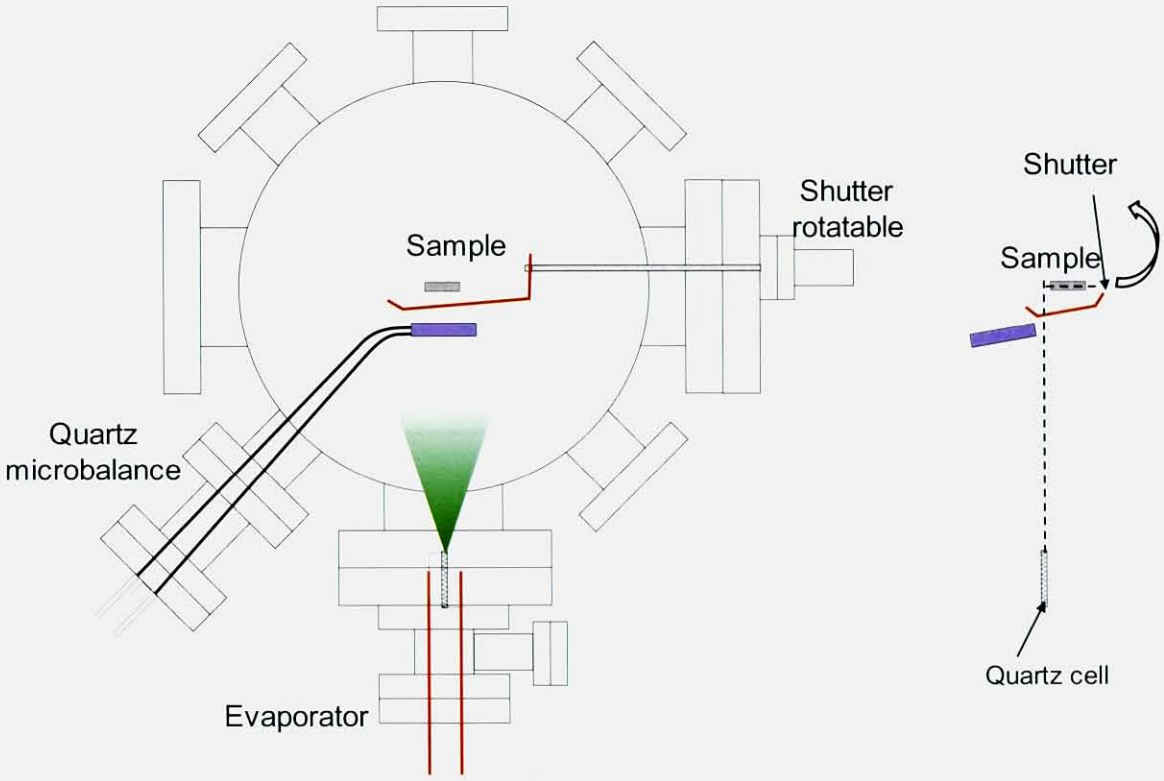

Fig. 3- 3. The configuration of the preparation chamber when PbPc is evaporated. The PbPc in the Quartz cell is heated resistitively. The deposition amount of the PbPc is controlled by open/close of the OFHC shutter. Thickness is monitored by quartz microbalance.

3. 2. 3. Sample mounting

In the 2PPE experiments, the sample should be stabilized in UHV because the electron energy analyzer detects photoelectron from focused small laser spot (~80 μm) on the sample. We employed a commercial manipulator, thermo vacuum Generator products, which has x, y and z axes micrometers and differentially-pumped θ sample rotating system. The sketch around the sample holder is shown in Fig. 3- 3. The sample mounted on OFHC insulated from the ground by sapphire plate. The sample can be easily cooled to be 90 K by introducing liquid nitrogen to the upper stainless steel tube. The sample temperature was monitored by chromel-alumel thermocouple. In the photoelectron spectroscopy, the electrically-charging around the sample is especially serious problem. Therefore, all insulating materials are set to the back of the sample and sealed by thin tantalum cover.

The sample was transferred to the preparation chamber when we perform the sample heating or evaporating PbPc molecule on the sample. The simple manipulator at the preparation chamber consists of electron bombardment sample heating system. The electrical connection is shown in Fig. 3- 4. The thermoelectrons are preferentially accelerated toward the backside of the sample by applying the sample bias of ~+150 V and sealed electrically negative plate behind the tungsten filament. Then the sample is preferentially heated and the temperature is achieved to at least 700 K.

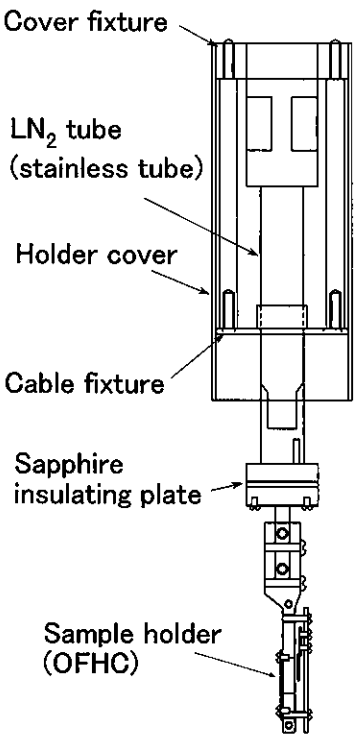

Fig. 3- 3. The sketch around the sample holder. The sample holder is insulated by sapphire plate. And the sample can be cooled at 90 K by thermal conduction from liquid nitrogen tube .

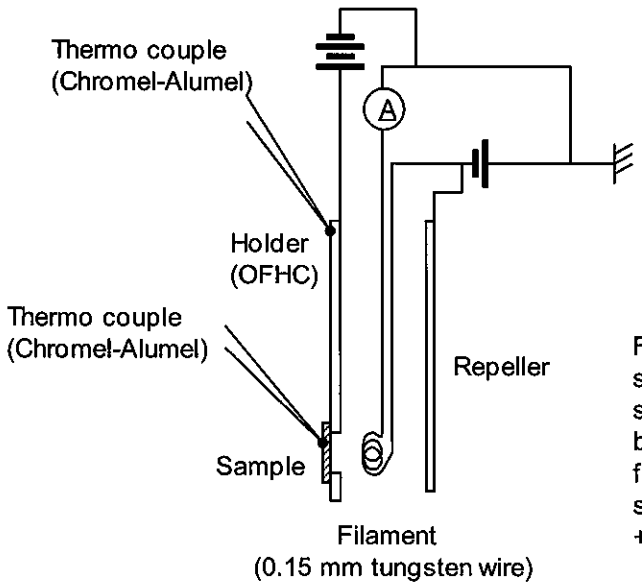

Fig. 3- 4 The electrical connections around the sample when the sample was prepared. The sample can be heated by an electron bombardment. The thermal electrons from the filament are efficiently accelerated to the sample by supplying the bias voltage of about +150 V

3. 3. Photoelectron spectroscopy

3. 3. 1. Hemispherical electron analyzer

Hemispherical electron energy analyzer is frequently used for the detection of the photoelectron. On the other hand, time of flight (TOF) spectrometer is also used when the amplified laser systems are employed together with optical parametric frequency conversion. However, the high repetition laser systems such as 76 MHz in our work results in very high signal to noise ratio even at low energies per pulse, which are necessary in order to avoid space charge effect [1]. Another advantage of the hemispherical type is its constant energy resolution at whole energy range while the resolution of TOF type should depend on the electron energy; the resolution of slower photoelectron should be better than higher than that for faster one. The theoretical energy resolution of hemispherical type is following below.

The schematic diagram of the hemispherical energy analyzer is shown in Fig. 3- 6. The energy of the photoelectron through the out slit (pass energy) E_0 is determined by

$$E_0 = \frac{eV_D}{\frac{R_2}{R_1} - \frac{R_1}{R_2}} \tag{3. 1}$$

where R_1 and R_2 is the radiuses of inside and outside the hemisphere, respectively and V_D is the difference of electrical potential between them [2]. By using the average of the radius R_0 (=$(R_1+R_2)/2$) and slit width of the analyzer W, the principle energy resolution ΔE of the analyzer is given as

$$\Delta E = \frac{W}{2R_0} E_0 \tag{3. 2}$$

Therefore, ΔE should change with E_0 and it is a quite problem. In generally, a spectrum is taken with the same E_0 at whole measurement and the velocity of photoelectron from the sample is controlled by scanning the voltage of electron lenses placed in front of the entrance slit. When the E_0 is set at lower energy, the energy resolution becomes better in cost of the signal to noise ratio. Normally, we set the pass energy to be 3 eV. Since the R_0 for the CLAM

4 is 150 mm [3], the principle energy resolution is 20 meV when $W = 2$ mm slit is chosen. The total energy resolution of the 2PPE system is given by the root-mean-square of the ΔE and the band width of the laser pulse of 18 meV (see 3. 4. 6) ,that is, $\sqrt{20^2 + 18^2} \cong 27$ meV.

The monochromated photoelectrons through the exit slit are amplified and detected by channeltron(s) in which high voltage (~+2 kV) is applied at the center of whorl. The CLAM 4 has a nine channeltrons which gives us sufficient signal to noise ratio.

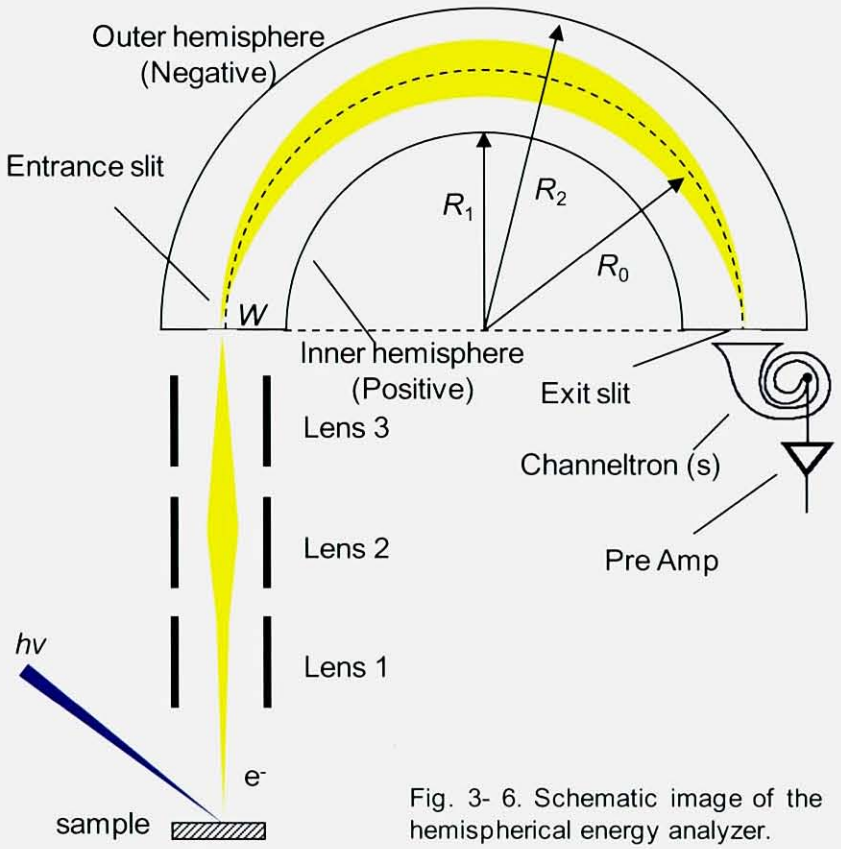

Fig. 3- 6. Schematic image of the hemispherical energy analyzer.

3. 4. The light source

3. 4. 1. The light source for 2PPE spectroscopy

Since the transition probability of 2PPE process is much less than that of 1PPE process, highly photon flax should be needed for efficient 2PPE signal. Mode-locked titanium sapphire pulsed laser and its high harmonics or optical parametric amplifier are often used as a light source of 2PPE experiment. In addition, high repetition rate of the pulse is used preferably in order to suppress the peak intensity of electric field per pulse which leads to space charge effect [1]. The optical components of our 2PPE experiment are already described in Fig. 3- 1. The detail descriptions of the pump laser (Nd: YVO_4, COHERENT, Verdi- 10), Ti: Sa laser (COHERENT, Mira-900F), and its frequency tripling with nonlinear crystals are explained in 3. 4.

3.4. 2. Nd: YVO_4 laser (COHERENT: Verdi-10)

We used Ti :Sa laser as a fundamental light source. Ti^{3+} in the sapphire crystal can absorb efficiently green or blue pumping light. In this work, we employed the Nd: YVO_4 laser (COHERENT, Verdi-10, CW-532 nm) for a pump laser. The laser medium of Nd: YVO_4 has a high absorption coefficient which allows a shorter crystal length and high stimulated emission cross section which is higher than that of Nd: YAG (yttrium aluminum garnet) laser medium [4]. With such a development of solid state laser, very stable Ti: Sa laser operation can be achieved with smaller power source.

In the Verdi-10, Nd^{+3} single resonance line of 1064 nm in the ring cavity pumped by diode lasers was frequency doubled by intra-cavity nonlinear crystal (LiB_3O_5: LBO) to generate continuous 532 nm green output. The phase matching between 1064 and 532 nm propagations in LBO crystal can be accomplished by temperature tuning of the crystal. In that case, the crystal temperature is kept at approximately 150 °C for successful phase matching.

3. 4. 3. Ti: Sa laser (COHERENT: Mira900-F)

Fig. 3- 7 shows the optical configuration of the Ti: Sa laser (COHERENT: Mira900-F) which were used as an oscillator in our apparatus [5]. The laser unit can be purged by dry N_2 at the normal operation. The pump beam from Verdi-10 is introduced to the Ti: Sa crystal with Brewster angle through M4 concave mirror. The laser cavity is constructed by M1 output coupler and M7 high reflector (solid line). The ultrafast laser oscillation can be achieved by mode-locking method which is mentioned in 3. 4. 4. The repetition rate and general pulse width of the Mira900-F oscillator are about 76 MHz and 100 fs, respectively, which are related with a cavity length and spectral width of net gain, as followed in 3. 4. 4. In order to simplify laser operation, intra cavity mode-locking starter is equipped. Central wavelength is easily tuned continuously by rotation of birefringence filter (BRF) between 750 and 950 nm which mainly depends on the reflectance character of the cavity mirrors. The general band width is about 10 nm, reflecting the pulse duration of 100 fs (see 3. 4. 6.). The group velocity dispersion in the laser cavity is compensated by a couple of intra-cavity SF10 prisms (BP1 and BP2). Stabilization of mode-locking is controlled by optimizations of BP2 and the slit in front of M1. Output laser from M1 is sampled by BS1 to monitor laser power and status of mode-locking [5].

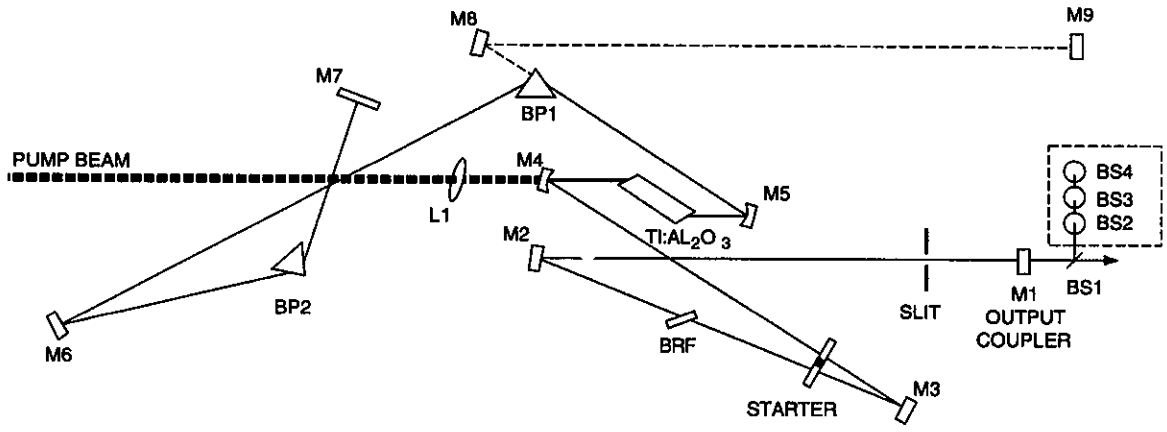

Fig. 3- 7. The optical configuration of COHERENT Mira900-F Ti: Sa laser.

3. 4. 4. Mode locking

The ultrashort laser pulses are achieved by mode locking technique, which is described mathematically in this section. An electric field can be established between two parallel mirrors only when a wave propagating in one direction adds constructively with the wave propagating in the reverse direction [6,7]. The result of superposition is a standing wave which is established if the distance L between the two mirrors is an integer multiple of the half wavelength of the light. Therefore, the standing wave condition is fixed to the value of the positive integer n, which written as

$$\nu = \frac{nc}{2L} \tag{3. 3}$$

where ν is the light frequency, and c is its velocity in the vacuum, 2.998×10^8 m/s. The cavity has a specific period of $T = n/\nu$, which is also round trip time of flight $T = 2L/c$ by remembering $\nu = c/\lambda$. For the Mira900-F which has L = 2.0 m, characteristic values of the cavity are about T = 13 ns and ν = 76 MHz.

The general laser spectrum is shown in Fig. 3- 8. In the efficient pumping condition, the number of modes can be emitted, depending on the band width of the net gain [7].

The basis of the mode-locking is to induce a fixed phase relationship between the each mode in a laser cavity. An total electric field in a laser cavity $E(t)$ is the sum of each mode, which written as

$$E(t) = \sum_m A_m \exp\{i2\pi\nu_m(t - \phi_m)\} \tag{3. 4}$$

where A_m, ϕ_m are the amplitude and phase of mode m, respectively. By using the central frequency of a laser cavity ν_0 and frequency difference of the neighboring mode is ν_F from eq, (3. 3)

$$E(t) = \exp\{i2\pi\nu_0(t - \phi_0)\} \cdot \sum_q A_q \exp\{i2\pi\nu_F(t - \phi_q)\} \tag{3. 5}$$

The phase parts ϕ_q's are generally independent of neighboring modes (continuous wave (CW) laser). However, when all ϕ_q's are constant (fixed to 0) by some optical techniques, the mode locking is achieved and the $E(t)$ results in

$$E(t) = \exp(i2\pi\nu_0 t) \cdot \sum_q A_q \exp(i2\pi q \nu_F t) \tag{3. 6}$$

where q = 0, ±1, ±2 · · ·±Q. For a comprehensive understanding, the A_q is set to be constant as 1. Then, the sum of series turns to be

$$E(t) = \exp(i2\pi\nu_0 t) \frac{\sin(\pi M t/t_c)}{\sin(\pi t/t_c)} \tag{3. 7}$$

where M is determined by $2Q$+1, and ν_F is $1/t_c$

The intensity of the light is proportional to square of $E(t)$. Therefore,

$$I(t) \propto \frac{\sin^2(\pi M t/t_c)}{\sin^2(\pi t/t_c)} \tag{3. 8}$$

The shape of the function of eq. (3. 8) is fixed with square hypobaric secant function sech^2 [6,7]. The repetition rate of the pulse is given by $\nu_F = 1/t_c$. Fig. 3- 9(a) shows the $E(t)$ modeled COHERENT: Mira900-F in which ν_0 is $3.75\times10^{14}\,\mathrm{s}^{-1}$ (λ = 800 nm), M is 7(q = 3), and L is 2.0 m (ν_F = 76 MHz). Fig. 3- 9(b) also shows the $E(t)$ when the each mode has random phase. In really, a large number of modes participate in the mode locking of Ti: Sa laser, and the laser pulse has extremely high electric field in the period of short duration compared with CW wave.

The pulse duration of mode locked laser is determined by numerator of right hand term in eq. (3- 8), that is, $\tau_p = t_c/M$. Therefore, the shorter pulse can be achieved when a large number of modes oscillates in the laser cavity. The capable wavelength of laser light is limited by spectral width of fluorescence of laser medium $\delta\nu$. When pumping of the laser medium is sufficient, M is neally same with $\delta\nu/\nu_F$, and then,

$$\tau_p \approx \frac{\nu_F}{\delta\nu} \cdot t_c = \frac{1}{\delta\nu} \tag{3. 9}$$

For example, $\delta\nu$ of Nd:YAG which is frequently used laser material in many application is about ~120 GHz. The ideal pulse width of the mode locked Nd:YAG laser is 8 ps from eq. (3. 9). On the other hand, Ti:Sa (titanium doped Al_2O_3) laser medium has extremely wider $\delta\nu$ than any other solid state laser material. The reported pulse duration of the Ti: Sa laser is shorter than few femto seconds which is a few optical cycles of the central frequency.

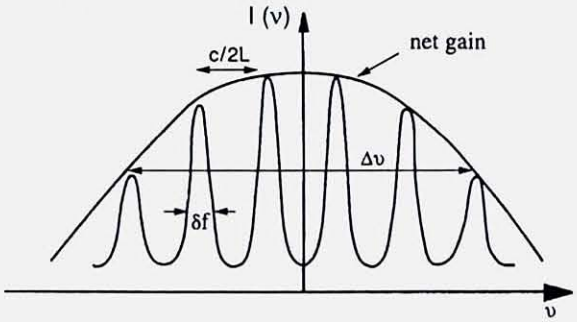

Fig. 3- 8. The spectral shape of the laser oscillation. The laser spectrum strongly depends on the properties of the laser cavity.

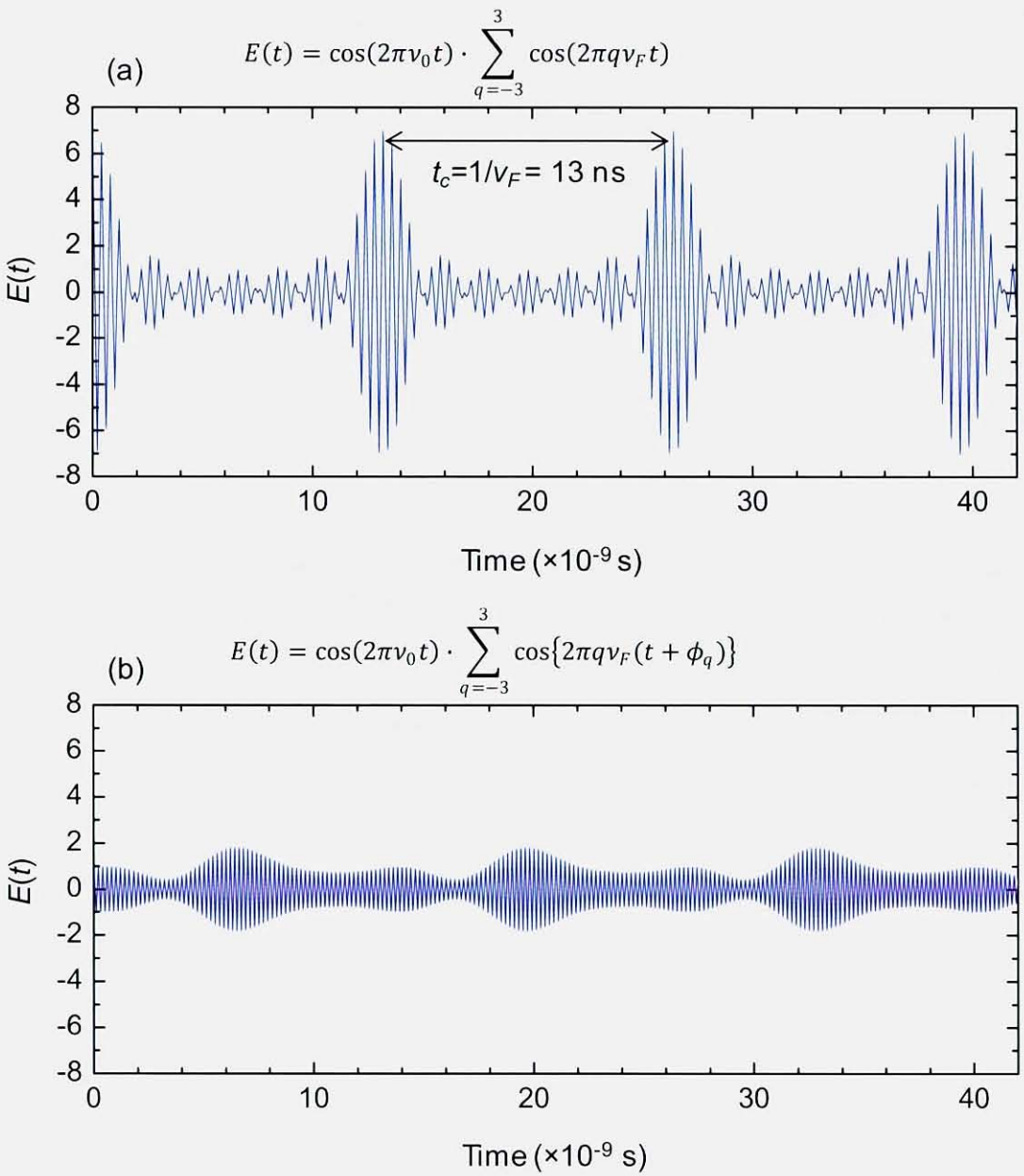

Fig. 3- 9. Illustration of electric field $E(t)$. (a) 7 modes with the same phase (ϕ = 0), (b) 7 modes with the random phase were modeled COHERENT:Mira900-F in which ν_0 is 3.75×10^{14} s^{-1} (λ = 800 nm), M is 7, and L is 2.0 m (ν_F = 76 MHz).

3. 4. 5. Mode locking method

The COHERENT Mira900-F employs the self mode-locking method based on the Kerr lens effect. The method can lock each phase of mode without inserting a saturable absorber or any external modulation in the laser cavity. High power electric field in the nonlinear medium can induce nonlinear refractive index depending on the light intensity I which written as

$$n = n_0 + n_2 I \tag{3. 10}$$

where n_2 is the nonlinear coefficient of refractive index [7]. Therefore, the Gaussian beam does not feel a homogeneous refractive index when it passes through such a nonlinear medium (Kerr effect). If n_2 is positive, a beam propagating through this medium is focused near the optical beam axis just like a lens where its intensity is stronger. This is called self-focusing by a Kerr lens effect which is shown schematically in Fig. 3- 10[7].

The Ti: Sa crystal has this nonlinear property. The low intensity part (CW beam) of the beam can be removed by a slit or pinhole. Thus high intensity maxima is survived in the cavity and much better amplified, then the laser reaches the condition of mode-locking to give short pulses.

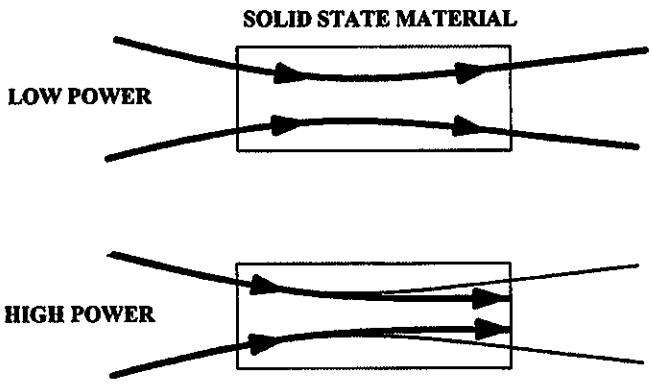

Fig. 3- 10. The schematically image of Kerr lens effect [7]. The high power component are focused in the nonlinear medium by its Kerr effect. The low power component is blocked by pinhole or slit and thus the high power component survives in the cavity.

3. 4. 6. Pulse duration and spectral width

Temporal pulse duration and spectral width of mode-locked laser pulse are related to each other through Fourier transform. Because the actual shape of the pulse is difficult to describe and calculate as fundamental mathematical functions, we have applied "general" pulse function to understand the essential behavior of ultrashort pulse. Most frequently, Gauss or square of secant hyperbolic ($sech^2$) have been used as the function [6,7]. Here, we discuss mainly about Gaussian pulse in order to consider the relation of temporal and spectral pulse widths.

The electrical field intensity of a central frequency ω_0 light is given by $\exp(-i\omega_0 t)$. The field of mode-locked laser pulse $\varepsilon(t)$ is the sum of many frequency which written as

$$\begin{aligned}\varepsilon(t) &= a_1 \cdot \exp(-i\omega_1 t) + a_2 \cdot \exp(-i\omega_2 t) + \cdots a_n \cdot \exp(-i\omega_n t) \\ &= \sum_n a_n \cdot \exp(-i\omega_n t) \\ &= \frac{1}{\sqrt{2\pi}} \int_{-\infty}^{+\infty} E(\omega) \cdot \exp(-i\omega t) d\omega \end{aligned} \quad (3.\ 11)$$

In the same way,

$$E(\omega) = \frac{1}{\sqrt{2\pi}} \int_{-\infty}^{+\infty} \varepsilon(t) \cdot \exp(-i\omega t) dt \quad (3.\ 12)$$

These equations have been well known as the formula of Fourier transform. Now we apply Gaussian function for the $\varepsilon(t)$ as

$$\varepsilon(t) = \exp(-t^2) \cdot \exp(-i\omega_0 t) \quad (3.\ 13)$$

where the ω_0 is central frequency of the laser pulse, therefore,

$$E(\omega) = \frac{1}{\sqrt{2\pi}} \int_{-\infty}^{+\infty} \exp(-t^2) \cdot \exp\{-i(\omega - \omega_0)t\} dt \quad (3.\ 14)$$

This integral can be solved by using the role of Gaussian integral, $\int_{-\infty}^{+\infty} \exp(-\alpha x^2) dx = \sqrt{\frac{\alpha}{\pi}}$, then,

$$E(\omega) = \frac{1}{\sqrt{2\pi}} \exp\left(-\frac{(\omega - \omega_0)^2}{4}\right) \quad (3.\ 15)$$

The power spectrum of the pulse is determined by,

(3. 16)

$$I(\omega) \propto E^*(\omega) \cdot E(\omega)$$
$$\propto \exp\left(-\frac{(\omega-\omega_0)^2}{2}\right) \quad (3.17)$$

while

$$I(t) \propto \varepsilon^*(t) \cdot \varepsilon(t) = \exp(-2t^2) \quad (3.18)$$

The FWHMs (full width at half maxima) of those dimensions for the pulse, Δt and $\Delta\omega$ are

$$\Delta t = \sqrt{2\ln 2}$$
$$\Delta\omega = 2\sqrt{2\ln 2}, \quad (3.19)$$

respectively. Therefore, the product of Δt and $\Delta\omega$ should be limited by (3.20)

$$\Delta t \cdot \Delta\omega = 4\ln 2 \approx 2.773 \quad (3.21)$$

The ideal laser pulse without any dispersion is called 'Fourier transform limited pulse'. For example, Fourier transform limited pulse which has 100 fs pulse duration leads to at least 18 meV spectral width.

In a general text book for quantum mechanics [8], the Heisenberg's uncertainty principle is written as

$$\Delta t \cdot \Delta E = \Delta t \cdot \hbar\Delta\omega \geq \hbar \quad (3.22)$$

in which Δt and $\Delta\omega$ are defined by the full widths at 1/e for both physical quantities.

3. 4. 7. Third harmonic generation

The third harmonic generation (THG) for 2PPE light source is generated by a couple of nonlinear crystals, β-BaB_2O_4 (BBO) [9]. Fig. 3- 11 shows the optical configuration of home-made TH generator. The output pulse of Ti:Sa oscillator is focused to the first BBO crystal of 1 mm thickness by an r = 200 mm dielectric concave mirror (M1) to generate the second harmonic generation (SHG) of fundamental wave (FW). After SHG and transmitted FW are collimated by an r = 200 mm dielectric concave mirror (M2), Polarization and time delay between the SHG and FW are compensated each other by $\lambda/2$ wave plate (WP2) and time plate (TP) in the right hand of Fig. 3- 11. Then both pulses are focused again to the second BBO crystal of 0.5 mm thickness by an r = 120 mm dielectric concave mirror (M3). Collimated and separated THG is introduced by concave mirror to the UHV chamber. The principle of harmonic generation by nonlinear crystal, time delay compensation by a TP and BBO nonlinear crystal are described in 3. 4. 8, 3. 4. 9 and 3. 4. 10, respectively.

For example, when the FW power is 980 mW at the 840 nm central wavelength, the THG power is normally 76 mW, that is, conversion efficiency of THG is ~8 %. The efficiency should depend on various factors such as the power of FW, pulse duration, cutting angle of the BBO crystal (see 3. 4. 10) the reflectance characters of M1~M3 in Fig. 3- 11, and adjustment of optical configuration of the TH generator. One of the general data for the FW and THG power plotted against the central wavelength of FW is shown in Fig. 3- 12. The FW tuning range is limited by a character of cavity mirrors in Mira-900.

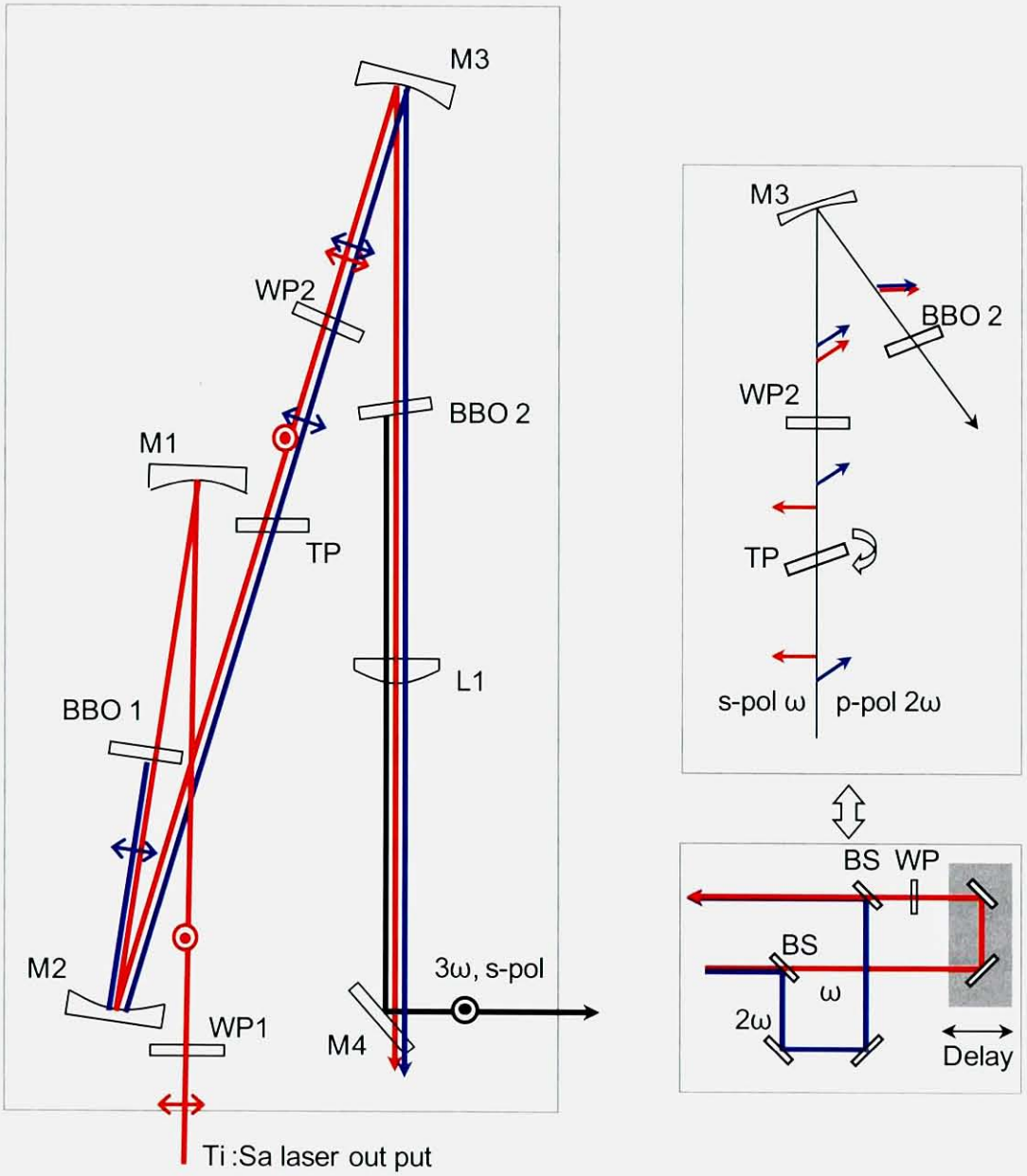

⊙	s-pol
↔	p-pol
BBO1	1.0 mm for SHG
BBO2	0.5 mm for THG
TP	Time plate(α-BBO)
L1	3ω Collimation lens

M1	ω reflect R=200 mm
M2	ω, 2ω reflect R=200 mm
M3	ω, 2ω reflect R=120 mm
M4	3ω reflect 45deg ,s-pol
WP1	for ω , 1/2Wave plate
WP2	for ω , 1/2Wave plate

Fig. 3- 11. The optical configuration of TH generator. The TH is generated by a couple of BBO crystals. Phase matching between fundamental wave and SH from first BBO(right top) can be achieved by time plate (TP) without a delay stage as displayed right bottom. TH is separated and introduced to the sample through quartz UHV window

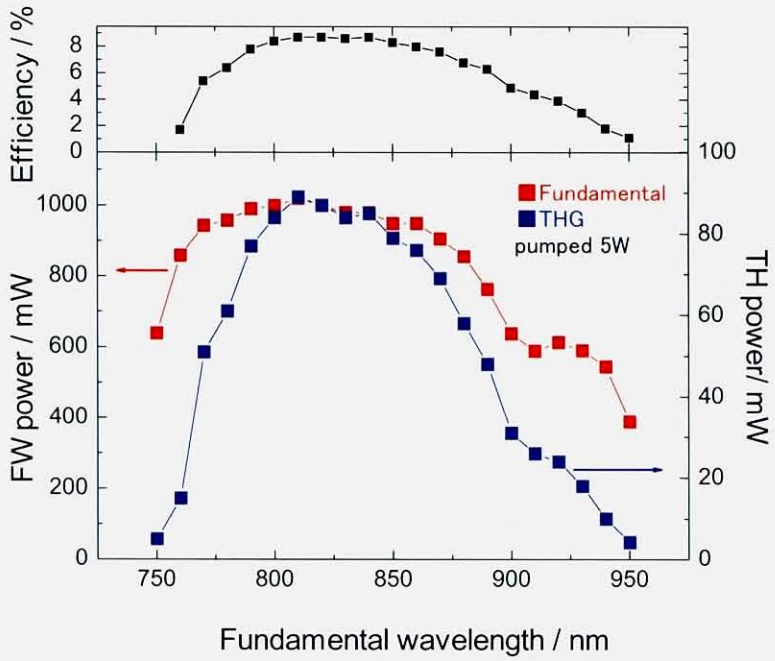

Fig. 3-12. The FW (red squares) and TH power (blue squares) plotted against the FW wavelength. Conversion efficiency (black squares) was also indicated at the upper part.

3. 4. 8. Principles of high harmonic generation

Nonlinear optical conversion like a second harmonic generation and sum frequency mixing can be accomplished in nonlinear crystal. When intense electric field **E** pass through a nonlinear medium, nonlinear polarization **P** should be induced in the material which is written as

$$\mathbf{P} = \varepsilon_0\left(\chi^{(1)}\mathbf{E} + \chi^{(2)}\mathbf{E}\cdot\mathbf{E} + \chi^{(3)}\mathbf{E}\cdot\mathbf{E}\cdot\mathbf{E} + \chi^{(n)}\mathbf{E}\cdot\mathbf{E}\cdots\mathbf{E}\right) \quad (3.\ 23)$$

where $\chi^{(1)}$ is liner optical susceptibility and other $\chi^{(n)}$'s are the n^{th} order nonlinear susceptibility[6,7]. The second right hand term of eq. (3. 23) is the second order nonlinear polarization $\mathbf{P}^{(2)}$ which is proportional to the square of **E**. By using the frequency of the electric field ω, the $\mathbf{P}^{(2)}$ is described by

$$\begin{aligned}\mathbf{P}^{(2)} &= \varepsilon_0\chi^{(2)}\mathbf{E}^2 \\ &= \varepsilon_0\chi^{(2)}{\mathbf{E}_0}^2\cos^2\omega t \\ &= \varepsilon_0\chi^{(2)}{\mathbf{E}_0}^2\frac{1-\cos 2\omega t}{2}\end{aligned} \quad (3.\ 24)$$

Thus the 2ω component in the eq. (3. 24) implies the second harmonic generation. However, such second order nonlinear phenomena arise only in the non-centrocymmetric medium. BBO is most frequently used as a nonlinear crystal.

By mixing of fundamental wave and its second harmonic in the second BBO, the sum frequency 3ω can be generated by

$$\begin{aligned}\mathbf{P}^{(2)} &= \varepsilon_0\chi^{(2)}\mathbf{E}\cdot\mathbf{E} \\ &= \varepsilon_0\chi^{(2)}\mathbf{E}_1\cos\omega t\cdot\mathbf{E}_2\cos 2\omega t \\ &= \varepsilon_0\chi^{(2)}\mathbf{E}_1\cdot\mathbf{E}_2\frac{\cos(2\omega+\omega)\,t+\cos(2\omega-\omega)t}{2}\end{aligned} \tag{3. 25}$$

The second term in the right hand in the bottom of eq. (3. 25) implies also difference frequency generation.

3. 4. 9. Time plate

In order to generate efficient THG, we have to compensate the time or phase difference between FW and its SH before BBO2 in Fig. 3- 11. Instead of harmonic separators and a delay stage such as shown in the inset of Fig. 3- 11, the time plate (TP) which made of high-temperature phase of BBO crystal (α-BBO) was used as an optics for the compensation. By using the TP, the THG can be thus easily generated in a small space. In this session, comprehensive description of the TP was displayed.

A light velocity in a material v_p is described by using its refractive index n and the light velocity in vacuum c as

$$v_p \equiv \frac{c}{n} \tag{3. 26}$$

Since the n in the material depends on the wavelength of light and is generally larger as shorter wavelength around the visible wavelength, SH is faster than FW in all material except for TP. The TP (α-BBO) is used as an optics for polarizer because of its scarce nonlinear effect. In the TP, SH of extraordinary ray (small n) is faster than FW of ordinary ray (large n) due to its birefringence. Therefore, we can compensate the time difference between FW and SH beams by rotating the crystal axis related with the index ellipsoid. The thickness and

cutting angle of the time plate depends on the thickness of BBO1, WP2 and other various factor. We obtain efficient TH signal with 2 mm thickness of AR coated time plate. The efficiency (see Fig. 3- 12) is almost same (or better) with general TH generator with delay line.

3. 4. 10. Details of BBO crystal

BBO crystal is generally used as not only SHG or THG but also optical parametric amplifier because of its high nonlinear coefficient, transmittance in ultraviolet region, and damage threshold. BBO is one of the optically uniaxial crystal which has crystal axis of a = b = 12.532 Å、 c = 12.717 Å. By using BBO, short wavelength limit of SH signal of 205 nm by nonlinear crystals has been reported [9]. THG by FW+SH can generate shorter wavelength less than 200 nm. Because BBO is sensitive to humidity, we have to be careful for the operation in atmosphere while the commercial crystals are generally coated for protection.

The cutting angle of the crystal should be determined to obtain adequate conversion efficiency. In the case of SHG, the phase matching condition between FW and generated SH is achieved by birefringent uniaxial crystal for which $n_e < n_o$, where n_e and n_o stand for the extraordinary and ordinary indices of refraction, respectively [6,7]. The extraordinary refractive ne in the crystal depends on the crystal axis which is given by

$$n_e(\theta)^{-2} = \frac{\cos^2\theta}{n_o^2} + \frac{\sin^2\theta}{n_e^2} \tag{3.27}$$

where θ is wave propagation angle related with the c-axis. Since n_o is independent of the crustal angle, the condition gives the angle of propagation of incident light with respect to the optic axis in which the n_e of the SH equals to that of n_o of the FW. When the indices of refraction of the FW and SH waves in the material are equal, i. e., $n_e(2\omega) = n_o(\omega)$, the phase matching condition is fulfilled. The phase matching condition can be demonstrated by the index of refraction ellipses as shown in Fig. 3- 13(a). The the phase matching angle θ_p corresponds to the intersection of the ordinary and the extraordinary index curves and is also calculated by

$$\theta_p = \sin^{-1}\sqrt{\frac{n_o(\omega)^{-2} - n_o(2\omega)^{-2}}{n_e(2\omega)^{-2} - n_o(2\omega)^{-2}}} \quad (3.28)$$

The phase matching by such a situation is called type I. The wavelength dispersion of the indices of BBO crystal are

$$n_o^2 = 2.7359 + \frac{0.01878}{\lambda^2 - 0.01822} - 0.01354\lambda^2 \quad (3.29)$$

$$n_e^2 = 2.3753 + \frac{0.01224}{\lambda^2 - 0.01667} - 0.01516\lambda^2 \quad (\lambda: \mu\text{m}) \quad (3.30)$$

which are given by Ref. 8. The calculated θ_p by using eq. (3. 28), (3. 29) and (3. 30) is plotted against the fundamental wavelength in Fig. 3- 14. For example, when the FW wavelength is 840 nm, the $\theta_p = 27.18°$. By tuning the crystal angle, the efficient SH is generated in the wide range.

In the same way, the phase matching angle (type I) for third harmonic is calculated by

$$3\omega \cdot n(3\omega, \theta) = \omega \cdot n_o(\omega) + 2\omega \cdot n_o(2\omega) \quad (3.31)$$

Therefore, the θ_p for 3ω is given as 41.45° at 840 nm FW and the refraction ellipses is displayed in Fig. 3- 13(b).

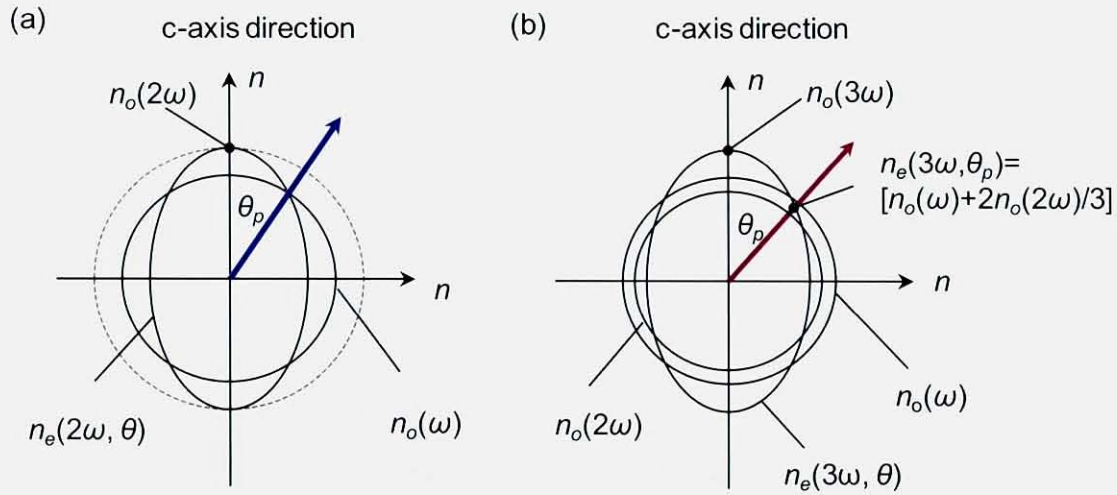

Fig. 3-13. The phase matching condition for (a) second harmonic (type-I)and (b)third harmonic with respect to the crystal c- axis direction. The phase matching angles θ_p correspond to the intersection of the index curves.

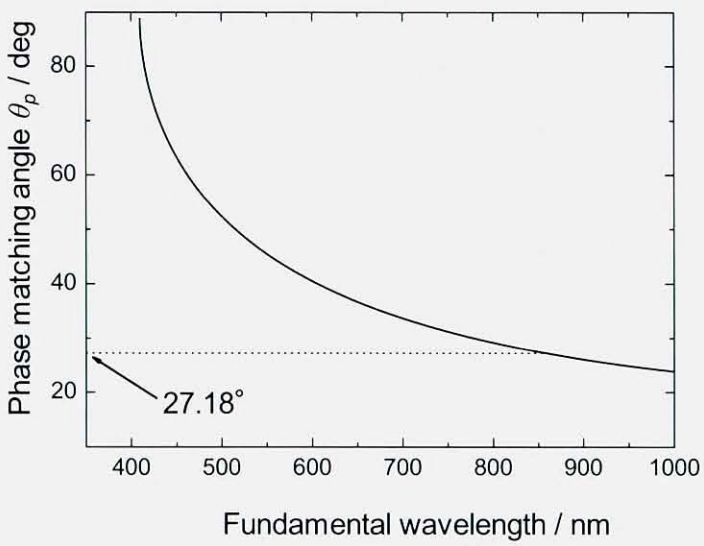

Fig. 3- 14. Phase matching crystal angle θ_p related with c-axis of BBO for frequency doubling the fundamental frequency

3. 5. Sample and its properties

3. 5. 1. Substrate: highly oriented pyrolytic graphite (HOPG)

HOPG is typically produced by the pyrolytic decomposition of carbonaceous vapors, where under suitably controlled condition (i.e. temperature of ~3000 °C and pressure of ~400 atm) [9]. The deposit is made of highly oriented basal layers so called honeycomb structure. In other words, the HOPG is said "polyclystaline graphite crystal". HOPG is generally used as a monochromater at X-ray region and standard sample of scanning tunneling microscope.

The ideal construction of graphite crystal is shown in Fig. 3- 15. The crystal lattice of graphite consists of an ordered **ABAB** stacking of honeycomb structure where carbon atoms locate within the plane. Each carbon atom in the plane is trigonally bounded to three neighboring carbon atoms by mainly sp^2. An unhybridized p_z orbital also participate in the bond as π interaction. The resulting inter atomic distance is 1.41 Å. The interaction between the basal planes of graphite is largely dominated by van der Waals interaction. The weaker interaction leads to the large interlayer spacing of 3.35 Å [10]. Therefore, it can be easily cleaved by scotch tape

We used ZYA grade HOPG procured from SPI. Inc. the In order to obtain clean HOPG substrate, it was cleaved in air and then heated in UHV to 673 K for at least 12 h. When we introduced new HOPG, the heating time should be longer at least 60 h to degas from honeycomb interlayer.

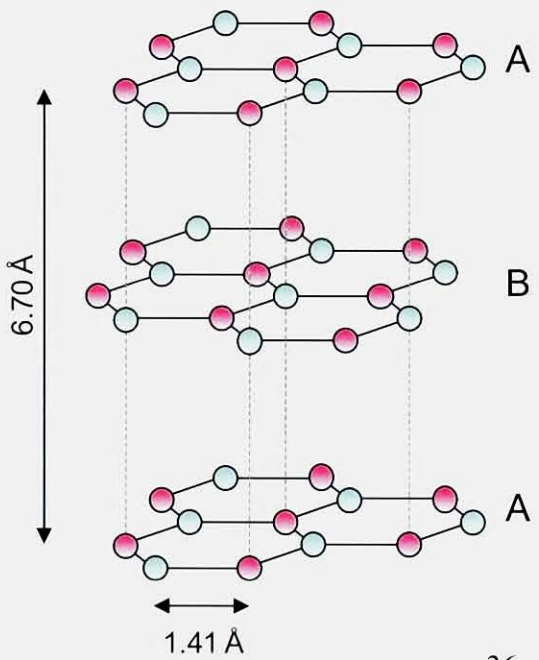

Fig. 3- 15. The crystal structure of hexagonal graphite. Each carbon atom within the basal plane is covalently bonded to three nearest neighbors by mainly sp^2 hybridized orbital. The weak interlayer interaction is largely due to van der Waals interaction

3. 5. 2. 2PPE spectrum for clean HOPG substrate

Fig. 3- 16 shows general 2PPE spectrum for HOPG substrate measured with *p*-polarized 4.43 eV photon energy at room temperature. The lower and upper horizontal axes were final and intermediate energy (final energy - $1h\nu$), respectively.. Work function of 4.45 eV for the substrate was determined by lower energy cut-off of the spectrum. Remarkable features of broad structure at around 1.7 eV intermediate energy and IPS (n = 1) were observed. Those features previously assigned to unoccupied structure by measuring the photon energy dependence of 2PPE spectra. The broad structure at E_F+1.7 eV was attributed to the unoccupied π^*-band of graphite [11]. The π^* structure has also been reported in the inverse photoemission spectroscopy [12-14].

The energy of IPS was +3.58 eV. Though slight sample or experimental dependence of the intensity ratio between π^*-band and IPS was observed, cleanliness of the substrate was confirmed by the value of work function and the width of IPS peak of less than 140 meV [15]. The general physical description of IPS is discussed in 3. 5. 3 and π^* structure was discussed in relation with the band structure of graphite and the result of PbPc film on HOPG in 6. 4. 1.

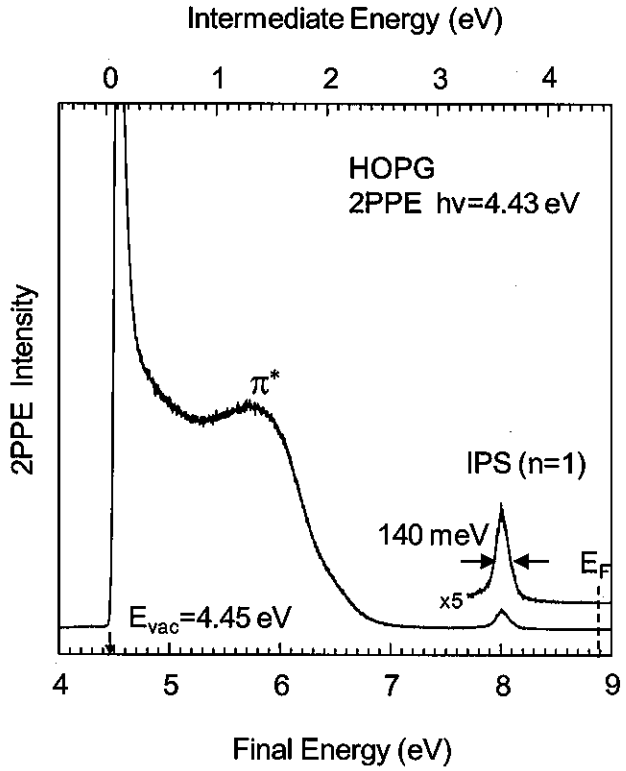

Fig. 3- 16. 2PPE spectrum for a HOPG substrate measured at room temperature. The lower and upper horizontal axes were final and intermediate energy, respectively. The photon energy was used p-polarized 4.43 eV. Work function of 4.45 eV was determined by lower energy cut-off of the spectrum. At 1.7 and 3.58 eV intermediate energies were due to π^*-band and IPS (n=1), respectively.

3. 5. 3. The description of image potential state

This part describes image potential state formed on the substrate. When the electron locates outside the surface, the electron feels the Coulomb potential as if the positive charge called image charge is in the bulk [16-18]. Fig. 3- 17 displays the image of the image charge.

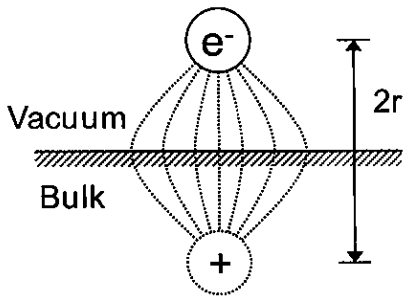

Fig. 3- 17. The inducement of an "image charge" in a surface opposite to a test charge distance from surface, *r*.

The work function is defined by the minimum energy required to remove an electron from a solid to sufficient distance outside the surface such that it no longer feels the effect of the image charge [16]. The surface Coulomb potential "image potential" is described by electromagnetic concept which is given by most simply

$$F(r) = \frac{e^2}{4\pi\varepsilon_0(2r)^2} \tag{3. 32}$$

where r, ε_0, and e are the distance between the surface and electron, dielectric constant of the vacuum, and elementary charge, respectively [17,18]. The potential energy is given with respect to the vacuum level E_{vac} which is defined the energy level of E_F+work function

$$V(r) = E_{vac} - \frac{e^2}{4\pi\varepsilon_0 \cdot 4r}. \tag{3. 33}$$

Equation (3. 33) has the same form as the radial part of the hydrogen problem. It differs only by a factor of 4 in the denominator. Therefore, the energy of the unoccupied levels so called image potential states (IPS's) are expect to form a discrete Rydberg series which result in

$$E_n = E_{vac} - \frac{Ry}{16(n+a)^2} - \frac{0.85}{(n+a)^2} \text{ (eV)} \tag{3. 34}$$

where n is the quantum number, a is the quantum defect depending on the band structure of the material, and Ry is a constant Rydberg energy of 13.6 eV [16,17]. As an example, the image potential curve and wavefunction of the IPS on Cu(100) surface were shown in Fig. 3-

18 [19]. The wave functions of the IPS's are expanded to more than 20 Å from the substrate.

In experimentally, the IPS's were firstly observed on the surface of liquid helium by absorption spectroscopy [20]. For the solid surface, the IPS's were reported by inverse photoemission spectroscopy [21-22] and now they have been most extensively studied by 2PPE spectroscopy up to $n = 3$ [17]. $n \geq 4$ IPS's were also detected by quantum beat spectroscopy based on the pump-probe 2PPE measurement [23]. Höfer and Harris have been deeply discussed the physical properties of the IPS by comparing the potential calculation [19,24-26]. For the 2PPE experiments, *p*-polarized light has to be chosen to excite the electron to the IPS because the transition can be induced with only the electronic field of surface normal direction.

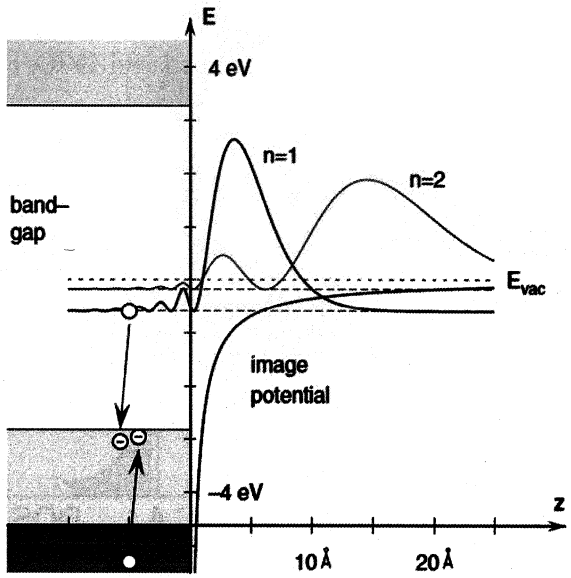

Fig. 3- 18. Energy diagram of Cu(100) surface and probability densities of first two IPS's referred from [19]. Discrete Rydberg series of hydrogen –like states are formed below the vacuum level E_{vac}. IPS's are penetrated into the bulk and spread far above a few nm from the surface.

3. 5. 4. Band structure of graphite

In order to consider the origin of broad π^*-band observed in 2PPE, the calculated band structure of graphite was shown in Fig. 3- 19 from Ref. 27. We measured photoelectrons emitted normal to the surface, that is, we probed the Γ-point of the surface Brillouin zone. The energy region between 0 and 4 eV above E_F at the Γ-point of bulk graphite is in the band gap and there is no unoccupied band. The π^*-band in the energy region between 1 and 2 eV is located at the momentum region from M, K to H points [27,28]. It seems as if no projected unoccupied band could be the intermediate state for the 2PPE process. Actually, the origin of the π^*-band in 2PPE can be explained by taking into account the electron-phonon interaction which is discussed together with the result of PbPc films on HOPG in 6. 4. 1.

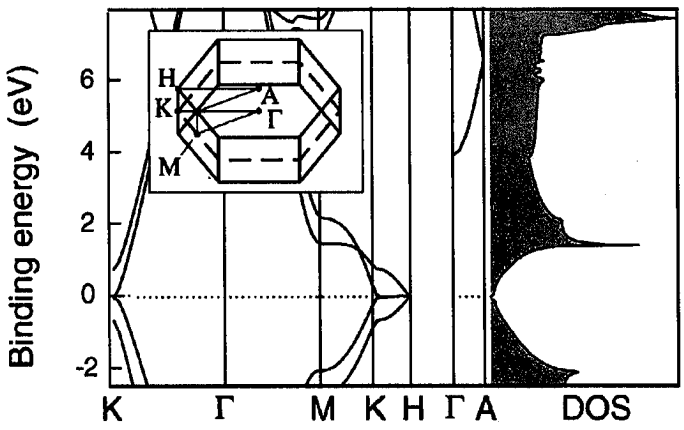

Fig. 3- 19. Band structure and density of state (DOS) of graphite from Ref 27. The Γ point is in a large band gap around the E_F. The saddle point is located at M and K point of Brillouin zone and high DOS is projected at E_F+1.7 eV.

3. 5. 5. Lead phthalocyanine (PbPc)

Phthalocyanine (Pc) is a very stable chemical compound which has porphyrin ring consisting of nitrogen, carbon, and hydrogen atoms. The molecule is able to coordinate hydrogen or many kinds of metal cations in its center (H- or M- Pc). Some Pc molecules have been used as a pigment in the field of the industry because its characteristic of visible absorbance. One of the pigment, cupper -Pc is most commonly found in blue line of Japanese Shinkansen. Today, the molecules have been interested many application [29,30] such as organic devices, oxidation-reduction catalyst, and optical nonlinear materials.

Lead-Pc (PbPc), we applied in this work as a material of organic films, is one of the most longtime organic semiconductors which is applied in field effect transistor. Fig. 3- 20 shows the molecular geometry of PbPc. In the case of PbPc, The Pc ring is deformed by a large lead atom like a shuttlecock type configuration. Therefore, the molecule has a C_{4v} symmetry and permanent molecular dipole moment directing perpendicular to the Pc ling [31-33]. The UPS work for PbPc films on HOPG has been performed by Ueno group and deeply discussed in relation with hole hopping mobility and reorganization energy [32-35]. One of the great advantages of the choice is that we can easily estimate the thickness of the films by monitoring the work function. Moreover, we can obtain the highly oriented molecular films of 1 ML and 2ML by suitable annealing process [32].

In this work, PbPc was purified by two-cycles of vacuum sublimation and carefully evaporated to the HOPG substrate at the constant rate of 0.05 nm / min with monitoring quarts micro valance.

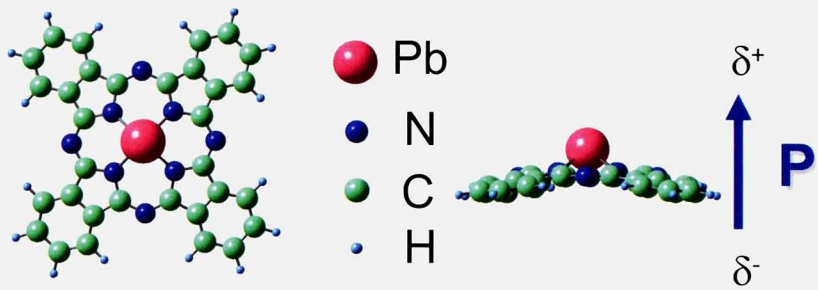

Fig. 3- 20. The molecular orientation of PbPc

References

[1] T. Munakata, M. Shibuta, M. Mikamori, T. Yamada, K. Miyakubo, T. Sugiyama, and Y. Sonoda, Proc. SPIE **6325**, 63250M (2006).

[2] T. Sagawa, OYOBUTHURI **41**, 851 (1972).

[3] V G Microtech. Inc.: CLAM 4 Systems Operating Manual.

[4] Verdi-10 Operator's Manual: COHERENT.

[5] Mira Model 900-F Operator's Manual: COHERENT.

[6] J. –C. Diels, W. Rudolph, *Ultrafast laser Pulse Phenomena* (Elsevier, 2nd edition, 2006).

[7] C. Rullière (ed.), *Femtosecond laser pulses* (Springer, 2nd edition, 2004).

[8] J. J. Sakurai, *Modern Quantum Mechanics* (Menlo Park, The Benjamin/Cummings Publishing Company, 1985)

[9] K. Miyazaki, H. Sakai, and T. Sato, Opt. Lett. **11**, 797(1986).

[10] M. N. Reynolds, *Physical properties of graphite* (Elsevier, Essex, 1968).

[11] J. Lehmann, M. Merschdorf, A. Thon, S. Voll, and W. Pheiffer, Phys. Rev. B **60**, 17037 (1999).

[12] B. Reihl, J. K. Gimzewski, J. M. Nicholls, and E. Tosatti, Phys. Rev. B **33**, 5770 (1986).

[13] I. Schäfer, M. Schlüter, and M. Skibowski, Phys. Rev B **35**, 7663 (1987)

[14] R. Claessen, H. Carstensen, and M. Skibowski, Phys. Rev. B **38**, 12582 (1988).

[15] I. Yamamoto, M. Mikamori, R. Yamamoto, T. Yamada, K. Miyakubo, N. Ueno, and T. Munakata, Phys. Rev. B **77**, 115404 (2008).

[16] Gary Atterd and Colin Banes, *Surfaces* (Oxford University press, New York, 1998).

[17] H. L. Dai, W. Ho, *Laser Spectroscopy and Photochemistry on metal Surfaces Part 1* (World scientific, Singapore, 1995).

[18] E. V. Chulkov, V. M. Silkin, P. M. Echenique, Surf. Sci. **437**, 330 (1999).

[19] J. Güdde, U. Höfer, Prog. Surf. Sci. **80**, 49 (2005).

[20] C. C. Grimes, T. R. Brow, Phys. Rev. Lett. **32**, 280 (1974).

[21] F. J. Himpsel, Comments Condens. Matter Phys. **12**,199 (1986).

[22] N. V. Smith, Rep. Prog. Phys. **51**, 1227 (1988).

[23] U. Höfer, I. L. Shumay, C. Reuß, U. Thomann, W. Wallauer, T. Fauster, Science **277**, 1480 (1997).

[24] C. B. Harris, N. –H. Ge, R. L. Lingle, Jr., J. D. McNeill, Annu. Rev. Phys. Chem. **48**, 711 (1997).

[25] A. Hotzel, G. Moos, K. Ishioka, M. Wolf, G. Ertl, Appl. Phys. B **68**, 615 (1999).

[26] W. Berthold, F. Rebentrost, P. Feulner, U. Höfer, Appl. Phys. A **78**, 131 (2004).

[27] G. Moos, C. Gahl, R. Fasel, M. Wolf, and T. Hertel, Phys. Rev. Lett. **87**, 267402 (2001).

[28] J. Lehmann, M. Merschdorf, A. Thon, S. Voll, and W. Pheiffer, Phys. Rev. B **60**, 17037 (1999)

[29] T. Yasuda, T. Thuthui, Jpn. J. Appli. Phys. **45**, L595 (2006).

[30] B. Mukherjee, A. K. Ray, A. K. Sharma, M. J. Cook, and I. Chambrier, J. Appl. Phys. **103**, 074507 (2008).

[31] K. Ukei, K. Takamoto, and E. Kanda, Phys. Lett. **45**, 345 (1973).

[32] S. Kera, H. Fukagawa, T. Kataoka, S. Hosoumi, H. Yamane, and N. Ueno, Phys. Rev. B **75**, 121305(R) (2007).

[33] H. Yamane, H. Honda, H. Fukagawa, M. Ohyama, Y. Hinuma, S. Kera, K.K. Okudaira, N. Ueno, J. Electr. Spectrosc. Relat. Phenom. **137-140**, 223 (2004).

[34] S. Kera, H. Yamane, and N. Ueno, Prog. Surf. Sci. **84**, 135 (2009).

[35] N. Ueno and S. Kera, Prog. Surf. Sci. **83**, 490 (2008).

4. Previous work and facing problem

4. 1. Summary of Previous results of Microspot- 2PPE

In the main body of this thesis, we focused on only 1 ML coverage, while the sample preparation, evaluation, and assignment of the observed energy levels were based on our previous microspot- 2PPE work [1] which covers in this part. The previous work carefully determined the ML and established the method to make well-ordered 1 ML film. The coverage dependence of microspot-2PPE spectra for PbPc/HOPG measured with $h\nu = 4.33$ eV is shown in Fig. 4- 1 [1]. The horizontal axis is the final energy of photoelectron with respect to E_F. By adsorption of PbPc, three peaks labeled L_1, H_1 and H_2 appeared in addition to IPS which was seen for the bare, 0.3 and 1ML films. The H_1, H_2 and L_1 shift to lower final energy with increasing coverage. The coverage was determined from the work function change. The work function decreased as the coverage increased up to 1 ML. According to Ref. 2, the decrease is due to the dipole layer formed on the graphite; PbPc molecules in the 1 ML film were lying flat on the substrate directing Pb atoms to vacuum side. When the second layer is adsorbed on the 1 ML film, the work function increased again. This indicates that the second-layer molecules stacked on the 1ML film forming PbPc dimmers [2]. Then, the dipole layer was canceled at 2 ML and work function was almost revived to that of the bare substrate. The molecular orientation at 1 ML and 2 ML were illustrated in the right hand of Fig. 4- 1. These behaviors were also reproduced with our microspot-UPS result [3]. Therefore, the 1 ML coverage was determined when the lowest work function was observed.

After suitable annealing at 100 °C for 1 hour, the IPS became sharp and L_1 split into L_0 and L_1 without changing the work function. The work function was 4.28 eV which is 0.19 eV lower than that for clean HOPG. The binding energy of IPS with respect to the vacuum level was -0.77 eV, slightly smaller than that for the bare HOPG, -0.89 eV. Since the IPS is very sensitive to surface flatness or defects, we could confirm that well ordered 1 ML PbPc film was really prepared. The IPS broadening at sub-ML coverage reflects the confinement of 2D free electron IPS in nm-size areas among molecular clusters but was not discussed here for sub- ML.

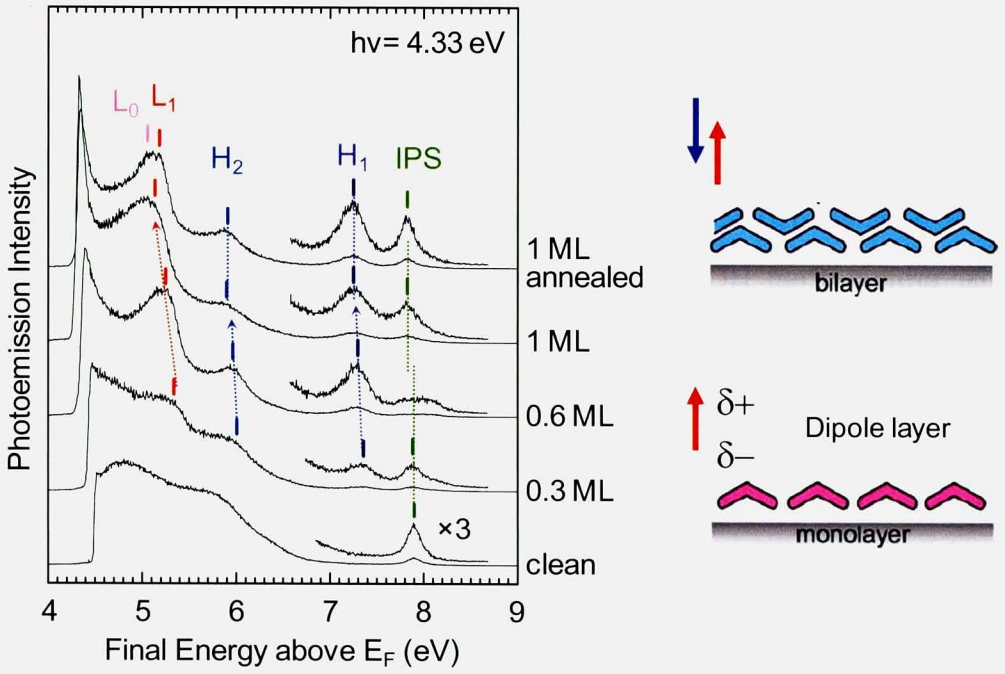

Fig. 4- 1. 2PPE results measured with p-polarized light at a photon energy of 4.33 eV for different coverages. 2PPE spectrum for an annealed 1 ML film is also shown at the top. The horizontal axis is the final energy of photoelectron with respect to E_F. All spectra were measured at room temperature. The shift of IPS (0.07 eV) is smaller than that of the vacuum level (0.19 eV). The right hand indicates the molecular orientation of the 1 ML and 2 ML films. 1 ML film is oriented with flat and directing lead atom to the vacuum.

In order to assign the observed peaks, microspot-2PPE spectra for well ordered 1 ML coverage measured with various photon energies were shown in Fig. 4- 2. The H_1 component split into two components labeled H_1 and L_2 at $h\nu \geq 4.38$ eV. The energies of these peaks are plotted as a function of photon energy in Fig. 4- 3. The data sets for Fig. 4- 3 accumulate the result of several experimental runs for 1 ML film. All the peak positions align well on the line of slope 1 or 2: the peaks on slope 1 lines are due to the photoelectrons from unoccupied levels and those on slope 2 are due to that from occupied levels. The energies of the occupied levels, H_1 and H_2, related to E_F were -1.33 and -2.76 eV (final energy $-2h\nu$), respectively. These energy positions for the occupied levels were well reproduced with UPS in Ref. 2 and our microspot-UPS. Then the peaks of H_1 and H_2 were assigned to originate from molecular derived HOMO and next HOMO (HOMO-1) levels. On the other hand, the energies for the

unoccupied levels, L_0, L_1, L_2, and IPS were 0.71, 0.87, 2.94, and 3.51 eV (final energy-1$h\nu$), respectively.

Fig. 4- 4 compares the observed energy level with the results of density functional theory (DFT) calculation. The molecular orbital energies are aligned with the experimental vacuum level. The DFT calculation was performed for PbPc free molecule with B3LYP method and LANL2DZ basis set. The results of the calculation were similar to those of Refs. 2 and 4. The molecular orbitals from HOMO-2 to LUMO+2 and were shown in the top of Fig. 4- 5. HOMO-1 is mainly composed of orbitals of Pb atom, and other occupied and unoccupied orbitals, HOMO, LUMO, LUMO+1, and LUMO+2, are composed of π-orbitals of phthalocyanine ring. The character table and direct product of C_{4V} is shown in the Fig. 4- 5.

The unoccupied levels L_0 and L_1 are related with the degenerate LUMO and LUMO+1. The degeneracy was released by adsorption. The unoccupied level of L_2 should be related with LUMO+2. According to the character table in Fig. 4- 5, optical transition from HOMO to LUMO+2 is forbidden. The observed resonance indicates that the adsorbed molecules are deformed from C_{4v} symmetry. Thus all occupied and unoccupied energy levels from HOMO-1 to LUMO+2 for this system could be obtained. In addition, the 2PPE resonances from HOMO to LUMO+2 and HOMO to IPS were observed at $h\nu$ of 4.3 and 4.8 eV. Now we expanded the work for well ordered PbPc film with improved signal to noise ratio, to obtain more details of excitation dynamics around the resonance

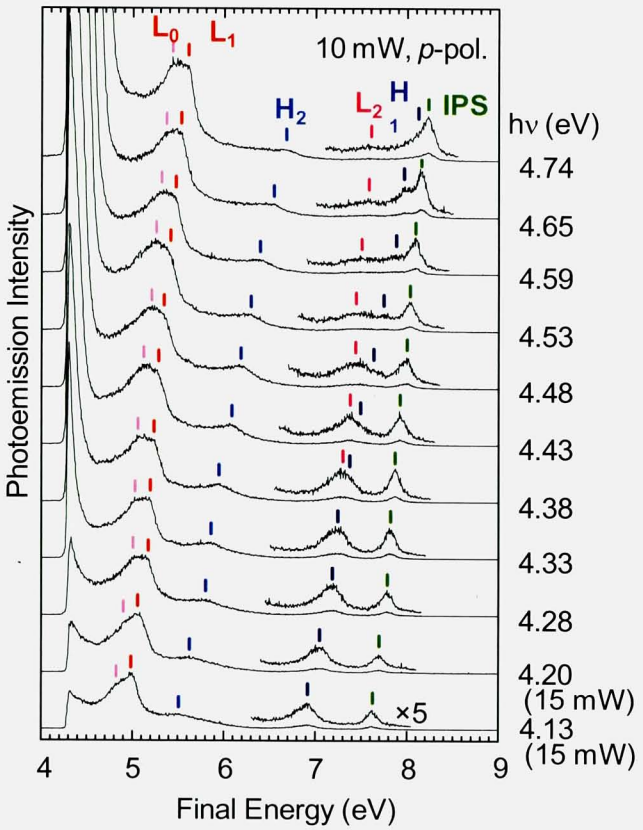

Fig. 4- 2. Photon energy dependence of 2PPE spectra for 1 ML coverage with microspot configuration. The photon energies are shown at the right-hand side. The spectra for hv > 4.38 eV were measured with nearly constant laser power of 10 mW. The spectra for photon energies of 4.20 eV and 4.13 eV were measured with the laser power of 15 mW. The energies of each peak are marked by bars. At photon energy higher than 4.3 eV, the peak H_1 split into two components, L_2 and H_1.

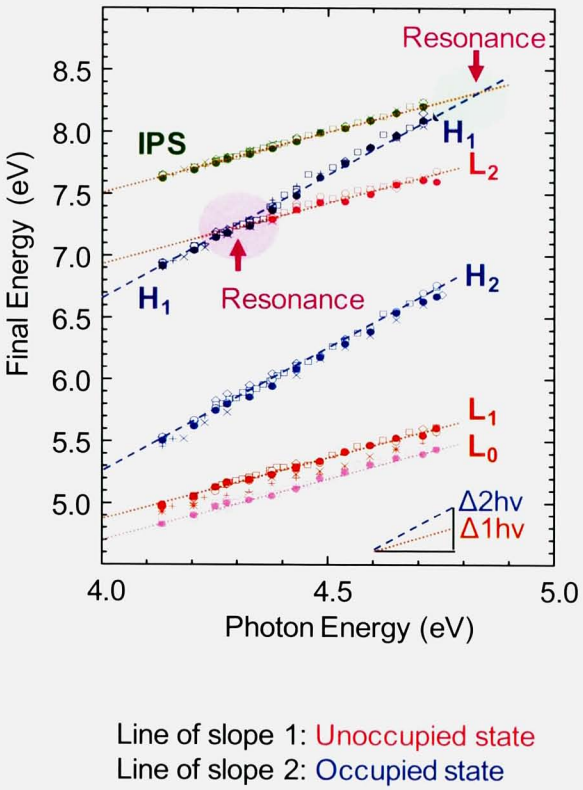

Fig. 4- 3. Final energies of the peaks for PbPc (1 ML)/HOPG are plotted as a function of photon energy. The result of several experimental runs for 1 ML film were plotted by distinguished symbols. The slopes of dotted and dashed lines are 1 and 2, respectively. The resonances were observed at photon energies of 4.3 and 4.8 eV.

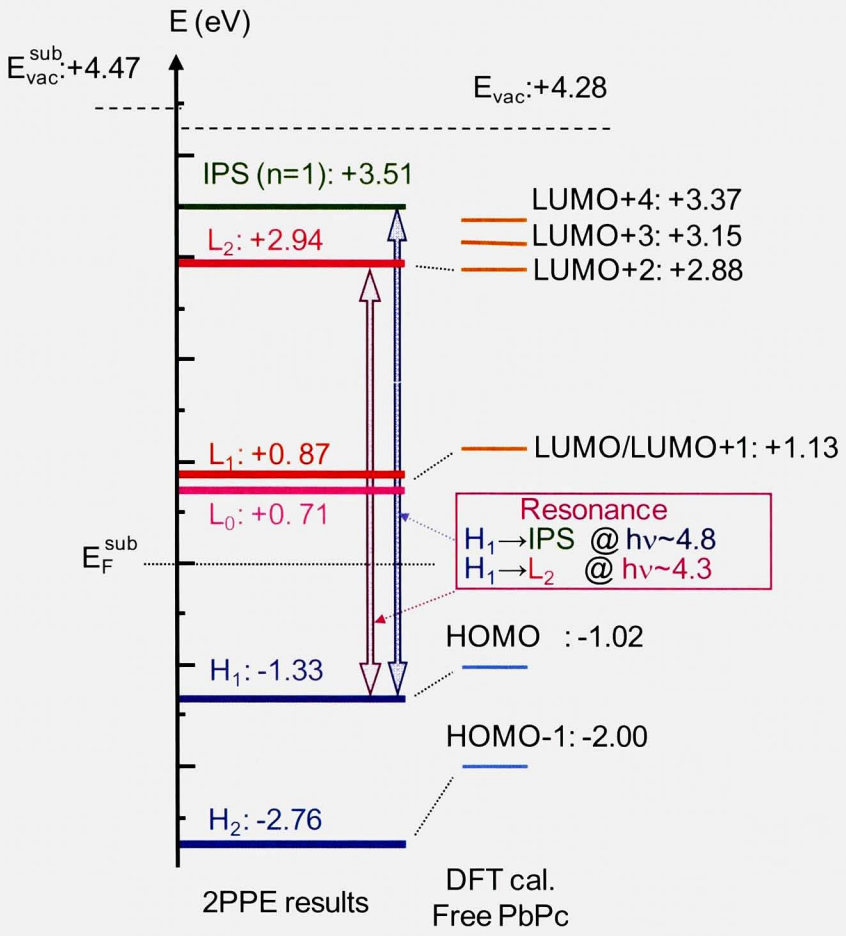

Fig. 4- 4. The energy levels of 1 ML PbPc/HOPG and the calculated molecular orbital energies from HOMO-1 to LUMO+4 of free PbPc molecule. The molecular orbital energies are aligned with the experimental vacuum level. LUMO and LUMO+1 are degenerated in a free PbPc molecule. The block-arrows show the observed resonances from the HOMO level to the LUMO+2-related level and to IPS.

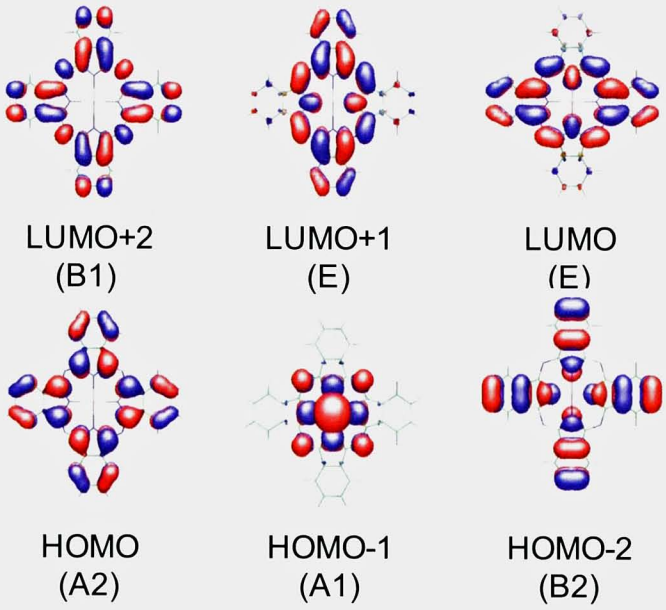

C_{4v} Character table

C_{4v}	E	$2C_4$	C_2	$2\sigma_v$	$2\sigma_d$	
A_1	1	1	1	1	1	z
A_2	1	1	1	- 1	- 1	
B_1	1	- 1	1	1	- 1	
B_2	1	- 1	1	- 1	1	
E	2	0	- 2	0	0	(x, y)

C_{4v} Direct product

C_{4v}	A_1	A_2	B_1	B_2	E
A_1	A_1	A_2	B_1	B_2	E
A_2		A_1	B_2	B_1	E
B_1			A_1	A_2	E
B_2				A_1	E
E					$A_1 + B_1 + B_2$

Fig. 4- 5. (top) the molecular orbital of PbPc from HOMO-2 to LUMO+2 calculated by DFT with B3LYP method and LANL2DZ basis set. Except for HOMO-1, the molecular orbitals mainly composed with π orbital of phthalocyanine ring. (bottom) character table and direct product of C_{4V}.

4. 2. Facing Problems for understanding 2PPE spectroscopy

This section clarified the facing problems for 2PPE spectroscopy. Though the 2PPE spectroscopy is an excellent method for the understanding the unoccupied state, some unresolved question still exists. Weinelt addressed this question as following in the next page [5]. He has been carefully measured the photon energy dependence of 2PPE spectra and pointed out the different resonance behavior in 2PPE between Si(100) and Cu(111) result.

In the case of 2PPE for Si(100), as shown at the yellow under line in the article, the unoccupied state (n = 1) was invisible below the resonance, and occupied state (D_{up}) was invisible above the resonance (see left hand of FIGURE 3). In other words, the 2PPE intensity was "switched" at the resonance.

In contrast, both occupied (n = 0) and unoccupied (n = 1) state were observed both below and above the resonance photon energy for Cu(111) (blue under line). The line width and intensity of 2PPE spectra for Cu(111) around the resonance have been deeply discussed by taking into account "dephasing" process (green box). This is supported by Ueba's 2PPE theory [6-8].

However, the intensity switching observed in 2PPE for Si(100) cannot be explained by "dephasing" process. The red box in the article addresses the clear contradiction of resonance behavior for Si(100). Similar intensity variations around the resonances were known for other transitions of Si(100) and Si(111) [9,10].

As mentioned in Introduction, it is the serious problem whether occupied and unoccupied states are detected. The unresolved question of the intensity variation should be a key to solve the problem. The intensity variation may reflect some important hidden physics which has not been taken into account in the existing theoretical works [6-8].

The PbPc film showed clear resonances, HOMO to LUMO+2 and HOMO to IPS. The system is an excellent example for understanding of the intensity variation around the resonance.

3.5 *Dephasing on* Si(100)

The reader not familiar with 2PPE might not be taken aback by the fact that the initial state D_{up} is probed below resonance but the intermediate state $n = 1$ is probed above resonance. Therefore, we present in Fig. 9a at first 2PPE spectra recorded on Cu(111) for overlapping pump and probe pulses. As already mentioned the surface-projected bulk band gap of Cu(111) supports an occupied Shockley surface state $n = 0$ as well as an unoccupied image-potential state $n = 1$ adjacent to the lower and upper band edges. The transition $n = 0 \rightarrow n = 1$ shows resonant enhancement at a UV photon energy of $3h\nu = 4.536$ eV [44, 45]. As spectra have been normalized to constant height this is not seen in Fig. 9a. More important and in contrast to Si(100), on Cu(111) both the occupied state and the unoccupied state are observed below and above the resonance ($h\nu = 1.512$ eV in Fig. 9a). As expected the $n = 0$ initial state shows a slope of $m = 4$ while a slope of $m = 1$ is observed for the unoccupied image-potential state $n = 1$ [46]. Thus, the energy spacing between the two peaks varies linearly with the UV pump pulse as $3 \times \Delta h\nu$. For a detuning of $\Delta h\nu = \pm 0.05$ eV from the resonance $h\nu \simeq 1.512$ eV, intensities of initial and intermediate states roughly match on Cu(111).

Figure 9b shows the outcome of a simulation of the Cu(111) spectrum at a photon energy of $h\nu = 1.57$ eV, i.e. $3\Delta h\nu \simeq 0.15$ eV above resonance. For the three-level system sketched at the bottom of Fig. 9b we solve optical Bloch equations in the rotating wave approximation [47]. We model transitions between initial $n = 0$, intermediate $n = 1$, and final states $|f\rangle$ above E_{vac} [48]. Process (a) corresponds to off-resonant excitation of the intermediate state and subsequent ionization of the transient population. Process (b) describes ionization of the initial state by direct two-photon absorption. Two parameters enter the simulation: the decay rate $\Gamma_1 = \hbar/\tau_1 = 36.5$ meV of the intermediate state with lifetime τ_1 [49, 50] and the dephasing rate Γ_{01}^* which describes the decay of the polarization, i.e. the decay of the dipole moment μ_{01} associated with the transition $n = 0 \rightarrow n = 1$. This so-called pure dephasing rate has been varied in the simulation keeping the lifetime constant. We assume

This is true for Cu(111), but it is not the case for the Si(100) surface. In Fig. 3a we marked the peak positions of D_{up} and $n = 1$ states expected for slopes of $m = 4$ and $m = 1$ by filled squares and open circles, respectively. At a photon energy of $h\nu = 1.55$ eV the contribution of the $n = 1$ state to the spectrum becomes negligible (filled square). Thus, one would conclude that the dephasing rate of the polarization driving the $D_{up} \rightarrow n = 1$ transition is rather small. In contrast, at a photon energy of $h\nu = 1.65$ eV we do not observe significant intensity at the position of the D_{up} peak (open circle). Now one would argue that the dephasing rate of the polarization driving the $D_{up} \rightarrow n = 1$ transition is rather large. Combining these observations suggests that dephasing sets in first when the photon energy is sufficient to resonantly populate the intermediate image-potential state. Comparable results have been obtained by Munakata and coworkers for Si(100) and Si(111) [55, 56]. The underlying microscopic mechanism remains to be clarified.

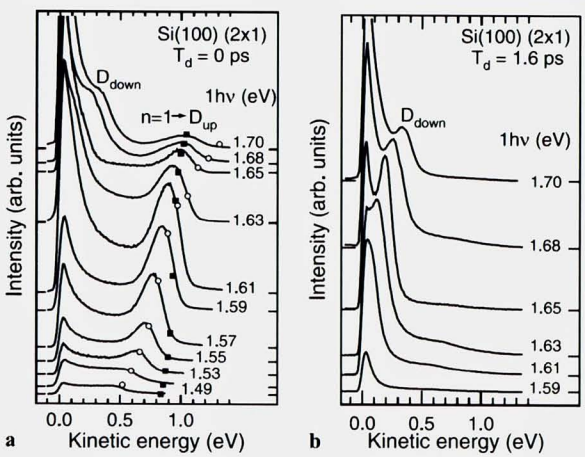

FIGURE 3 Bichromatic two-photon photoemission spectra from a Si(100) (2 × 1) surface. The photon energy of $h\nu$ refers to the IR fundamental. (**a**) For overlapping pump and probe pulses $T_d = 0$ ps the occupied dangling-bond state D_{up} and the surface-state resonance $n = 1$ are probed. Peak positions expected for a slope m of 4 and 1 are marked by *open circles* and *filled squares*, respectively. (**b**) The unoccupied dangling-bond state D_{down} is accessible at higher photon energies and best resolved at a time delay of $T_d = 1.6$ ps between IR pump and UV probe pulses

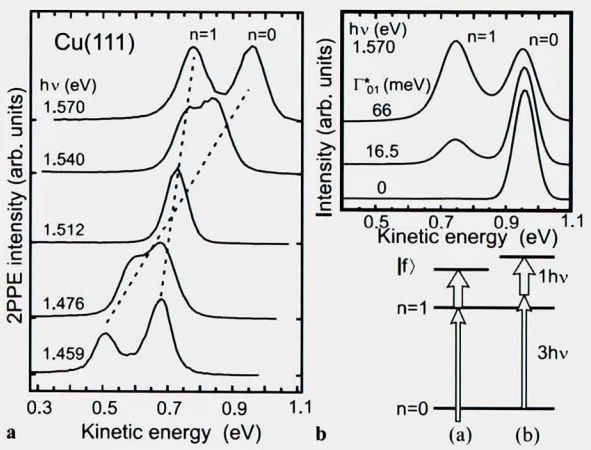

FIGURE 9 (**a**) Two-photon photoemission spectra from Cu(111) for various photon energies $h\nu$ below and above resonance ($h\nu = 1.512$ eV). The spectra are normalized to the same height. The $n = 0$ initial state and the $n = 1$ intermediate state show slopes of $m = 4$ and $m = 1$. (**b**) Simulated spectra for an IR photon energy of $h\nu = 1.57$ eV. Γ_{01}^* is the respective dephasing rate (see text). Processes (a) and (b) outline off-resonant excitation of the $n = 1$ intermediate state and two-photon ionization of the $n = 0$ initial state

References

[1] I. Yamamoto, M. Mikamori, R. Yamamoto, T. Yamada, K. Miyakubo, N. Ueno, and T. Munakata, Phys. Rev. B **77**, 115404 (2008).

[2] S. Kera, H. Fukagawa, T. Kataoka, S. Hosoumi, H. Yamane, and N. Ueno, Phys. Rev. B **75**, 121305(R) (2007).

[3] I. Yamamoto, N. Matsuura, M. Mikamori, R. Yamamoto, T. Yamada, K. Miyakubo, N. Ueno, T. Munakata, Surf. Sci. **602**, 2232 (2008).

[4] Y. Zhang, X. Cai, X. Zhang, H. Xu, Z. Liu, J. Jiang, Inter. J. Quantum Chem. **107**, 952 (2007).

[5] M. Kutschera, M. Weinelt, M. Rohlfing, T. Fauster, Appl. Phys. A **88**, 519 (2007).

[6] H. Ueba, Surf. Sci. **334**, L719 (1995).

[7] H. Ueba, T. Mii, Appl. Surf. Sci. **169-170**, 63 (2001).

[8] H. Ueba, B. Gumhalter, Prog. Surf. Sci. **82**, 193 (2007).

[9] K. Shudo, S. Takeda, and T. Munakata, Phys. Rev. B **65**, 075302 (2002).

[10] K. Shudo and T. Munakata, Phys. Rev. B **63**, 125324 (2001).

5. Vibrationally resolved 2PPE spectroscopy for PbPc film on graphite

5. 1. Introduction

The interaction of electron and hole with phonon is a key for electric conduction in solids as well as at interfaces. As for carrier transportation in organic semiconductors, the role of vibronic coupling has been discussed [1,2]. The hole-vibrational coupling at interfaces between organic molecular films and substrates has recently been resolved in photoemission spectroscopy and was discussed in relation to the hole-hopping mobility and the reorganization energy [3,4]. Experimental detection of the nuclear motion of molecule triggered by injection of electron into an unoccupied state is the next step to be explored for deeper understanding of electron transportation at the interface between inorganic substrate and organic film. Nuclear wave packet motion of adsorbed atoms in an unoccupied state was reported as the real-time observation of a surface photochemical reaction [5]. On the other hand, vibration of molecule in an electronic excited state can be resolved only for thick films, and is hardly resolved for the first adsorbed layer because lifetime of the excited state becomes too short by interaction with the substrate [6]. 2PPE spectroscopy gives spectroscopic and dynamic information on both occupied and unoccupied energy levels. Vibrational structure in 2PPE spectroscopy for adsorbed molecules will provide rich information on carrier dynamics at surfaces and interfaces, though vibrational resolution in 2PPE for adsorbed molecules was not very clear so far [7]. Here, we report vibrationally resolved features in 2PPE spectra for lead phthalocyanine (PbPc) films formed on HOPG graphite.

In our former 2PPE work for PbPc/HOPG, we have identified molecule-derived levels due to HOMO-1, HOMO, LUMO, LUMO+1, LUMO+2 as well as the first IPS. Resonant excitation from the HOMO level to the LUMO+2 level was observed [8]. In this paper, we examined the detailed spectral profiles of the HOMO- and LUMO+2-derived peaks at photon energies below and above the resonance. The vibrational satellite of the HOMO peak was found to be dependent on the excitation photon energy. The dependence was attributed to the nuclear motion of the molecule in the LUMO+2-related intermediate state.

5. 2. Experiment

The 2PPE experiments were performed in an UHV chamber. The light source was the *p*-polarized third harmonic output of a titanium sapphire laser operated at a pulse duration of 100 fs and a repetition rate of 80 MHz. The light was focused by a concave mirror of 350 mm focal length onto the sample surface at an incidence angle of 60°. Photoelectrons emitted to the surface normal were detected with a hemispherical energy analyzer (VG-CLAM4 with nine channeltrons) of 20 meV energy resolution. The acceptance angle of the analyzer was limited to be ±1° with a specially modified electron entrance lens. HOPG substrate was cleaved in air and cleaned by heating at 673 K for 50 h in UHV. The cleanliness was confirmed by the work function (4.45 eV) and the peak width of the IPS feature (140 meV) measured with 2PPE spectroscopy for the bare HOPG. Note that focusing of the light to a sub-μm spot as in Ref. 8 was not employed here. The spot size of the light in this experiment was estimated to be about 80 μm. The large spot size was advantageous to increase the photoemission intensity while suppressing the broadening of spectrum due to the space charge effect [9]. Then the uniformity of the films was a key of this experiment. Our microspot-2PPE [8] and photoemission electron microscopy [10] experiments showed that well ordered films of 1 monolayer (ML) thickness were prepared by annealing PbPc films of 0.4 nm thickness (reading of a quartz microbalance) at 373 K for 1 h. Formation of uniform films of sub-ML or > 1 ML thickness was not successful [8], and only the 1 ML films were used in this experiment.

5. 3. Results and discussions

The 2PPE spectrum for the PbPc film at the room temperature measured with photon energy of 4.59 eV is shown in the top of Fig. 5- 1. The lower horizontal axis is the initial energy (final energy - $2h\nu$, where hν is the photon energy) with respect to the E_F, the upper one, the intermediate energy defined as (final energy - $1h\nu$). The 1PPE result measured at 90 K with a He-I light source was plotted on the initial energy scale at the bottom. The 1PPE spectrum reproduced that of Ref. 11. The 1PPE feature at -1.33 eV initial energy was assigned to originate from the HOMO-derived level. Molecules in the film were lying flat on the substrate directing Pb atoms to vacuum side [11]. The HOMO-derived feature was deconvoluted with two Voigt functions of 157 meV FWHM, as shown by thin blue curves. The FWHM's of the fitted functions were 50 and 140 meV for Gaussian and Lorentzian, respectively. The small component at -1.47 eV was attributed to the vibronic structure in the final state [3,4,11]. The structure should be composed of several vibrational modes [3] though detail was not reported. Higher vibronic structures and an additional component at right-hand side of the main HOMO peak reported in Ref. 11 were not involved in the present fitting. In the 2PPE result, three clear peaks appeared. The peak at -1.33 eV initial energy was in agreement with the 1PPE result, and was assigned to direct two-photon photoemission from the HOMO level. Note that the vibronic structure of the HOMO feature is only faintly visible in the 2PPE result. Because of the weak vibronic feature, it seems as if the HOMO-derived 2PPE peak was sharper than that of 1PPE. In reality, the width of the main HOMO peaks in 2PPE measured at 90 K (see Fig. 5- 2) was about 155 meV and there was no difference from the 1PPE result. The peaks at +2.87 and +3.52 eV intermediate energies were absent in the 1PPE result. These were due to the LUMO+2-derived unoccupied state and the IPS (n = 1) formed on the PbPc films, respectively [8].

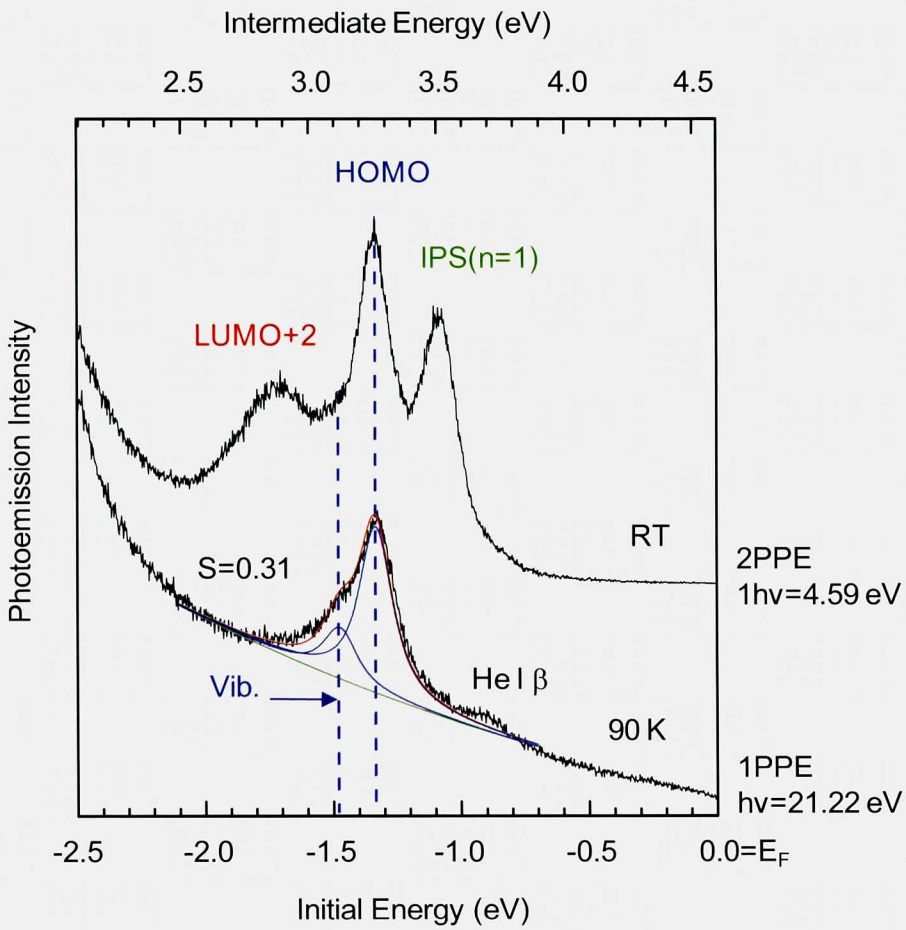

Fig. 5- 1. 1PPE (bottom) and 2PPE (top) spectra for the well annealed 1 ML PbPc film on HOPG. Sample temperatures were 90 K and room temperature for 1PPE and 2PPE, respectively. The temperature difference caused no significant effects. The upper horizontal axis, valid only for 2PPE, is the intermediate energy above E_F. The main HOMO peaks were at -1.33 eV for both spectra. The LUMO+2 and IPS (n=1) peaks were observed in the 2PPE result. The width of the LUMO+2 feature was about 0.25 eV. The HOMO feature of the 1PPE spectrum was deconvoluted into two vibronic components (blue curves) separated by 140 meV. The fitted curve was shown by red line. The peak width and the S value (see text) were 157 meV and 0.31, respectively. The vibronic structure of the 2PPE result is significantly weaker than that of 1PPE. The hump at -0.9 eV is due to the HOMO-1 (-2.78 eV) feature excited by He Iβ.

In order to see the origin of the weak vibronic structure, 2PPE spectra measured at 90 K with different photon energies were shown in Fig. 5- 2. The sample was prepared in another experimental run. Except for sharpening of spectral features at the low temperature, no significant temperature dependence of the vibronic structure was identified (see Appendix I). The peaks due to LUMO+2 and IPS shifted with the photon energy in the initial energy scale, while the peaks due to HOMO aligned at the fixed initial energy. The shifts of peak positions were accurately in accordance with the 2PPE processes: With the increase of the photon energy by $\Delta h\nu$, the occupied state feature shifts with $2\Delta h\nu$, and the unoccupied feature, with $1\Delta h\nu$ [8]. The details of these unoccupied features will be discussed in Chapter 6 and we here focus our attention on the HOMO feature. The HOMO peak and the LUMO+2 peak overlapped at the photon energy of 4.28 eV, where the pump photon was closely resonant with the energy separation between the HOMO- and LUMO+2-derived levels [8]. Disregarding (c) and (d), the HOMO peaks for (a), (b), (e), and (f) were accompanied by clear shoulders at -1.47 eV in a similar way as in the 1PPE result. The shoulder was seen at around half height of the main HOMO peak, indicating that the intensities of the vibronic structures in these 2PPE spectra were similar to that of 1PPE. On the other hand, the vibronic structure in (d) was weakly seen at the valley between the peaks due to HOMO and LUMO+2. The 2PPE results in (d) and Fig. 5- 1 indicates that the photon energy slightly above the resonance caused something in the photoemission process to decrease the vibronic structure.

As a quantitative analysis, the HOMO feature was deconvoluted into components of 0-0 and 0-1 vibrational transitions, as shown by smooth lines (blue) in Fig. 5- 2. The intensity ratio S of the components, defined as S=I(0-1)/I(0-0), was determined from the deconvolution. The spectrum (c) at the photon energy of 4.28 eV was not deconvoluted because of the heavy overlapping of the LUMO+2 and HOMO features. Except for (d), the S values were 0.34, 0.26, 0.27, and 0.34 for spectra (a), (b), (e) and (f), respectively. The error of the S value caused by the overlapping of the spectral features was less than ± 0.05. The S value of about 0.3 is very close to the value of 0.31 for the 1PPE result (see Fig. 5- 1) and 0.33 reported in Ref. 12. The similarity of the S value is reasonable because coherent two-photon excitation results in the same final state as 1PPE. Slightly smaller S values of 0.26 and 0.27 for (b) and (e) may have some meaning, but we cannot discuss them because of the limited certainty. In contrast to these cases, the S value at 4.65 eV photon energy (d) was 0.10, significantly

smaller than that of the 1PPE value or other 2PPE results. Decrease of the S value was always found at photon energies slightly higher (< 0.4 eV) than the resonance.

The enhancement of the HOMO peak at the resonance is seen by traces (a) to (c) in Fig. 5-2. The HOMO peak enhancement and the appearance of the LUMO+2 peak indicate the formation of the real intermediate state at the photon energies higher than 4.28 eV. The molecule in the LUMO+2-related intermediate state should be in several vibrational states of different vibrational modes. As schematically shown in Fig. 5- 3, when nuclei in the molecule move along relevant normal coordinates before suffering any relaxation process, the second photon leads to the HOMO peak of modified vibrational distribution. The vibrational potential curves in Fig. 5- 3 were drawn by considering the electronic structure of a free molecule. Molecular structure of the excited state in which the bonding electron in HOMO is excited to antibonding LUMO+2 is rather similar to that of the molecular cation in which the bonding HOMO electron is removed. The equilibrium distance of the ground state molecule is shorter than those of the excited state and the cation. The smaller S value, that is, smaller vibrational excitation by photoemission corresponds to elongation of the bond lengths in the intermediate state associated with LUMO+2. Assuming the molecular vibrational energy in the intermediate state to be 140 meV similar to the ionic state, the time of the molecular vibration cycle is estimated to be about 30 fs. The time for the nuclear motion in the state should be a fraction of the vibrational cycle, that is, a few fs. The width of the LUMO+2 feature in Fig. 5-1 was about 0.25 eV. The width indicates that the lifetime of the intermediate state produced by 4.59 (Fig. 5- 1) and 4.65 (Fig. 5- 2(d)) eV photon is longer than a few fs (see Appendix II). The lifetime is sufficient for the nuclear motion. The energy window of 0.4 eV for the small S value may be related to the sum of the widths of the occupied and unoccupied levels. The photon energies are within tail part of the resonance.

Even at photon energies far above the resonance ((e) and (f)), the LUMO+2-derived intermediate state was populated through some relaxation process. The off-resonantly populated intermediate state does not affect the vibronic structure. This is deduced from the width of the LUMO+2 feature. The width of the LUMO+2 feature increased as the photon energy exceeded the resonance, and became about 0.4 eV at photon energy of 4.77 eV. The main origin of the broadening is tentatively considered to be related with the hole scattering effect in the intermediate state [13] rather than a final state effect because the change of the

final state energy in the photon energy range is small (4.77-4.59 = 0.18 eV). The broadened LUMO+2 feature suggests that the lifetime of the intermediate state is less than few fs. Then nuclei cannot move within the lifetime.

At photon energy below the resonance, the LUMO+2 feature was not observed. Considering the widths of the relevant energy levels and the dephasing processes discussed in 2PPE process [14,15], it seems the feature should appear even at photon energies below the resonance. This is in contradiction to the observation. The 2PPE intensity variation around the resonant photon energy is the unresolved question [16]. Anyway, the intermediate state was not excited at the low photon energy. Thus the S values for (a) and (b) are similar to that of 1PPE. Time-resolved pump-probe experiment was performed by compressing the UV laser pulse width to 60 fs. The lifetimes of the HOMO- and the LUMO+2-peaks were shorter than our time-resolution of 30 fs, in consistency with the very rapid process discussed above. The short report for the result is shown in Appendix III. In order to consider a contribution of higher order processes, we measured 2PPE spectra at 4.59 eV photon energy by changing the laser power from 3 to 16 mW which summarized in Appendix IV. No significant change of the S value was detected.

At the photon energy of 4.8 eV, the intermediate state from the HOMO level becomes close to the resonance with IPS [8]. It is interesting that the S value at 4.77 eV photon energy was not affected by the resonance. The molecular vibration may not couple with the 2-dimentional free electron orbital of IPS. This may be reasonable for in-plane molecular vibrations, but it is speculative that out-of-plane vibrations and molecule-substrate vibrations may couple with the IPS orbital. Rather drastic change of the electronic structure by the molecule-substrate distance is known for several organic films [17]. Analysis of vibronic structure around the resonance with IPS may be informative for such systems.

Though wave packet motions in electronic excited states have been extensively studied in gas and liquid phases [18,19], such motions are difficult to be detected for adsorbed molecules because lifetimes of electronic excited states are typically shorter than vibrational cycle. The motion of adsorbed atom along a repulsive potential of an excited state was observed in photodesorption of Cs from Cu(111), and coherent control of the photodesorption was demonstrated [5,20]. Similarly, vibronic structure in 2PPE spectroscopy will be fruitful to know very fast dynamics within few fs occurring at interfaces between organic molecule and

inorganic substrate.

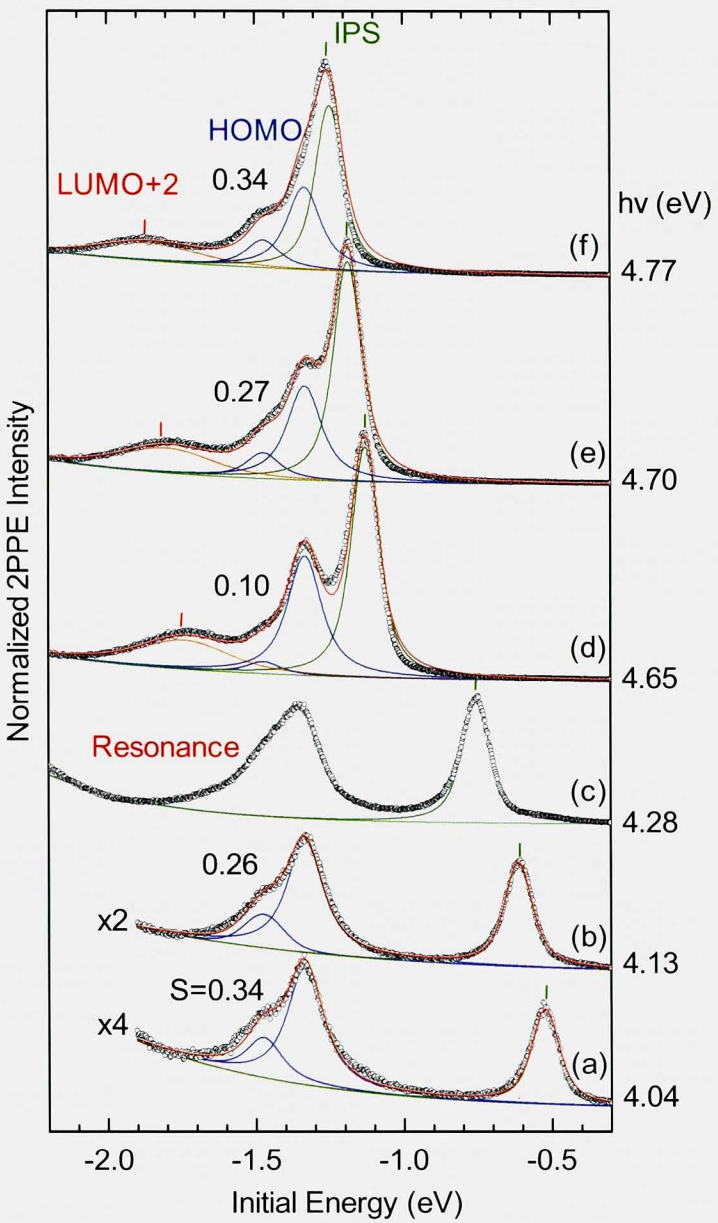

Fig. 5- 2. 2PPE spectra (open circles) for the 1 ML PbPc film measured with photon energies below and above the HOMO-LUMO+2 resonance were plotted on the initial energy scale. The photon energies were shown on the right-hand side. The lower two spectra were expanded by the indicated factors. The spectra were deconvoluted with Voigt functions for IPS peak (green), HOMO peak with the vibronic structure (blue), and the LUMO+2 peak (orange). The red lines overlapped with the experimental points were the fitted curves. The spectrum (c) was not deconvoluted. The S values were shown at the left side of the HOMO peaks. The S value for (d) was significantly smaller than those for other spectra.

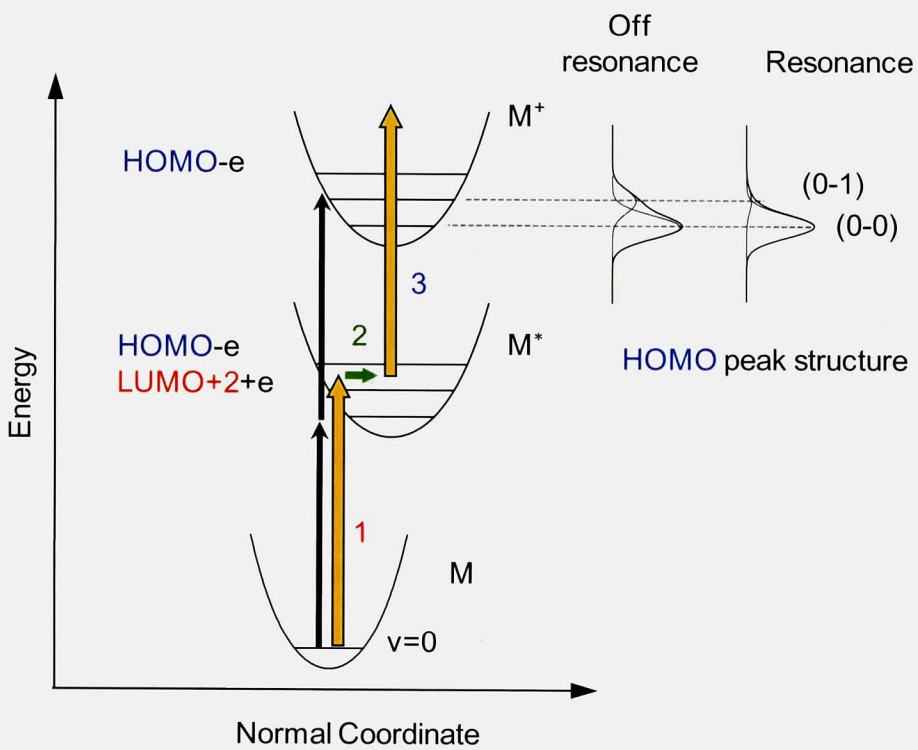

Fig. 5- 3. Vibrational potential curves against a normal mode coordinate are schematically shown. The curves for the ground, neutral excited, and ionic states are denoted by M, M^*, and M^+, respectively. At off-resonant condition (black arrows), the vibrational distribution of the ion is mainly determined by the Franck-Condon factor between M and M^+. At photon energy just above the resonance (open orange arrow 1), the M^* molecules should be in several vibrational states of different vibrational modes. When neclei move (horizontal green arrow 2) along the normal coordinate before suffering any relaxation processes, the second photon (open orange arrow 3) leads to M^+ of a modified vibrational distribution. The change of the S value is a result of the nuclear motion in M^*. The right-hand curves schematically show the HOMO features at off- and on-resonant conditions.

References

[1] J.-L. Brédas, D. Biljonne, V. Coropceanu, and J. Cornil, Chem. Rev. **104**, 4971 (2004).

[2] V. Coropceanu, J. Cornil, D. A. da S. Filho, Y. Olivier, R. Silbey, and J.-L.Brédas, Chem. Rev. **107**, 926 (2007).

[3] S. Kera, H. Yamane, and N. Ueno, Prog. Surf. Sci. **84**, 135 (2009).

[4] N. Ueno and S. Kera, Prog. Surf. Sci. **83**, 490 (2008).

[5] H. Petek and S. Ogawa, Annu. Rev. Phys. Chem. **53**, 507 (2002).

[6] Ph. Avoulis and J. E. Demuth, J. Chem. Phys. **75**, 4783 (1981).

[7] T. Munakata, T. Sakashita, M. Tsukakoshi, and J. Nakamura, Chem. Phys. Let. **271**, 377 (1997).

[8] I. Yamamoto, M. Mikamori, R. Yamamoto, T. Yamada, K. Miyakubo, N. Ueno, and T. Munakata, Phys. Rev. B **77**, 115404 (2008).

[9] T. Munakata, M. Shibuta, M. Mikamori, T. Yamada, K. Miyakubo, T. Sugiyama, and Y. Sonoda, Proc. SPIE **6325**, 63250M (2006).

[10] I. Yamamoto, N. Matsuura, M. Mikamori, R. Yamamoto, T. Yamada, K. Miyakubo, N. Ueno, and T. Munakata, Surf. Sci. **602**, 2232 (2008).

[11] S. Kera, H. Fukagawa, T. Kataoka, S. Hosoumi, H. Yamane, and N. Ueno, Phys. Rev. B **75**, 121305(R) (2007).

[12] N. Ueno, S. Kera, K. Sakamoto, K. K. Okudaira, Appl. Phys. A **92**, 495 (2008).

[13] M. Sakaue, T. Munakata, H. Kasai, and A. Okiji, Phys. Rev. B **68**, 205421 (2003)

[14] W. Wallauer and Th. Fauster, Surf. Sci. **374**, 44 (1997).

[15] H. Ueba and B. Gumhalter, Prog. Surf. Sci. **82**, 193 (2007)

[16] M. Kutschera, M. Weinelt, M. Rohlfing, and Th. Fauster, Appl. Phys. A **88**, 519 (2007).

[17] L. Kilian, A. Hauschild, R. Temirov. S. Soubatch, A. Schöll, A. Bendounan, F. Reinert, T.-L. Lee, F. S. Tautz, M. Sokolowski, and E. Umbach, Phys. Rev. Lett. **100**, 136103 (2008).

[18] E. Schreiber, *Femtoscond real-time spectroscopy of small molecules and clusters* (Springer, Berlin, 1998).

[19] S. Takeuchi, S. Ruhman, T. Tsuneda, M. Chiba, T. Taketsugu, and T. Tahara, Science **322**, 1073 (2008).

[20] H. Petek, H. Nagano, M. J. Weida, and S. Ogawa, J. Phys. Chem. B **105**, 6767 (2001).

6. Resonant effects on 2PPE spectroscopy: Line widths and intensities of occupied and unoccupied features for PbPc films on graphite.

6. 1. Introduction

The electronic structure and the exited electron dynamics in the vicinity of the E_F at interfaces between organic thin films and inorganic substrates are the key issues to understand the functionalities of organic films. Though occupied energy levels have been extensively studied by both experimental and theoretical works [1,2], investigation for unoccupied levels are still challenging [3,4]. 2PPE spectroscopy based on ultrafast laser pulses is a promising method to probe the unoccupied levels and electron dynamics in the levels [3-6]. In 2PPE, a first light pulse excites electron from an occupied level to an unoccupied level. The excited electron is probed by photoemission with the second pulse (denoted as 1ω process). In one-color 2PPE experiment, the final energy of photoelectron E_K from 1ω process is written as

$$E_K = h\nu + E_m, \qquad (6.1)$$

where $h\nu$ is the photon energy and E_m (> 0) is the energy of the unoccupied level with respect to E_F. The two-step process competes with the coherent two-photon process (denoted as 2ω process) which results in the photoelectron of

$$E_K = 2h\nu + E_i, \qquad (6.2)$$

where E_i (< 0) is the initial energy of the occupied level. One of the key advantages of 2PPE spectroscopy is the competition of the two processes. From the 1ω and 2ω peaks we can know the occupied and unoccupied levels at the same time. With photon energy of E_m - E_i, 2PPE signal is resonantly enhanced. Optical transition probability between the levels is also important to understand the character of the electron wave functions. The photon energy dependence of the 2PPE signals due to 1ω and 2ω processes around the resonance has been studied by several theoretical works [7-11]. The theoretical results were carefully compared with experiments for the resonance between the occupied Shockley state and the first IPS of

Cu(111) surface [5,7,12]. On the other hand, experiments for different surfaces showed resonance behaviors deviated from the theories [13-15]. Understanding of the resonance behavior is essentially important to know the physical meaning of the unoccupied level detected by 2PPE experiment. The issue is especially serious for organic films in which addition or removal of electron in/from a molecular orbital causes significant change of the energy levels.

Here, we extended our former works on 2PPE of PbPc films formed on a substrate of HOPG [16-17]. We have resolved occupied levels due to HOMO and the next HOMO (HOMO-1. Also clearly resolved were the molecule-derived unoccupied levels (denoted as LUMO, LUMO+1, LUMO+2 in the order of energy) and the first IPS's on HOPG and on the PbPc films. Moreover, resonance between HOMO and LUMO+2, as well as that between HOMO and the IPS were observed at $h\nu$ = 4.3 eV and 4.8 eV, respectively [16]. The system which involves two resonant excitations is a highly suitable example for detailed analysis of the resonances in 2PPE. We have measured 2PPE spectra for 1 ML films of PbPc on HOPG with improved signal-to-noise ratio. By analyzing the photon energy dependence of the line shapes and the intensities, excitation processes in 2PPE spectroscopy were revealed.

6. 2. Experimental

In our former 2PPE work for PbPc films, we employed a microspot method in which laser radiation was focused on the sample to the spot of 0.6 μm diameter [16]. The microspot method was effective to selectively observe laterally homogeneous surface areas, while the number of photoelectrons from the small probe areas was limited to suppress the space charge effect [18]. In this work, the laser light was focused with a concave mirror of 35 cm focal length onto the sample surface in an UHV chamber at the incident angle of 60°. With the large light spot size of about 80 μm diameter, larger number of photoelectrons were emitted while keeping the density of the photoelectron low sufficient to avoid the space charge effect. In cost of the spatial resolution, signal to noise ratio of 2PPE spectrum was fairly higher than the microspot configuration [17]. We disregarded the lateral inhomogeneity of the films in this work because we have found in our former works that highly uniform 1 ML films were made

by a suitable annealing process [16,19]. Note that formation of the uniform films was achieved only for 1 ML coverage, and was not for sub-ML films. Annealed sub-ML films seemed to be homogeneous when the surface image was measured with photoemission from the HOMO band [19], but they were not homogeneous when the unoccupied levels were measured with the microspot-2PPE. The inhomogeneity of unoccupied levels will be discussed elsewhere. The light source of the 2PPE experiments was the *p*-polarized third harmonics (4.04 eV~4.77 eV) of a tunable titanium sapphire laser. Repetition rate and pulse width of the third harmonics were 80 MHz and 100 fs, respectively. The power of the incident light was controlled to be less than 0.19 nJ/pulse. Photoelectrons emitted to the surface normal were detected with a hemispherical energy analyzer (VG-CLAM4 with nine channeltrons detector) of 20 meV resolution. The analyzer was modified to limit the electron acceptance angle to be ± 1°.

HOPG was cleaved in air and heated in UHV at 673 K for more than 50 h. Cleanliness of HOPG was confirmed by the work function (4.45 eV) and the width of the $n = 1$ IPS feature. The IPS peak was narrower than 140 meV [16]. Purified PbPc was deposited by sublimation on the HOPG surface in an UHV preparation chamber with a rate of 0.05 nm/min as monitored by a quartz microbalance. The deposition and annealing conditions were similar to those in the former works [16,19]. The coverage was determined from the work function change. The well ordered 1 ML films were formed by annealing the deposited films of 0.4 nm thickness at 373 K for 1 h. The work function was 4.27 eV for the 1 ML film. The decease of the work function was due to the uniform dipole layer at the interface [20].

6. 3. Results

6. 3. 1. General spectral features for 1 ML films

The 2PPE spectrum for the 1 ML film measured at $h\nu$= 4.65 eV was compared with a 1PPE spectrum in Fig. 6- 1. The sample was at RT. The 1PPE spectrum [16], measured by the microspot configuration with $h\nu$= 8.86 eV, reproduced photoemission spectra with He-I resonance line [17,20] except for slight broadening due to the space charge effect. Molecules in the annealed 1 ML films were lying flat on the substrate directing Pb atoms to vacuum side [20] (see Fig. 4- 1). In the 2PPE spectrum, the peaks due to the first (n = 1) IPS on the films, the HOMO derived occupied level, and the LUMO+2 derived unoccupied level were clearly observed. The HOMO derived peak was at -1.33 eV for both 2PPE and 1PPE spectra. The vibronic structure appeared as a shoulder at -1.47 eV in the 1PPE trace, while it was very weak in the 2PPE result. The weak vibronic structure is due to the nuclear motion in the electronic excited state associated with the LUMO+2 level [17], as discussed in Chapter 5. The HOMO-1 derived peak appeared at -2.78 eV for both spectra, but the spectral shapes were largely different. The peak was sharp and enhanced in 2PPE when compared with the broad shoulder in 1PPE. The broad 1PPE feature reproduced that of Ref. 20 measured with $h\nu$ = 21.2 eV.

The 2PPE spectra measured at different photon energies for the film of 90 K were shown in Fig. 6- 2. The peaks were assigned previously as indicated [16] in Chapter 4. According to a DFT calculation (B3LYP with LANL2DZ basis set) for a free molecule (see Fig. 4- 5), HOMO-1 is mainly composed of orbitals of Pb atom, and other occupied and unoccupied orbitals, HOMO, LUMO, LUMO+1, and LUMO+2, are composed of π-orbitals of phthalocyanine ring. The LUMO and LUMO+1 levels are degenerated in a free molecule. The degeneracy was lifted by the adsorption [16]. The split levels appeared as two features at 0.71 and 0.88 eV, labeled by L0 and L1, respectively.

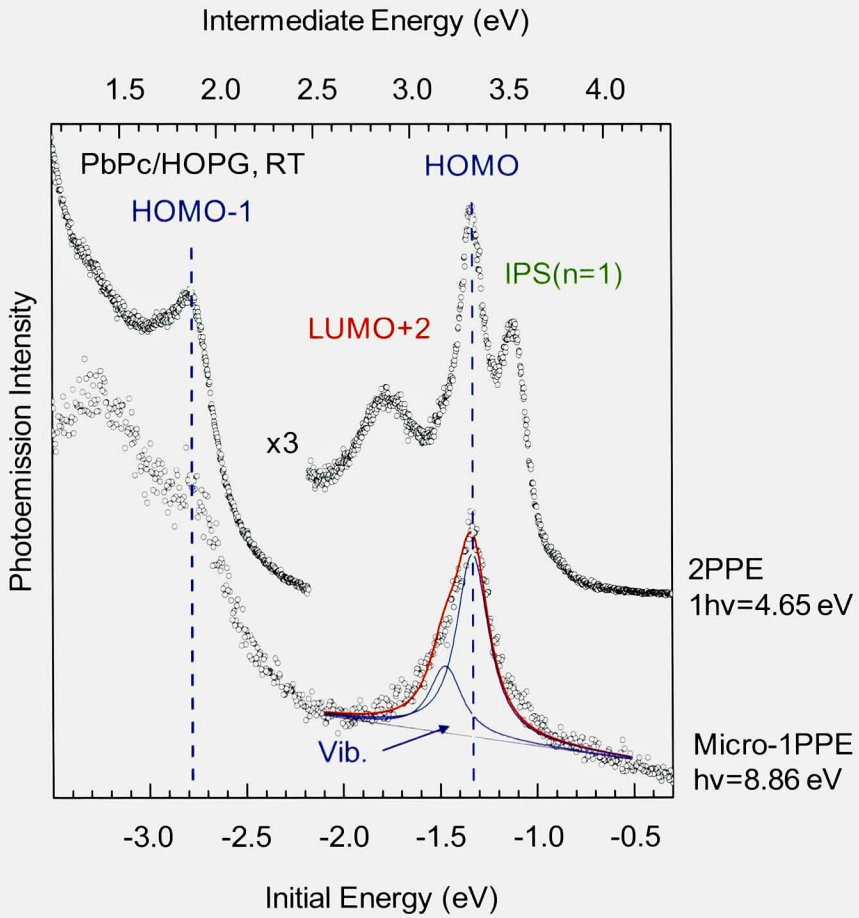

Fig. 6- 1. Micro-1PPE (bottom) and 2PPE (top) spectra for the well annealed 1 ML PbPc film on HOPG. The photon energies were shown at right hand side. The upper horizontal axis was the intermediate energy (final energy-1*hv*) for 2PPE. The 2PPE trace in the right-hand was magnified by a factor of 3 to that in the left-hand side. Peaks due to IPS and molecule-derived levels (HOMO, LUMO+2 and HOMO-1) were clearly resolved. The main HOMO peaks were at -1.33 eV initial energy for both spectra. The vibronic structure of the HOMO feature shown by deconvoluted thin curves of the 1PPE spectrum was very weak in the 2PPE as discussed in Ref. 17. The HOMO-1 feature appeared as a sharp peak in the 2PPE spectrum, while that in the 1PPE spectrum was a broad shoulder.

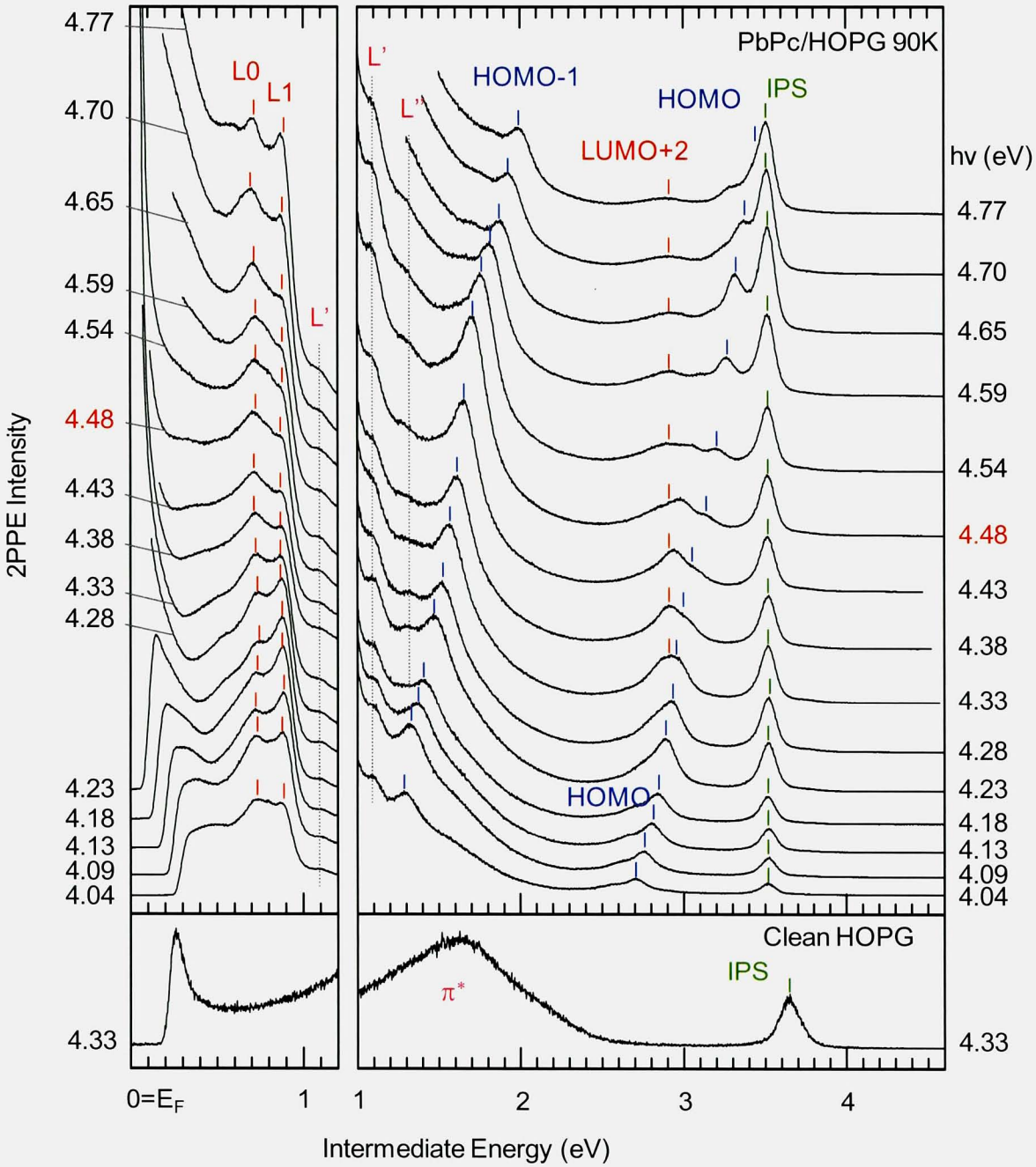

Fig. 6- 2. Photon energy dependence of 2PPE spectra for 1 ML PbPc/HOPG measured at 90 K. The photon energies were shown at both left and right hand sides of the spectra. The bottom spectrum was for the clean HOPG measured at RT. The horizontal axis was the intermediate energy. The HOMO-1 peak was enhanced at 1.7 eV intermediate energy. In addition to the peaks appeared in Fig.6- 1, the LUMO and LUMO+1 derived levels appeared as split features, labeled L0 and L1 at energy region lower than 1 eV. The intensity ratio between L0 and L1 changed as the change of the photon energy. Weak features labeled as L' and L'' were left unassigned.

6. 3. 2. The HOMO-1 peak

The HOMO-1 peak in Fig. 6- 2 was sharply enhanced at $h\nu$= 4.48 eV. From the initial energy of the HOMO-1 peak of -2.78 eV, the intermediate energy for the enhancement was 1.70 (= 4.48 - 2.78) eV. In order to confirm the enhancement of the HOMO-1 feature, expanded spectra measured at RT were shown in Fig. 6- 3. The HOMO-1 peak became sharp and enhanced at photon energy of 4.48 eV, reproducing Fig. 6- 2. By comparing Figs. 6- 2 and 6- 3, we identified no significant temperature dependence for the HOMO-1 enhancement. The enhancement is discussed in 6. 4. 1.

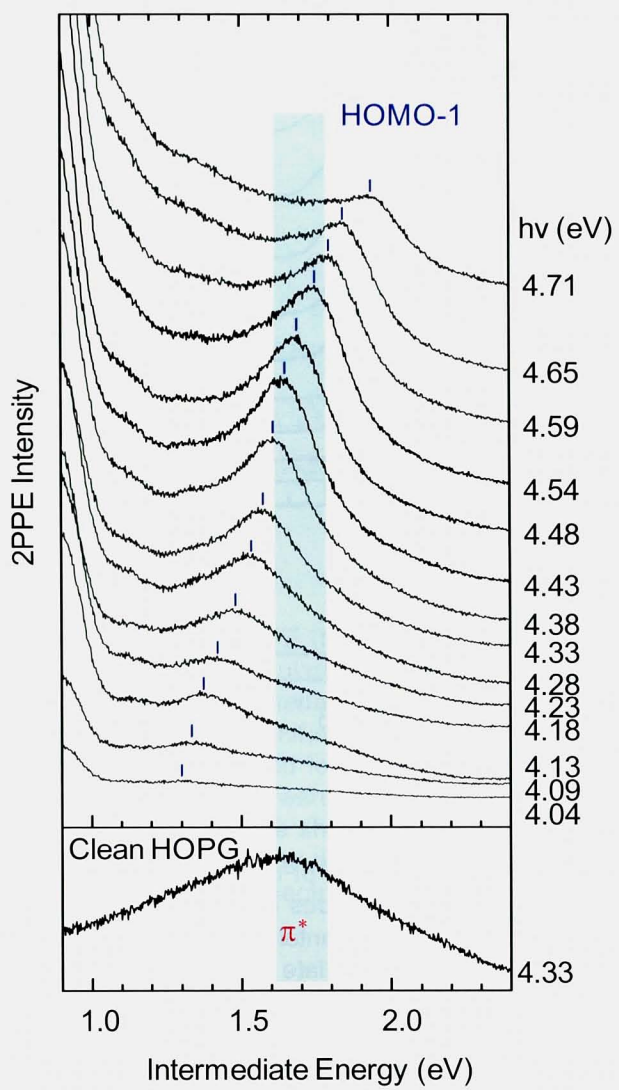

Fig. 6- 3. Close up of the HOMO-1 derived peak measured at RT. The photon energies were indicated at right-hand side. The bottom trace was the 2PPE spectrum for the clean HOPG substrate. The broad peak for HOPG at 1.7 eV intermediate energy, marked by a vertical bar, was due to the unoccupied π^*-band of graphite. The enhancement of the HOMO-1 peak at 1.7 eV intermediate energy is due the resonance with the π^*-band . Note that the π^*-band was not visible for the PbPc film.

6. 3. 3. The LUMO+2, HOMO and IPS peaks

The LUMO+2, HOMO, and IPS features appeared at the energy region above 2.5 eV as can be seen in Fig. 6- 2. The photon energy dependence of their intensities and widths were rather complicated. The HOMO derived peak became stronger as the photon energy increased from 4.04 eV to 4.23 eV. At $h\nu$= 4.23 eV, the peak was sharp and intense: The enhancement is due to the resonance between the HOMO and LUMO+2 derived levels [16]. At $h\nu$> 4.33 eV, the HOMO and LUMO+2 peaks split. The peak was mainly composed of the LUMO+2 component, and the HOMO component was resolved as a weak shoulder at $h\nu$ = 4.38 and 4.43 eV. The intensity of the HOMO peak was switched to that of the LUMO+2 peak when the photon energy became higher than the resonance energy. These intensity changes are clearly seen in Fig. 6- 4 where selected spectra were shown in an expanded scale. The HOMO peak became strong again at $h\nu$> 4.48 eV. The intensity increase was due to the resonance between the HOMO derived level and IPS [16]. The LUMO+2 peak was not observed at photon energies lower than 4.18 eV. The peak became prominent at the HOMO-LUMO+2 resonance and gradually became weaker as the photon energy increased. The width of the LUMO+2 peak became wider with increasing photon energy (see Fig. 6- 4). In contrast to these molecule-derived peaks, the IPS peak appeared for all spectra and became stronger with increasing photon energy. The IPS peak nearly merged with the HOMO peak at $h\nu$= 4.77 eV (the HOMO-IPS resonance). The width of the IPS peak was almost constant throughout the photon energy region.

For a quantitative analysis, the 2PPE spectra were fitted with four Voigt functions and some characteristic results were shown in Fig. 6- 4. The fitting was made as follows: The initial energies for the HOMO peak and its vibronic structure were fixed to -1.33 and -1.47 eV, respectively. The intermediate energies for the LUMO+2 and IPS peaks were also fixed to +2.91 and +3.52 eV, respectively. Thus the energy for the HOMO-LUMO+2 resonance was 4.24 eV, and that for the HOMO-IPS resonance, 4.85 eV. In order to reduce the number of adjustable parameters, the Lorentzian and Gaussian widths, W_L and W_G, of the IPS peak were fixed to 80 and 60 meV, respectively. The width parameters of the LUMO+2 peak were adjustable with equal W_L and W_G. The main HOMO peak was fitted with a fixed W_G value of 60 meV and adjustable W_L. The width parameters for the vibronic structure were set to be the

same as those of the main HOMO peak. The fixed width parameters for the IPS and HOMO peaks were determined from the spectrum at $h\nu = 4.13$ eV. Fitting results for all spectra are shown in Appendix V.

The areas and full widths at half maxima (FWHMs) of the peaks were plotted against the photon energy in Fig. 6- 5. At $h\nu = 4.28$ and 4.33 eV, the HOMO and LUMO+2 peaks were too heavily overlapped for the fitting, and the intensity and the width of the HOMO peak were not determined. The intensities at $h\nu > 4.7$ eV were not very reliable because the photon energy was close to the limit of the tuning range of our laser. The variation of the intensities and the widths are discussed in 6. 4. 2.

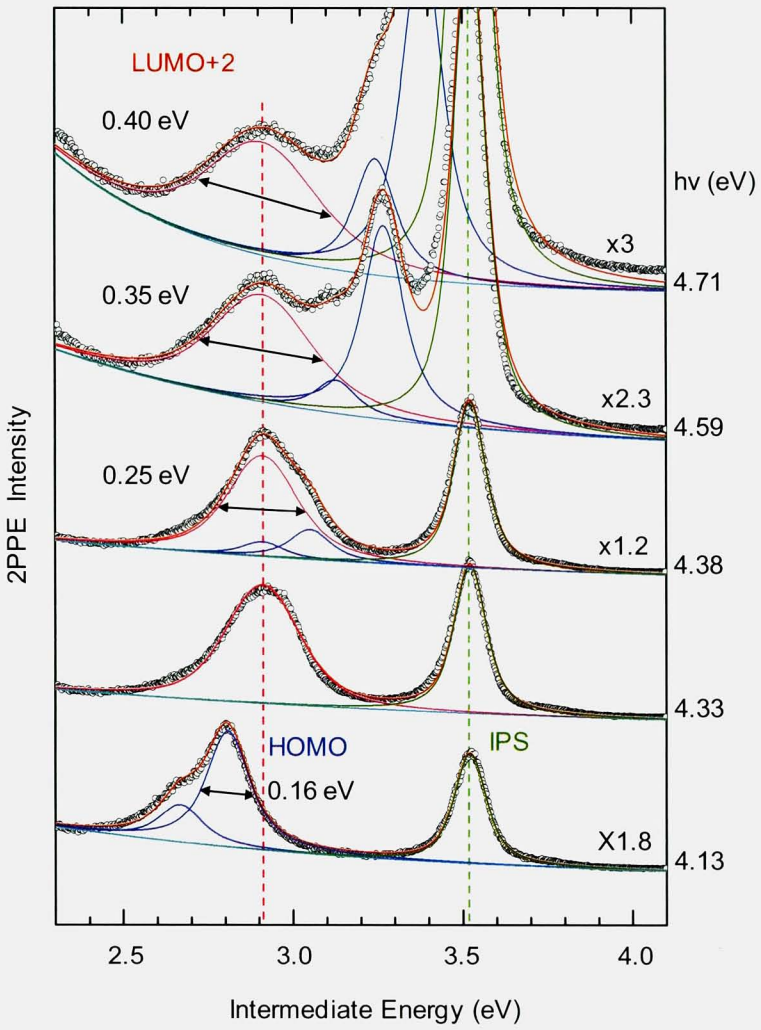

Fig. 6- 4. 2PPE spectra were fitted with Voigt functions for the IPS (green), HOMO (blue), and LUMO+2 (pink) features. The photon energies were shown at the right-hand side. The magnification factors relative to the spectrum at $h\nu$ = 4.33 eV were indicated. At $h\nu$ = 4.13 eV, the width of the HOMO peak was 0.16 eV, and the LUMO+2 peak was not observed. The HOMO peak was much weaker than the LUMO+2 peak at $h\nu$ = 4.38 eV. The LUMO+2 peak became broader as the photon energy increased above the resonance at 4.24 eV. The widths were shown at left-hand sides of the LUMO+2 peaks.

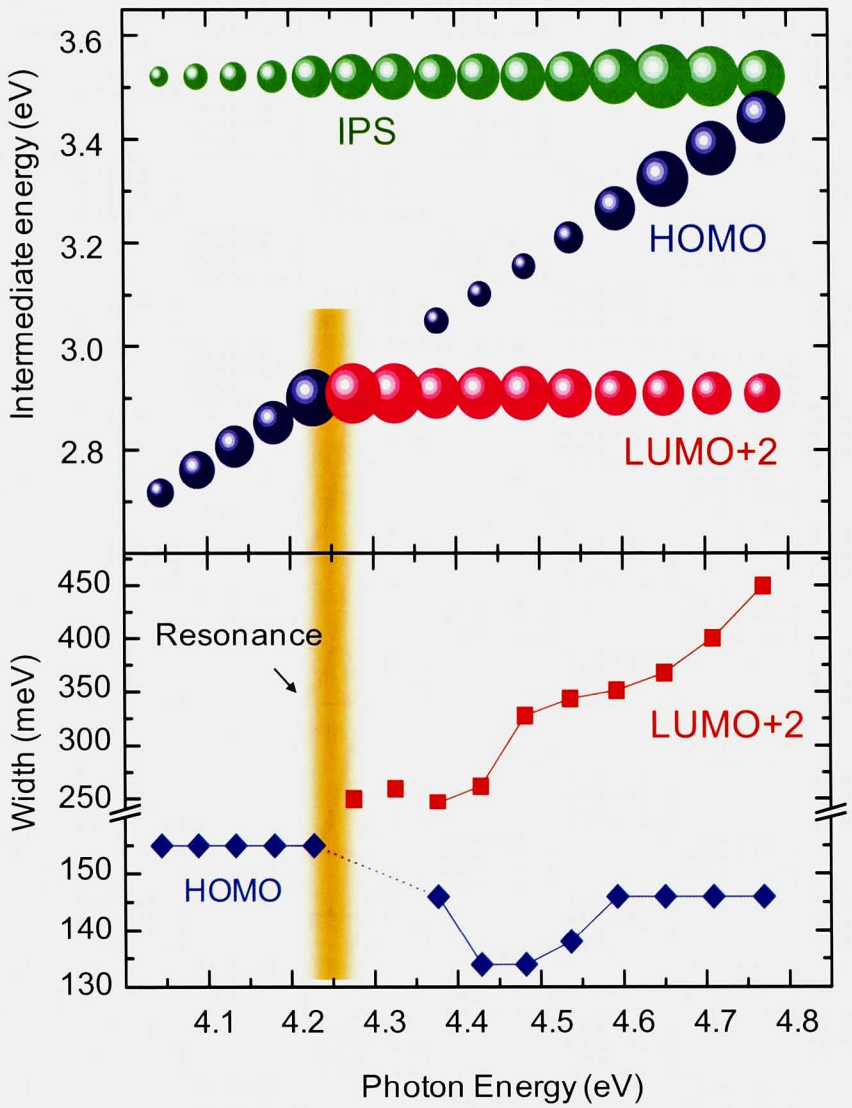

Fig. 6- 5. Fitted results for the spectra in Fig. 6- 2. (top) The intensities of the HOMO, LUMO+2, and IPS peaks were represented against the photon energy by the areas of the blue, pink, and green circles, respectively. (bottom) The widths of the HOMO and LUMO+2 peaks were shown by blue diamonds and red squares, respectively. For $h\nu$ = 4.28 and 4.33 eV, the width and intensity of the HOMO peaks were not determined. The width of the HOMO peak became narrower within a photon energy range up to 0.4 eV above the resonance. The LUMO+2 peak became broader as the photon energy increased. The HOMO-LUMO+2 resonance was marked by a vertical bar.

6. 3. 4. The L0 and L1 features

The intensity ratio between L0 and L1 changed by increasing the photon energy (see Fig. 6- 2). At $h\nu$= 4.04 eV, both features were weak and the L0 component was slightly higher than the L1 component. The features became intense as the photon energy increased. The intensity of L1 exceeded L0 at $h\nu$= 4.18~4.28 eV. The L0 feature became higher again at $h\nu$ > 4.33 eV. At $h\nu$ > 4.65 eV, the further enhanced peaks showed slightly changed spectral shapes. The $h\nu$ dependent change is discussed in 6. 4. 4. The weak peaks at 1.10 and 1.32 eV in Fig. 6- 2, labeled by L' and L", respectively, were not resolved in Ref. 16. The unoccupied levels for the L' and L" peaks should be another split components of the LUMO and LUMO+1, but were left unassigned here.

6. 4. Discussions

6. 4. 1. The HOMO-1 derived peak

The sharp HOMO-1 feature in the 2PPE spectra was in clear contrast to the shoulder-like feature in the 1PPE result. This indicates that the intrinsic width of the HOMO-1 level is not so broad as suggested by the 1PPE result. The enhancement of the HOMO-1 derived structure at the intermediate energy of 1.7 eV should be a resonance with an unoccupied level at the energy. In order to clarify the origin of the unoccupied level, the 2PPE spectrum for clean HOPG substrate measured at $h\nu = 4.33$ eV was shown at the bottoms of Figs. 6- 2 and 6- 3 (see also in Fig. 3- 16). The broad structure at the intermediate energy of 1.7 eV in the clean HOPG spectrum was attributed to the unoccupied π^*-band of graphite [21]. The π^*-structure was also observed in the inverse photoemission spectroscopy [22-24]. Because the π^*-derived peak coincided with the energy for the HOMO-1 enhancement, we attribute the enhancement to the resonance between the HOMO-1 level and the unoccupied π^*-band of graphite.

Before concluding the assignment, we mention the band structure of graphite [21,25]. We measured photoelectrons emitted normal to the surface, that is, we probed the Γ-point of the surface Brillouin zone. The energy region between 0 and 4 eV above E_F at the Γ-point of bulk graphite is in the band gap and there is no unoccupied band. The π^*-band in the energy region between 1 and 2 eV is located at the momentum region from M, K to H points [21-25]. It seems as if no projected unoccupied band could be the intermediate state for the 2PPE process. In this respect, real intermediate states within the projected band gap were known in the 2PPE works for Cu(111) [26-28]. Petek discussed the role of phonon assisted process as the origin of the real unoccupied states within the band gap [26] (see Appendix VI). In order to compare our HOPG result with the Cu(111) case, temperature dependence of 2PPE spectra was measured as shown in Fig. 6- 6(a). The intensity of the π^*-band for clean HOPG decreased by decreasing the temperature, suggesting that the π^*-band for clean HOPG was related with thermal phonon. Similarly to Cu(111), the broad π^* peak at 1.7 eV for clean HOPG should arise from the phonon-coupled states which is essentially the momentum integrated density of state of the unoccupied π^* band.

Another interesting feature of the π^* peak is that the π^* feature of the substrate became

almost invisible for the 1 ML covered surface. The electron mean free path of the low energy photoelectrons is fairly larger than the thickness of the films. The disappearance of the π^* peak cannot be attributed to the attenuation of the photoelectrons by the films. In contrast to the clean HOPG in Fig. 6- 6(a), the intensity of the HOMO-1 peak was insensitive to the temperature as shown in Fig. 6- 6(b), suggesting that the thermal phonon was not contributing to the intensity of the HOMO-1 peak. The surface phonon of graphite should be largely disturbed by adsorbed PbPc, and the phonon-assisted process inducing the π^* peak for the clean surface became less effective. Then the π^* peak disappeared for the PbPc covered surface. In place of the phonon coupled process, we consider that electron scattering by PbPc molecules is responsible for the resonant excitation from HOMO-1 to the π^*-band. The electron scattering should be effective in 2PPE when the electronic transition is coupled with the molecule. Thus the HOMO-1 peak was resonantly enhanced by the unoccupied π^*-band. The HOMO-1 peak was observed throughout the photon energy region of Figs. 6- 2 and 6- 3. The variation of the peak height with the photon energy reflects the density of state of the π^*-band.

As can be seen in Fig. 6- 6(a), the intensity of the IPS peak for HOPG decreased at low temperature, suggesting that the IPS peak for bare HOPG arose by an indirect transition from occupied states at high momentum regions. The indirect transition became effective by phonon assisted momentum conservation. On the other hand, the IPS peak for the PbPc film was rather insensitive to the temperature. The IPS on the film is related with a molecule-derived unoccupied level as is discussed in 6. 4. 2.

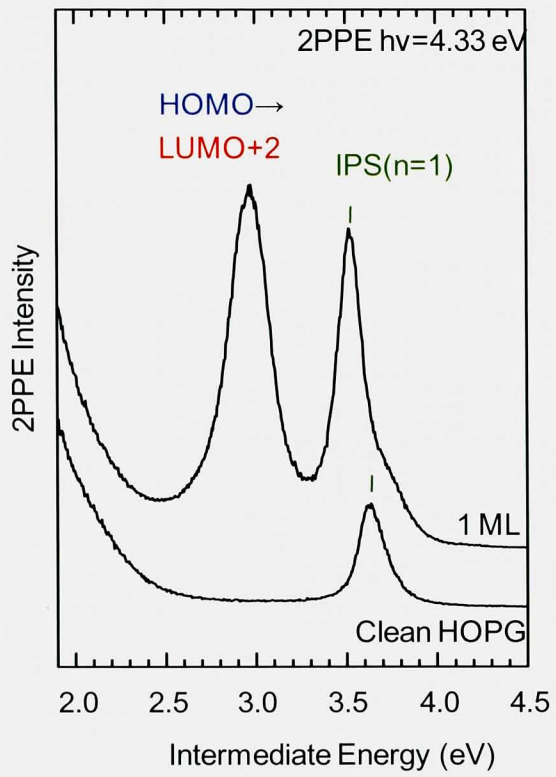

Fig. 6- 6. Close up of 2PPE spectra for clean HOPG (bottom) and the 1 ML PbPc/HOPG (top) measured at 4.33 eV photon energy. The IPS peak for the film was significantly higher than that for the clean HOPG. The enhancement indicates that the IPS was mixed with an unoccupied level of the PbPc film.

6. 4. 2. The HOMO, LUMO+2 and IPS peaks

The intensity of the IPS peak monotonically increased as the photon energy became closer to the HOMO-IPS resonance. The intensity increase indicates that electrons in the IPS were excited from both the HOMO level and the bulk band of graphite. It is interesting that the intensity of the IPS feature for the 1 ML PbPc film was higher than that for the clean HOPG as shown in Fig. 6- 7. The binding energies from the vacuum level were 0.85 eV for the clean HOPG and 0.73 eV for the PbPc films, respectively. The increase of the intensity is in contradiction to the frequently used model of dielectric isolation layer [29-32]. When the film acts as the dielectric layer, the wave function of the IPS penetrates into the substrate by less extent and the intensity of the IPS peak becomes weaker than that for clean surface. On the other hand, the increase of the intensity of the IPS peak indicates that the PbPc film is not the simple isolation layer. As an origin of the enhancement, we consider a hybridization of the

IPS with a molecule-derived unoccupied level. Our DFT calculation [16] for a free molecule showed that higher lying levels such as LUMO+3 or 4 located close to the IPS (see Fig. 4- 4). By mixing of the molecule-derived unoccupied level with IPS, the IPS wave function is not dumped, but becomes large within the film. Then the penetration of the IPS wave function into the substrate is enhanced, and the IPS peak became stronger. The mixing also caused the HOMO-IPS resonance by the intra-molecular transition.

It is interesting that the LUMO+2 feature was observed only at photon energies higher than the HOMO-LUMO+2 resonance at 4.24 eV. The width of the HOMO level was 0.16 eV at photon energy below the resonance and that of the LUMO+2 peak was about 0.25 eV at $h\nu$= 4.38 eV (see Figs. 6- 4 and 6- 5). Simply considering that the intensity variation of the unoccupied peak around the resonance is determined by convolution of the density of states for relevant occupied and unoccupied levels, the LUMO+2 peak is expected to get intensity at the photon energy region higher than 4.04 (= 4.24-(0.16+0.25)/2) eV. But no trace of the LUMO+2 peak was observed at the photon energy region from 4.04 to 4.18 eV. On the other hand, the intensity of the HOMO peak increased as $h\nu$ increased from 4.04 eV to 4.13 eV, reflecting the resonance. As can be seen in Figs. 6- 4 and 6- 5, the HOMO peak suddenly lost intensity as the photon energy exceeded the resonance, and the LUMO+2 contribution suddenly rose up at $h\nu$= 4.23 eV. The intensity switching between the HOMO and LUMO+2 peaks is strange in the view of the simple resonance.

According to 2PPE results for Cu(111), the n = 1 IPS feature due to 1ω process was observed even at photon energy lower than the resonance between the occupied Shockley state and IPS [7,12,13], which is also demonstrated in our Cu(111) study (Appendix VII). The intensity variations of the IPS peak due to 1ω process and the Shockley state peak due to 2ω process were symmetric with respect to the resonant photon energy. The intensity variation as a function of the pump photon energy was discussed based on the dephasing process [7-10,12]. When the present PbPc results are compared with the known trend, the intensity variation around the HOMO-IPS resonance may be viewed as to be similar to the Cu(111) case: both the HOMO peak (2ω) and the IPS peak (1ω) became stronger as the photon energy increased closer to the HOMO-IPS resonance. In contrast to the HOMO-IPS resonance, the intensity variations around the HOMO-LUMO+2 resonance were asymmetric: the intensities of the HOMO (2ω) and LUMO+2 (1ω) peaks were switched at the resonance. Similar intensity

switching at the resonance has been reported for several systems [13-15]. The asymmetric intensity variation is not specific to the present molecular film. The detailed mechanism for the intensity variation of 2PPE features awaits for further understanding on the 2PPE process as was suggested by Weinelt [13,33].

The LUMO+2 peak due to 1ω process was observed at photon energies far above the resonance. If only the HOMO level was the initial state, energy conservation was not fulfilled. A possible mechanism may be an optical transition from the HOMO level to some resonantly excited state followed by relaxation to populate the LUMO+2 level. But such a resonant state was not observed and is not very probable for the film with the clearly resolved energy levels. Rather, we consider a contribution of occupied bulk bands of the substrate as the initial state. The contribution is considered below when the width of the LUMO+2 peak is discussed.

Fig. 6- 5 shows that the width of HOMO was 0.16 eV at $h\nu < 4.23$ eV and became narrower to 0.13 eV at the resonance. It became about 0.15 eV again at $h\nu > 4.59$ eV. According to Ueba's theory of resonance narrowing [8], the peak width at the resonance is determined by the product of the occupied and unoccupied density of states. Taking the widths of the HOMO and LUMO+2 levels to be 0.16 and 0.25 eV, respectively, the width of the product function is estimated to be about 0.13 eV ($1/0.16^2 + 1/0.25^2$). The value close to the observed width supports the narrowing mechanism. However, we present with reservation the coincidence of the observed and estimated values, because the functional forms of the intrinsic density of states are not accurately known. The narrowing was observed at the photon energy range of about 0.4 eV wide. The energy range should be correlated with the widths of the HOMO and LUMO+2 levels and is similar to photon energy window of 0.4 eV for the suppression of the HOMO vibronic structure [17].

The width of the LUMO+2 peak became broader with increasing photon energy above the HOMO-LUMO+2 resonance. The broadening is not expected when a fixed intermediate state is assumed. Sakaue predicted that the line width of 1ω peak becomes broader at photon energy higher than resonance by the hole scattering [11]. According to the theory, the hole partially exists in the bulk band. As the photon energy increased, the hole is formed at deeper energy to fulfill the energy conservation. As the result of the increased phase space to fill the hole, the lifetime of the intermediate state including the hole and the excited electron, becomes shorter and the 1ω peak becomes broader. The concept of the theory is shown

schematically in Appendix VIII. The mechanism seems to be helpful to consistently understand the broadening of the LUMO+2 peak and also the appearance of the peak at the high photon energy region above the resonance. The discussion also leads to a conclusion that the LUMO+2 level observed in 2PPE spectroscopy is not a molecular exciton in which the hole and electron are localized within a molecule. On the other hand, the theory cannot interpret why the LUMO+2 peak did not appear below the resonance.

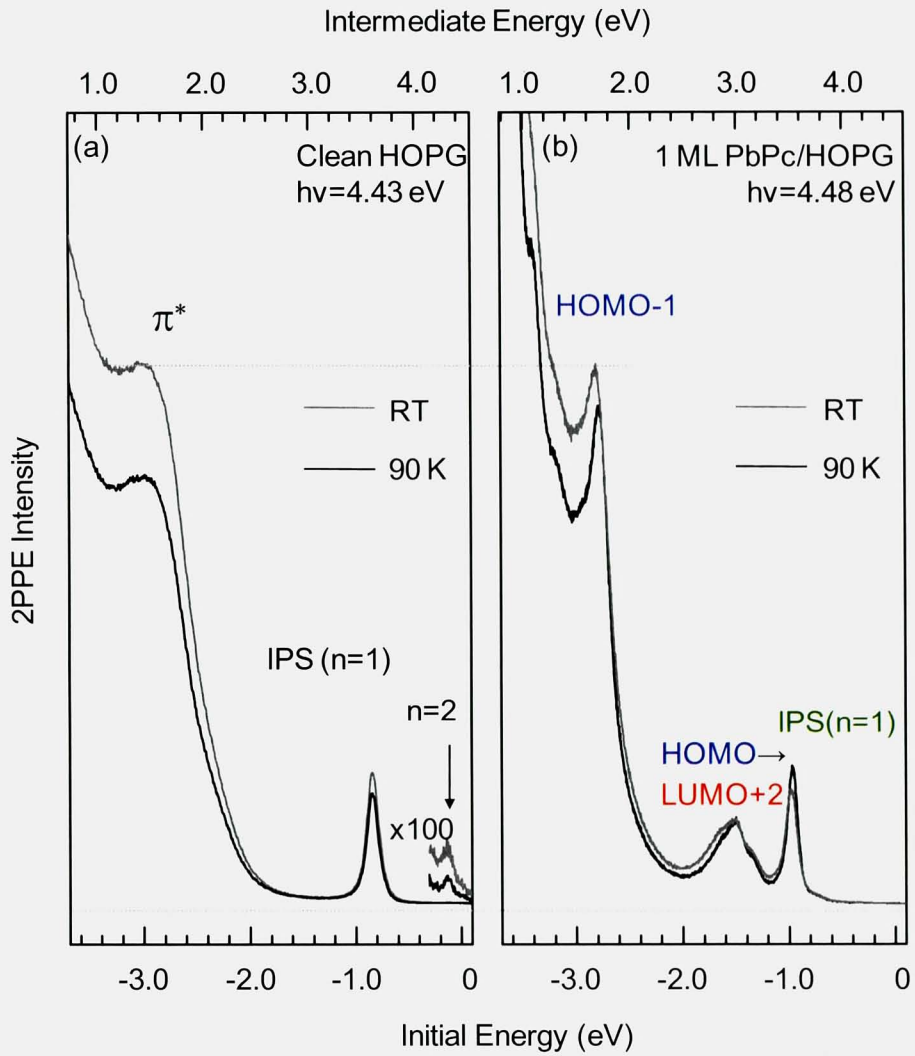

Fig. 6- 7. Temperature dependence of 2PPE spectra for (a) clean HOPG and (b) 1 ML PbPc/HOPG. The gray and black traces were for RT and 90 K, respectively. The RT spectra for (a) and (b) were normalized (gray horizontal line) to the intensities at the -2.8 eV initial energy. For clean HOPG, the intensity of the π^*-band at around 1.7 eV intermediate energy decreased as temperature decreased, indicating that the π^*-band arose by phonon assisted process. The IPS peak also became weak by decreasing the temperature. On the other hand, the intensities of the HOMO-1 peak and the IPS peak for the film were nearly independent of the temperature. The low energy backgrounds in these spectra were higher than those in Figs.6- 2 and6- 3 because of the different experimental conditions.

6. 4. 3. The L0 and L1 features

The intensity ratio of the split components, L0 and L1, changed with the photon energy increase as can be seen in Fig. 6- 2. The change can be understood by considering resonant excitations from occupied levels deeper than HOMO-1. Fig. 6- 8 showed energy levels for a free PbPc molecule obtained by the DFT calculation and the 2PPE spectra measured with characteristic photon energies. The energy scale for the calculated levels was adjusted to reproduce the initial energies of the HOMO and HOMO-1 peaks. The occupied levels below HOMO-1 were grouped as (A) to (C). The lengths of vertical arrows were proportional to the photon energies used in the upper 2PPE spectra. The resonance from HOMO-1 to the graphite π^*-band, discussed in 6. 4. 1, was shown by an open gray arrow. At low $h\nu$ of 4.04 eV, the L0 and L1 levels are not resonant with any occupied levels. The resultant 2PPE features were weak. The photon energy of 4.18 eV is sufficient to resonantly excite the L0 and L1 levels from the occupied levels of the group (A) and the intensities of the 2PPE features became higher. The L1 component was higher than the L0 component by favorable resonance from the high-lying level of the group. At slightly higher photon energy of 4.38 eV, another occupied levels labeled (B) participate in the initial states to excite the L0 level. The intensity ratio of the L0 and L1 components was reversed by the contribution. At $h\nu$ = 4.70 eV, the group (C) occupied levels participate in the initial states to populate the L0 and L1 levels resulting in the increased intensity and the change of the spectral features. Thus the L0 and L1 levels are considered to be populated by resonant excitations from the occupied levels. The broad 1PPE feature at the energy region of occupied levels deeper than HOMO-1 does not means that the deeper energy levels are intrinsically broad and forms continuous electronic states (see Appendix IX; the UPS spectrum from Ref. 20 is superimposed in Fig. 6- 8). The resonant 2PPE process is effective to resolve the congested occupied levels which cannot be resolved in 1PPE.

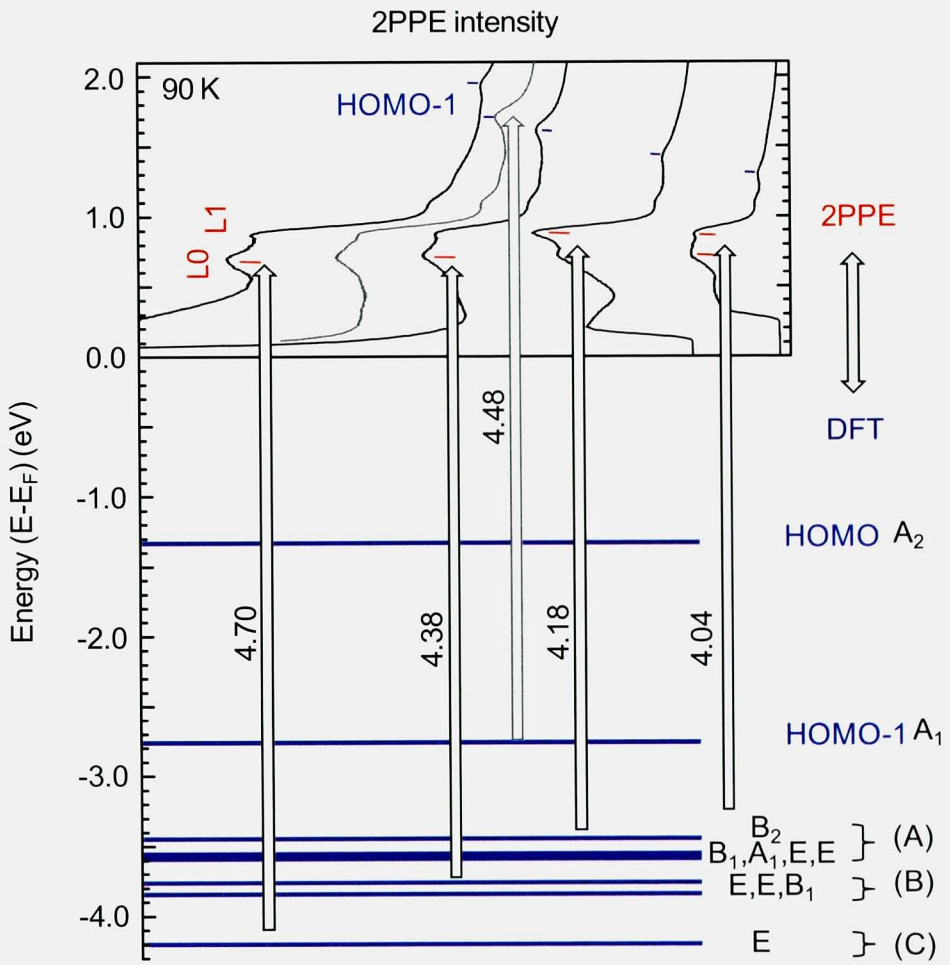

Fig. 6- 8. Photon energy dependence of 2PPE spectra at the L0 and L1 region (top) and the energy levels of a free PbPc molecule obtained by the DFT calculation (bottom). The photon energies of the 2PPE spectra were shown at the vertical arrows the lengths of which were proportional to the photon energies. The intensity variations of the L0 and L1 peaks were interpreted by the resonant excitations from deeper occupied levels shown by groups of (A) to (C).

References

[1] H. Ishii, K. Sugiyama, E. Ito, and K. Seki, Adv. Mater. **11**, 605 (1999).

[2] N. Ueno, S. Kera, Prog. Surf. Sci. **83**, 490 (2008).

[3] M. Muntwiler, Q. Yang, W. A. Tisdale, and X. -Y. Zhu, Phys. Rev. Lett. **101**, 196403 (2008).

[4] A. G. Borisov, V. Sametoglu, A. Winkelmann, A. Kubo, N. Pontius, J. Zhao, V. M. Silkin, J. P. Gauyacq, E. V. Chulkov, P. M. Echenique, and H. Petek, Phys. Rev. Lett **101**, 266801 (2008).

[5] P. M. Echenique, R. Berndt, E. V. Chulkov, Th. Fauster, A. Goldmann, U. Höfer, Surf. Sci. Rep. **52**, 219 (2004).

[6] J. Stähler, M. Meyer, D. O. Kusmierek, U. Bovensiepen, and M. Wolf, J. Am. Chem. Soc. **130**, 8397 (2008)

[7] K. Boger, M. Roth, M. Weinelt, Th. Fauster, P. -G. Reinhard, Phys. Rev. B, **65** 075104 (2002).

[8] H. Ueba, Surf. Sci. **334**, L719 (1995).

[9] H. Ueba, T. Mii, Appl. Surf. Sci. **169-170**, 63 (2001).

[10] H. Ueba, B. Gumhalter, Prog. Surf. Sci. **82**, 193 (2007).

[11] M. Sakaue, T. Munakata, H. Kasai, and A. Okiji, Phys. Rev. B **68**, 205421 (2003).

[12] W. Wallauer, Th. Fauster, Surf. Sci. **374**, 44 (1997).

[13] M. Kutschera, M. Weinelt, M. Rohlfing, T. Fauster, Appl. Phys. A **88**, 519 (2007).

[14] K. Shudo, S. Takeda, and T. Munakata, Phys. Rev. B **65**, 075302 (2002).

[15] K. Shudo and T. Munakata, Phys. Rev. B **63**, 125324 (2001).

[16] I. Yamamoto, M. Mikamori, R. Yamamoto, T. Yamada, K. Miyakubo, N. Ueno, and T. Munakata, Phys. Rev. B **77**, 115404 (2008).

[17] M. Shibuta, K. Yamamoto, K. Miyakubo, T. Yamada, and T. Munakata, Phys. Rev. B **80**, 113310 (2009).

[18] T. Munakata, M. Shibuta, M. Mikamori, T. Yamada, K. Miyakubo, T. Sugiyama, and Y. Sonoda, Proc. SPIE **6325**, 63250M (2006).

[19] I. Yamamoto, N. Matsuura, M. Mikamori, R. Yamamoto, T. Yamada, K. Miyakubo, N. Ueno, T. Munakata, Surf. Sci. **602**, 2232 (2008).

[20] S. Kera, H. Fukagawa, T. Kataoka, S. Hosoumi, H. Yamane, and N. Ueno, Phys. Rev. B **75**, 121305(R) (2007).

[21] J. Lehmann, M. Merschdorf, A. Thon, S. Voll, and W. Pheiffer, Phys. Rev. B **60**, 17037 (1999).

[22] B. Reihl, J. K. Gimzewski, J. M. Nicholls, and E. Tosatti, Phys. Rev. B **33**, 5770 (1986).

[23] I. Schäfer, M. Schlüter, and M. Skibowski, Phys. Rev B **35**, 7663 (1987).

[24] R. Claessen, H. Carstensen, and M. Skibowski, Phys. Rev. B **38**, 12582 (1988).

[25] G. Moos, C. Gahl, R. Fasel, M. Wolf, and T. Hertel, Phys. Rev. Lett. **87**, 267402 (2001).

[26] H. Petek and S. Ogawa, Prog. Surf. Sci. **56**, 239 (1997).

[27] E. Knoesel, A. Hotzel, and M. Wolf, Phys. Rev. B **57**, 12812 (1998).

[28] H. Petek, H. Nagano, M. J. Weida, S. Ogawa, Chem. Phys. **251**, 71 (2000).

[29] R. L. Lingle, Jr., N. -H. Ge, R. E. Jordan, J. D. McNeill, C. B. Harris, Chem. Phys. **205**, 191 (1996).

[30] J. D. McNeill, R. L. Lingle, Jr., R. E. Jordan, D. F. Padowitz, and C. B. Harris, J. Chem. Phys. **105**, 3883 (1996).

[31] W. Berthold, F. Rebentrost, P. Feulner, U. Höfer, Appl. Phys. A **78**, 131 (2004).

[32] A. Hotzel, G. Moos, K. Ishioka, M. Wolf, G. Ertl, Appl. Phys. B **68**, 615 (1999).

[33] M. Kutschera, T. Groth, C. Kentsch, I. L. Shumay, M. Weinelt, and Th. Fauster, J. Phys.: Condens. Matter **21**, 134006 (2009).

7. Conclusion

For well ordered 1 ML PbPc films on HOPG, clear viblational structure of the ionic HOMO derived level was observed with high resolution. Weak vibronic structure at the resonance photon energy with LUMO+2 derived level indicates the nuclear motion in the excited state within the few fs. Though, such ultrafast nuclear motion in the excited state at the interface is the key for electric conduction in the molecules, it has not been identified by any experiment. Therefore, vibronic structure in 2PPE spectroscopy will be fruitful to know very fast dynamics within few fs occurring at interfaces between organic molecule and inorganic substrate.

Photon energy variable 2PPE spectroscopy has been applied to probe the resonance behavior for 1 ML PbPc firms on graphite. By comprehensive analysis of the on/off resonant 2PPE line shapes, we have identified all the relevant occupied and unoccupied pairs. In addition, we have demonstrated that the 2PPE experiment is effective to probe not only unoccupied levels but also occupied levels which are buried in complicated 1PPE features. Thus all the unoccupied levels in the present system were produced by direct photoexcitations from the occupied levels, and were not populated by electron transfer from the substrate. The intensity variations of the 1ω and 2ω peaks around the resonance provided clear evidences of the unresolved signal generation mechanisms for 2PPE processes. Theoretical analysis of the resonance behavior is highly required for understanding the excitation mechanism and carrier dynamics at the interface between adsorbed molecules and the substrate. Detailed understanding of the nature of the unoccupied levels observed in 2PPE experiment is indispensable to compare with other experimental results such as inverse photoemission, optical spectroscopy and so on.

Angle resolved 2PPE and time resolved 2PPE, which are already started, will provide more dynamical information for the adsorbed system. These information must be helpful to understand the electric conduction at the interface.

Appendix

I. Temperature dependence of 2PPE spectra

Fig. A- 1 shows the expanded photon energy dependence of 2PPE spectra measured at RT (blue trace) superimposed upon that of measured at 90 K(right blue trace) for the same sample. Both spectra were measured with laser incident power of 16 mW. Significant temperature dependence of those peak behaviors with photon energy were not identified except for sharpening of spectral features at the low temperature. Very small upshift of IPS for 90 K spectrum may have some physical meaning but that cannot be discussed here in detail.

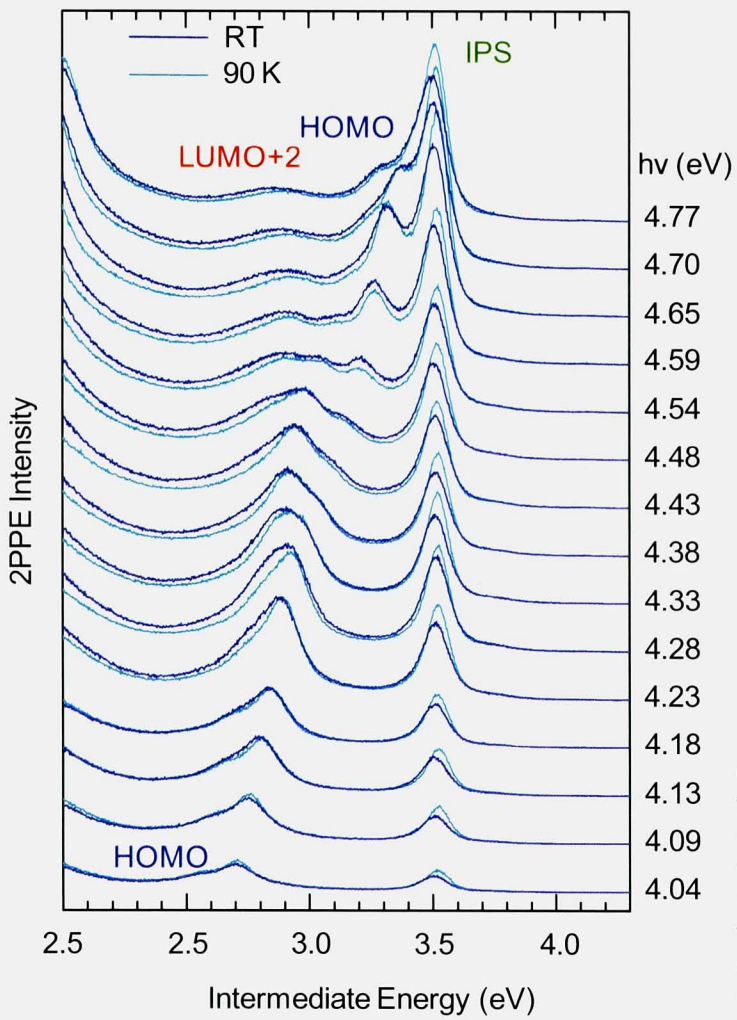

Fig. A- 1. Temperature dependence of 2PPE spectra. The sample temperatures were RT(blue) and 90 K(light blue), respectively. The temperature dependence of those peak behaviors with photon energy were not identified, except for slight sharpening of spectral features at 90 K.

II. Estimation of the time scale for the nuclear motion

Assuming the molecular vibrational energy in the intermediate state to be $h\nu$ = 140 meV similar to the ionic state, the frequency of the vibration, ν is about 3.4×10^{13} s^{-1}. Then the time of the molecular vibration cycle ($T = 1/\nu$) is estimated to be about 30 fs. The time for the nuclear motion in the state should be a fraction of the vibrational cycle, that is, a few fs. The width of the LUMO+2 feature in Fig. 6- 1 was about 0.25 eV. The width γ indicates that the lifetime of the intermediate state produced by 4.59 (Fig. 5- 1) and 4.65 eV (Fig. 6- 1). The life time (τ) is estimated by using uncertainty relation of $\tau = \hbar/\gamma$. Therefore, τ should be longer than a few fs and is sufficient for the nuclear motion.

III. Time resolved measurement for observed unoccupied levels

We performed time resolve measurement for the 1ML PbPc films in order to investigate the change of electronic structure within the fs time scale. The interferometer for the time resolved 2PPE is shown in Fig. A- 2. The 3ω beam is separated and combined by BS1 and BS2. The mechanical delay stage is equipped at one pass to scan the delay time Δt of between two pulse. The minimum step of the delay stage is Δx = 50 nm and thus that of delay time is 0.33 fs (= 2×50 nm / 2.998×10^{8} ms^{-1}). To avoid light interference, the two pulses should 'not' be overlapped before the sample but separated for ~5 mm. Fig. A- 3 shows time resolved 2PPE spectra for the films measured at $h\nu$ = 4.33 eV which nearly corresponds to the resonance energy between HOMO and LUMO+2. The pulse width of the incident laser was 89 fs determined by autocorrelation width of 126 fs. Each spectrum in Fig. A- 3 was subtracted with the smoothed zero delay spectrum fixed the HOMO-1 height of maximum delay (24000 fs) from low data and the time delays are indicating at right hand side. All spectra were dumped at lower side of the cut off because of the 1PPE signal in which its intensity is independent of the time delay. The decays of HOMO-1 ,HOMO→LUMO+2 and IPS peaks were very fast while L0, L1 and secondary signals seem slow decays reflecting the life time of excited electron. Fig. A- 4 also shows magnified time resolved 2PPE spectrum

measured with 4.59 eV photon energy in which small vibronic structure was observed as discussed in Chapter 5. The pulse width of the incident laser was 112 fs at the measurement. No significant change of spectral shape was not observed in both photon energies. These results indicate no attracting phenomena such as electron solvation or exciton state at 1 ML film is identified, i.e. the excited electrons on the film rapidly attenuate to the substrate. Therefore the wavefunctions of both graphite and HOPG are fairly mixed each other at the interface.

To measure the intrinsic life time of observed unoccupied levels accurately, the laser pulse was compressed to 58 fs by improvement of laser and by a pair of prisms. The central wavelength of the fundamental light is fixed to 834 nm (1.49 eV) to obtain shorter pulse. Fig. A- 5 shows the time resolved 2PPE trace of the characteristic unoccupied levels, L0, LUMO+2 and IPS. The sample was cooled at 30 K by He refrigerator. But large temperature dependence of the trace was not identified which cannot be discussed here. The horizontal axis is the delay time between the incident two pulses by scanning the delay stage. The determined life time of L0 and IPS are 92 and 40 fs, respectively, by considering $I(2PPE) \propto \exp(\Delta t/\tau)$. The life time of LUMO+2 derived level could not identify because of the limited time resolution of the system (~30 fs). Two-color 2PPE (ω+3ω or 2ω+3ω) will give more accurate information of the life time.

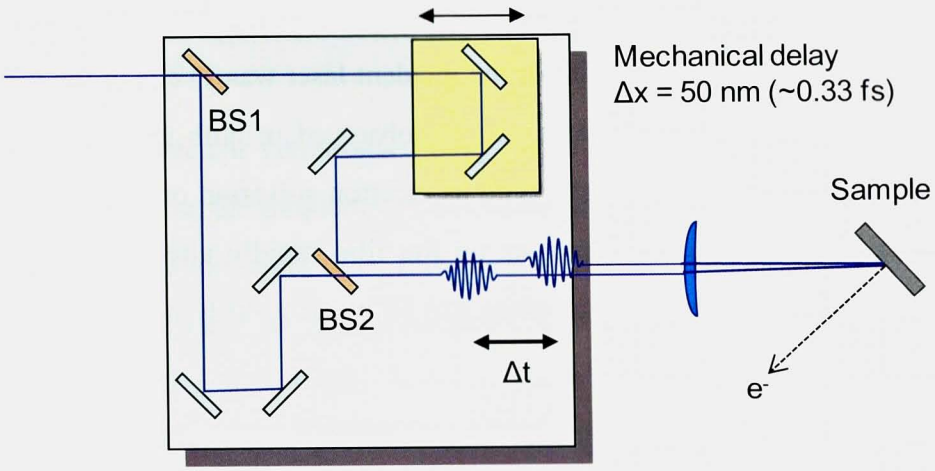

Fig. A- 2. Interferometer for time resolved 2PPE. The 3ω beam is separated and combined by BS1 and BS2. The mechanical delay stage is equipped at one pass to scan the delay time Δt of between two pulse. To avoid light interference, the two pulse should 'not' be overlapped before the sample but separated for ~5 mm .

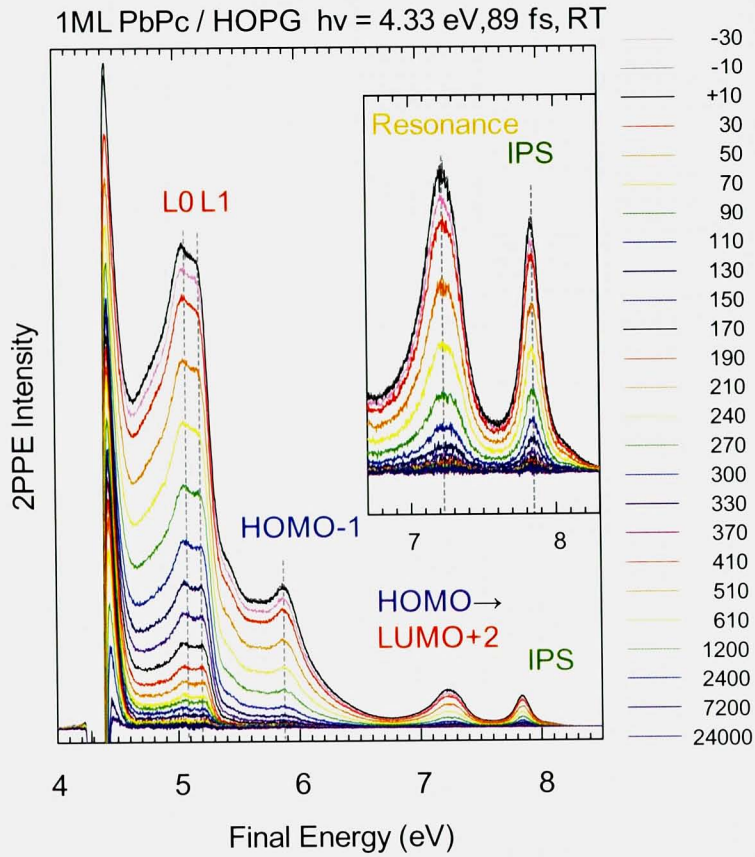

Fig. A- 3. Time resolved 2PPE spectra for 1 ML PbPc/HOPG measured at *hv* = 4.33 eV which nearly corresponds to the resonance energy between HOMO and LUMO+2. Pulse width of the incident laser was 89 fs. Each spectra were subtracted with the smoothed zero delay spectrum from low data and the each time delays are indicated at the right hand side. Significant change of spectral shape within fs time scale is not observed.

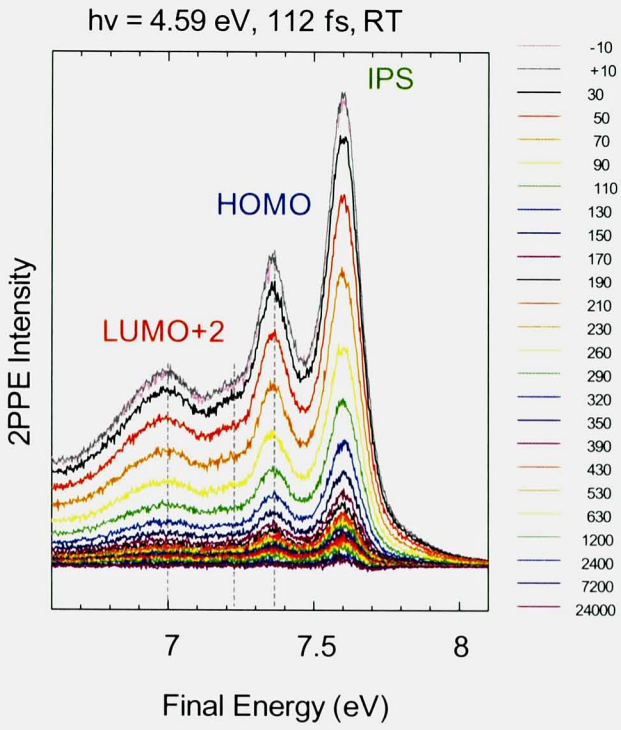

Fig. A- 4. Magnified time resolved 2PPE spectra for 1 ML PbPc/HOPG measured at *hv* = 4.59 eV in which the small vibronic structure of HOMO was observed. Pulse width of the incident laser was 112 fs. But attractive change of the spectral shape was not identified.

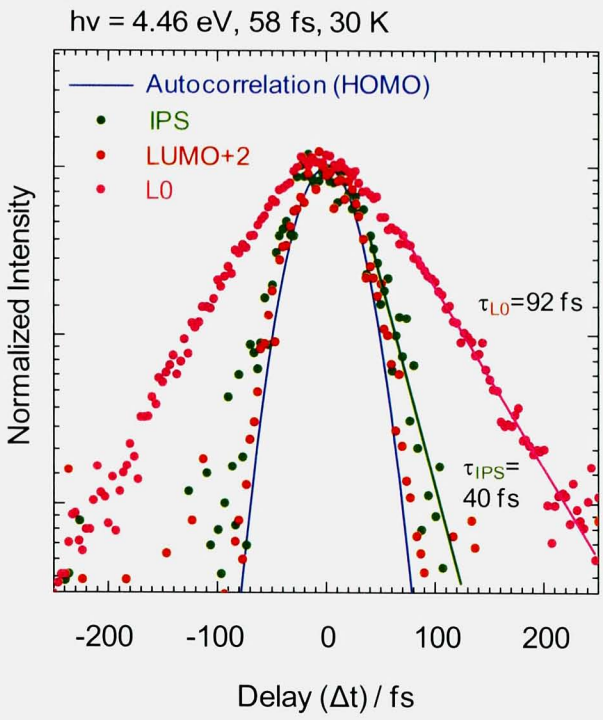

Fig. A- 5. Delay scan trace of characteristic unoccupied levels for the 1 ML film cooled at 30 K. Pulse duration was compressed to 58 fs by changing the laser condition and by a pair of prisms for fundamental output. The life time of L0 and IPS are 92 and 40 fs, respectively, while that for LUMO+2 could not determined because of the limit of time resolution of ~30 fs.

IV. Incident power dependence of 2PPE feature

To consider the high-order process which was mentioned in 5. 3, the 2PPE spectra for 1 ML PbPc on HOPG measured various incident laser powers are shown in Fig. A- 6. Each spectrum was normalized to the peak height of IPS. The photon energy was 4.59 eV which is slightly above the resonance energy from HOMO to LUMO+2. The HOMO-derived feature seemed sharper than that for 1PPE result (see Fig. 5- 1) because of the weak vibronic structure reflecting nuclear motion in the excited state as discussed in 5. 3. If high-order nonlinear process occurs, the spectral feature should depend on the laser power. But all spectra were completely reproduced and such high-order phenomena does not participate in the spectral feature i.e. all detecting photoelectrons are by exact 2PPE process.

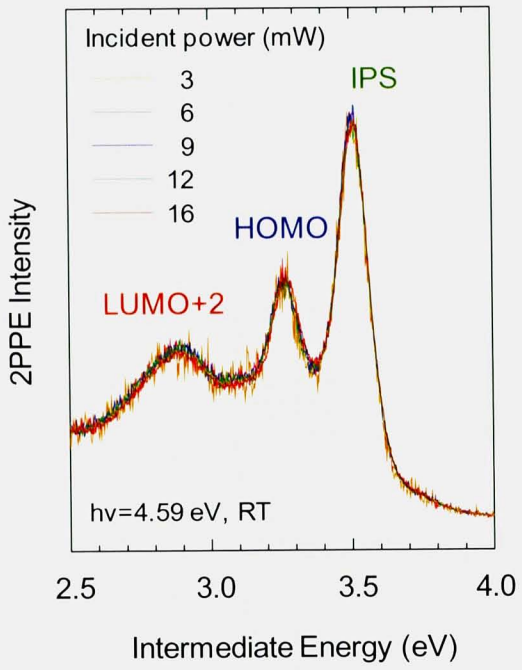

Fig. A- 6. Normalized and superimposed 2PPE spectra for 1 ML PbPc films measured with different incident power of 3, 6, 9, 12, and 16 mW. The photon energy was 4.59 eV which is slightly higher energy than resonance from HOMO to LUMO+2. Spectral features were perfectly overlapped each other and thus no higher nonlinear phenomena could not be identified.

V. Fitting result for all spectra in the capable photon energies

Fitting results for all spectra around the region of HOMO, LUMO+2 and IPS were shown in Fig. A- 7. Each spectrum was not normalized. Voigt function was tentatively chosen for the curve fitting as the peak function, because the 2PPE line shape should be determined by a convolution of the Gaussian spectral shape of laser pulse and the Lorentz type line shape of the energy levels reflecting the life time of the level. The fitting was made with the following parameter in the bottom of Fig. A- 7 and also in 6. 3. 3.

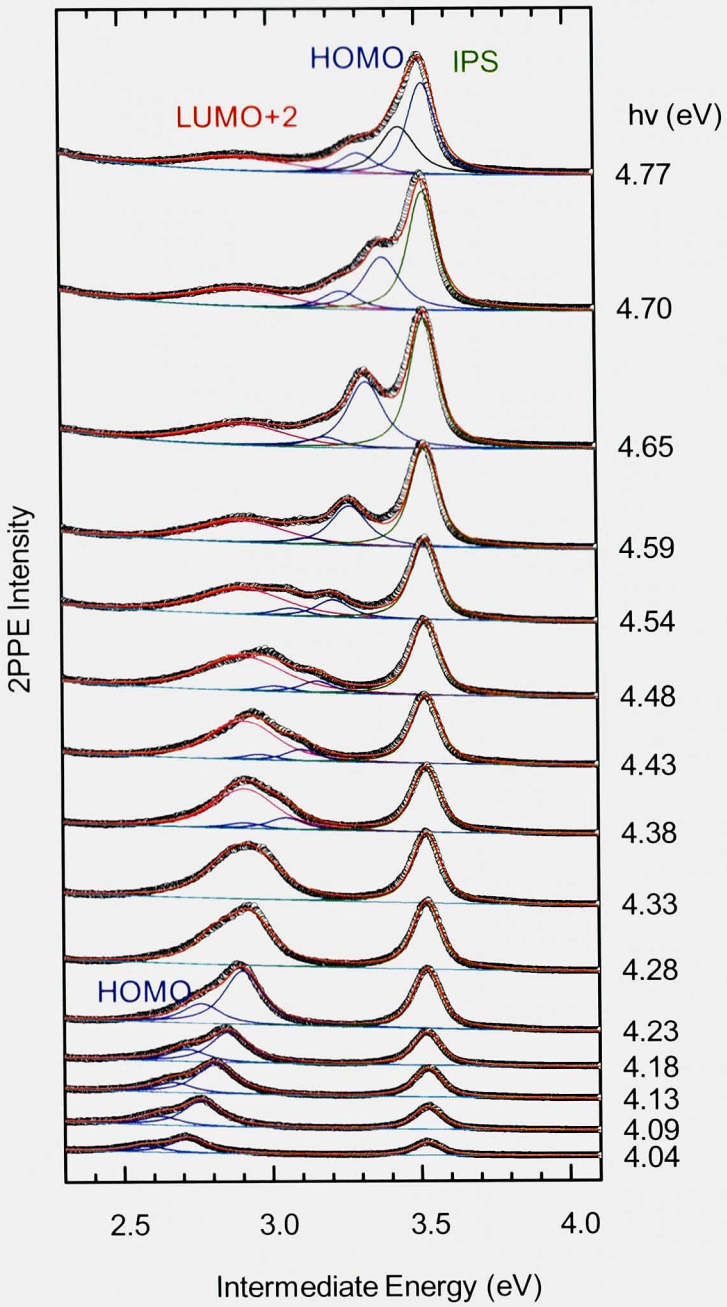

	Energy Position(eV)	Width(Gauss) W_G(meV)	Width(Lorentz) W_L(meV)
LUMO+2	+2.91	available (share)	
HOMO	-1.33	60	available
HOMO-vib	-1.47	60	available
IPS	+3.52	60	80

Fig. A- 7. Fitting all results for HOMO, LUMO+2 and IPS region. The fitting was performed for 2PPE spectra measured at 90K. Voigt function applied as a peak function Parameters of the fitting were indicated at the bottom table. The adjustable parameters were reduced as follows in the table for meaningful fitting. The fixed width parameters for the IPS and HOMO peaks were determined from the spectrum at $h\nu$ = 4.13 eV.

VI. Drude process in the band gap :The case of Cu(111)

In order to consider the appearance of π^* structure at the Γ point, we compare the result for Cu(111) case. Fig. A- 8(a) shows the time resolved 2PPE result for hot electrons of low index surfaces of Cu referred from [H. Petek and S. Ogawa, Prog. Surf. Sci. 56, 239 (1997)]. Finite life time have been reported even Cu(111) surface in which large band gap exists around E_F and they discussed the role of phonon assisted process so called Drude process as the origin of the real unoccupied states within the band gap. Fig. A- 8(b) shows schematic image of phonon coupled excited electron that can be photoemitted from different momentum.

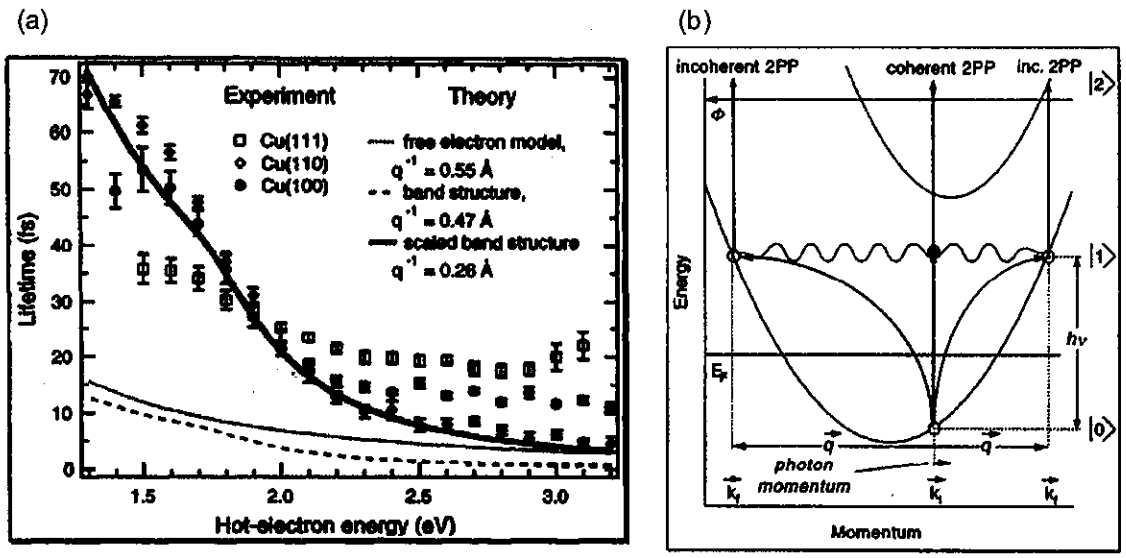

Fig. A- 8. (a) Life time of hot electron for low index surfaces of copper referred from [H. Petek and S. Ogawa, Prog. Surf. Sci. **56**, 239 (1997)]. Finite life time have been reported even Cu(111) surface in which large band gap exists around E_F. (b) schematic image of phonon assisted process so called Drude process as the origin of the real unoccupied states within the band gap. Phonon coupled excited electron can be photoemitted from different momentum.

VII. Resonance behavior for the case of Cu(111): Our study

As an example of resonance behavior in our study, right hand of Fig. A- 9 shows the 2PPE spectra for Cu(111) surface measured with various photon energies. All spectra were normalized by peak height. Occupied Shockley surface state (SS) and unoccupied IPS (n = 1) were perfectly in resonance each other at $h\nu$ = 4.48 eV. in contrast to the result for PbPc/HOPG, the unoccupied IPS feature due to 1ω process was observed even at $h\nu$ lower than the resonance and the occupied SS due to 2ω process was observed even at $h\nu$ higher than the resonance. Thus, the intensity variations of 1ω process and 2ω process were symmetric with respect to the resonant photon energy. This resonance behavior has been reported and discussed by Fauster and Ueba with comparing 2PPE calculation based on the dephasing process. According to Ueba's theory of resonance narrowing, the peak width at the resonance is determined by the product of the occupied and unoccupied density of states. Fig. A- 9 demonstrates the resonance narrowing; the width of the resonance peak at $h\nu$ = 4.48 eV is clearly narrower than that of SS or IPS at off resonance (see inset).

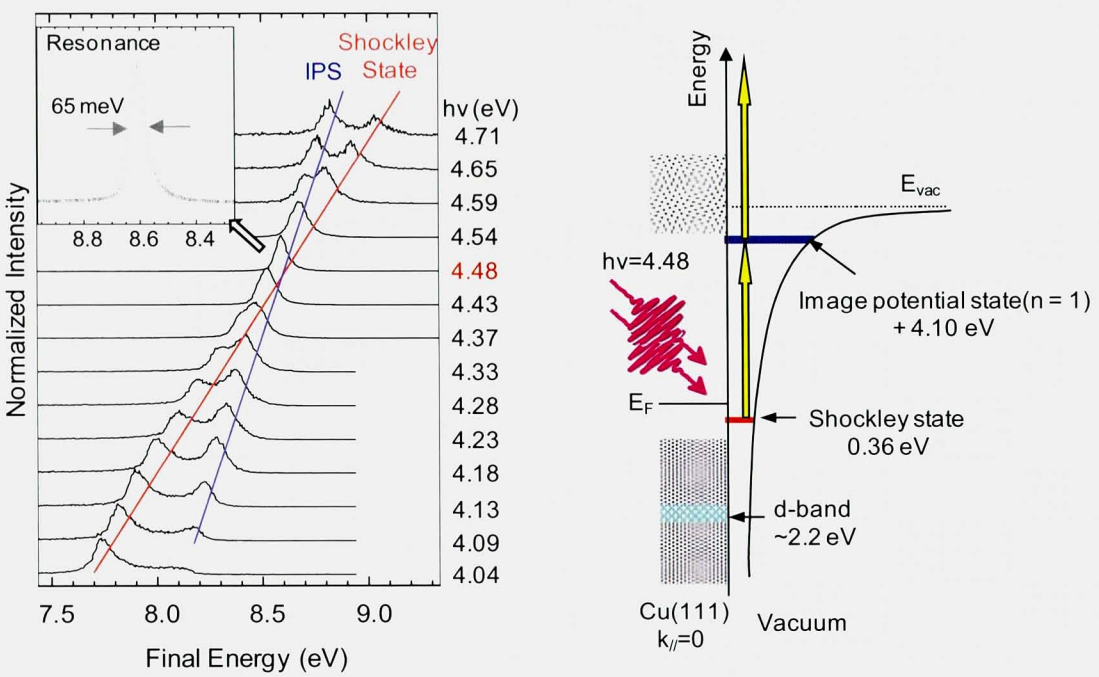

Fig. A- 9. (left) Photon energy dependence of 2PPE spectra for the Cu(111) surface and (right) its energy diagram. Occupied Shockley surface state (SS) and unoccupied IPS locate at projected band gap of the Cu(111) surface. SS and IPS were perfectly in resonance each other at $h\nu$ = 4.48 eV. The intensity variation of the levels are symmetric below and above the resonance. At $h\nu$ < 4.09 eV, IPS was invisible because electron can not excite to the level. The peak width at the resonance was clearly narrower than the intrinsic width of SS and IPS indicating resonance narrowing by Ueba theory.

VIII. The concept of Sakaue theory

Sakaue predicted that the line width of 1ω peak becomes broader at photon energy higher than resonance by the hole scattering. The broadening of calculated IPS width for Cu(111) at photon energy above the resonance was shown as a diamond square at the left hand of Fig. A-10. According to the theory, the hole partially exists in the bulk band. As the photon energy increased, the hole is formed at deeper energy to fulfill the energy conservation. The simple image of the situation is also shown at the right hand side of Fig. A- 10. As the result of the increased phase space to fill the hole, the lifetime of the intermediate state including the hole and the excited electron, becomes shorter and the 1ω peak becomes broader. The mechanism seems to be helpful to consistently understand the broadening of the LUMO+2 peak and also the appearance of the peak at the high photon energy region above the resonance.

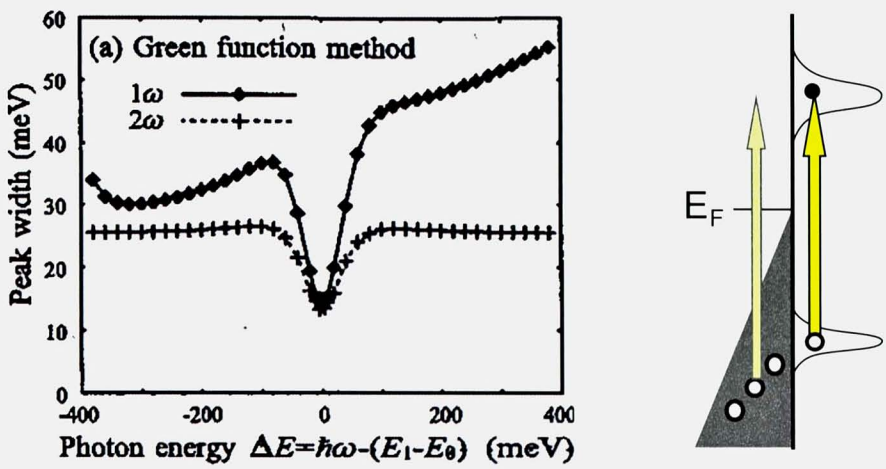

Fig. A- 10. Calculated line width of SS and IPS on Cu(111) by Sakaue [Phys. Rev. B **68**, 205421 (2003)]. The horizontal axis is the detuning of photon energy rerated with the resonance. According to the theory, the unoccupied level should be broader when photon energy is higher than the resonance, qualitatively supporting our width behavior of LUMO+2. The hole partially exists in the bulk band. As the photon energy increased, the hole is formed at deeper energy to fulfill the energy conservation. As a result of the increased phase space to fill the hole, the lifetime of the intermediate state including the hole and the excited electron, becomes shorter and the unoccupied peak becomes broader.

IX. Change of L0 and L1 feature: Comparing with UPS result

In addition to 2PPE and DFT calculation (Fig. 6- 8), the UPS result from Ref. [S. Kera, et. al., Phys. Rev. B **75**, 121305(R) (2007)] was also superimposed as a pink trace in Fig. A- 10. The HOMO-1 and deeper occupied levels than HOMO-1 were observed as a broad and shoulder-like structure.

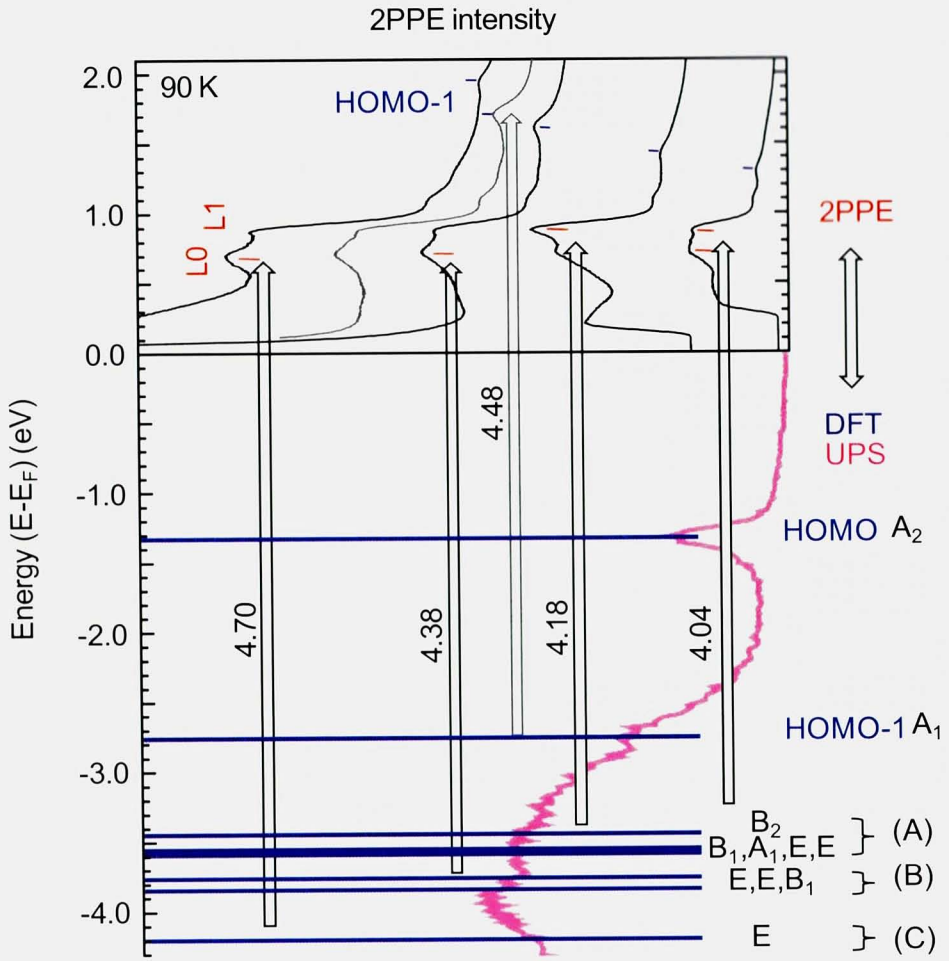

Fig. A- 11. In addition to 2PPE and DFT calculation (Fig. 6- 8), the UPS result from Ref. [S. Kera, et. al., Phys. Rev. B **75**, 121305(R) (2007)] was also superimposed as a pink trace in Fig. A- 10. The HOMO-1 and deeper occupied levels than HOMO-1 were observed as a broad and shoulder-like structure.

The list of publications (~Jan. 2010, partially in Japanese)

1. Papers

(1) **The Evolution of Diverse Self-Assembled Superstructures of Naphthalene on Cu(111)**

T. Yamada, **M. Shibuta**, Y. Ami, Y. Takano, A. Nonaka, K. Miyakubo, and T. Munakata

J. Am. Chem. Soc. submitted.

(2) **Resonant effects on two-photon photoemission spectroscopy: Line widths and intensities of occupied and unoccupied features for lead phthalocyanine films on graphite**

M. Shibuta, K. Yamamoto, K. Miyakubo, T. Yamada, and T. Munakata

Phys. Rev. B submitted.

(3) **Vibrationally resolved two-photon photoemission spectroscopy for lead phthalocyanine film on graphite**

M. Shibuta, K. Yamamoto, K. Miyakubo, T. Yamada, and T. Munakata

Phys. Rev. B **80**, 113310 (2009).

(4) **One-and two-photon photoemission micro-spectroscopy for organic films**

T. Munakata, **M. Shibuta**, M. Mikamori, T. Yamada, K. Miyakubo, T. Sugiyama, Y. Sonoda

Proc. of SPIE, **6325**, 63250M-1 - 63520M-9 (2006).

2. Presentation at international conference

Oral presentations (presenter*)

(1) **Vibrationally Resolved Two-Photon Photoemission for PbPc Films**

T. Munakata*, **M. Shibuta**, K. Yamamoto, K. Miyakubo, and T. Yamada

The 5th Electronic Structure and Processes at Molecular-Based Interfaces (ESPMI-V), Chiba, Japan, Jan. 2009

(2) **Unoccupied Electronic States at the Organic Film/Graphite Interface**

M. Shibuta*, K. Yamamoto, R. Yamamoto, T. Yamada, K. Miyakubo, and T. Munakata

The International Workshop on Molecular Information and Dynamics 2008, SP-10, Taiwan, Nov. 2008

(3) **Unoccupied electronic states at the lead phthalocyanine (PbPc)/Graphite interface measured with two-photon photoemission microspectroscopy**

M. Shibuta, R. Yamamoto, T. Yamada, K. Miyakubo, T. Munakata*

Ultrafast Surface Dynamics 6 (USD6), Kloster Banz, Germany, July 2008

(4) **Electronically Exited States at the Lead Phthalocyanine (PbPc)/Graphite interface studied by Two-Photon Photoemission Micro-spectroscopy**

M. Shibuta, R. Yamamoto, T. Yamada, K. Miyakubo, T. Munakata*

Electronic structure and Processes at Molecular- based interfaces (ESPMI-08), C.6, Princeton, USA, June 2008

Poster presentations

(5) **Correlation between Adsorbed Structures and Electronic States of Naphthalene on Cu(111)**

T. Yamada*, M. Shibuta, Y. Ami, Y. Takano, K. Miyakubo and T. Munakata

The 5th Electronic Structure and Processes at Molecular-Based Interfaces (ESPMI-V), Chiba, Japan, Jan. 2009

(6) **Effects of Vibrational Excitation and Hole Scattering in Two-Photon Photoemission from Thin Organic Films on Graphite**

M. Shibuta*, K. Yamamoto, T. Yamada, K. Miyakubo, and T. Munakata

11-th International Conference on Electronic Spectroscopy and Structure (ICESS-11),8AP03, Nara, Japan, Oct. 2009

(7) **Adsorbed States of Naphthalene on Cu(111) Studied by STM, LEED and 2PPE**

T. Yamada*, M. Shibuta, Y. Ami, Y. Takano, K. Miyakubo, and T. Munakata

11-th International Conference on Electronic Spectroscopy and Structure (ICESS-11), 6AP16, Nara, Japan, Oct. 2009

(8) **Resonant Excitation in Two-photon Photoemission for Lead Phthalocyanine (PbPc) on Graphite**

M. Shibuta*, K. Yamamoto, T. Yamada, K. Miyakubo, T. Munakata

26th European Conference on Surface Science (ECOSS-26), Mo-DYN-P-047, Parma, Italy, Aug. 2009

(9) **Novel Overlayer Growth of Naphthalene on Cu(111) Studied by STM, LEED and 2PPE**

T.Yamada*, **M. Shibuta**, Y. Ami, Y. Takano, K. Miyakubo, T. Munakata

26th European Conference on Surface Science (ECOSS-26), Mo-MOL-P-016, Parma, Italy, Aug. 2009

(10) **Adsorbed States and Electronic Structures of Naphthalene on Cu(111)**

T.Yamada*, A. Nonaka, **M. Shibuta**, K. Miyakubo and T. Munakata

25th European Conference on Surface Science (ECOSS-25), MO-P17, Liverpool, UK, July 2008

(11) **Adsorption -induced states Measured by Two -Photon Photoemission**

M. Shibuta*, T. Murakami, T. Yamada, K. Miyakubo, and T. Munakata

The 4th Japan-Sweden Workshop on Advanced Spectroscopy of Organic Materials for Electronic Applications(ASOMEA-4), P-9, Chiba, Oct. 2007

(12) **Comparative 2PPE study of naphthalene adsorption on Cu(111) and HOPG**

M. SHIBUTA*, T. MURAKAMI, T. YAMADA, K. MIYAKUBO, T. MUNAKATA

15th International Conference on Vacuum Ultraviolet Radiation Physics (VUV XV), Tue-Pos123, Berlin, Germany, July 2007

3. Presentations in domestic conference

Oral presentations

(1) **共鳴2光子光電子分光による鉛フタロシアニン薄膜の電子励起ダイナミクス**

渋田 昌弘*, 山本 健太, 南 隆文, 山田 剛司, 宮久保 圭祐, 宗像 利明

表面・界面スペクトロスコピー2009, 札幌, 2009 年 12 月

(2) **鉛フタロシアニン薄膜での共鳴励起と振電相互作用**

山本 健太*, **渋田 昌弘**, 宮久保 圭祐, 山田 剛司, 宗像 利明

分子科学討論会 2009, 1D19, 名大, 2009 年 9 月

(3) **高分解能2光子光電子分光法による鉛フタロシアニン(PbPc)分子薄膜の共鳴励起と振動構造**

渋田 昌弘*, 山本 健太, 南 隆文, 宮久保 圭祐, 山田 剛司, 宗像 利明

第4回有機デバイス院生研究会, 阪大, 2009 年 6 月

(4) **鉛/銅フタロシアニン薄膜の顕微 2 光子光電子分光**

山本 亮太*, 渋田 昌弘, 高野 康弘, 阿弥 曜平, 宮久保 圭祐, 山田 剛司, 宗像 利明

第 89 回日本化学会年会, 2E4-09, 日大, 2009 年 3 月

(5) **鉛フタロシアニン/グラファイト表面の 2 光子光電子分光法での共鳴過程**

渋田 昌弘*, 山本 健太, 山田 剛司, 宮久保 圭祐, 宗像 利明

第 89 回日本化学会年会, 2E4-08, 日大, 2009 年 3 月

(6) **Cu(111)表面上におけるナフタレンの吸着構造と電子状態**

山田剛司*, 渋田昌弘 ,高野康弘, 宮久保圭祐, 宗像利明

日本物理学会 2009 年春期年会, 27pTE-4, 立教大, 2009 年 3 月

(7) **2 光子光電子分光法によるフタロシアニン薄膜の電子状態計測**

山田 剛司*, 渋田 昌弘, 山本 勇, 山本 亮太, 山本 健太, 宮久保 圭祐, 宗像 利明

表面・界面スペクトロスコピー2008, 大阪, 2008 年 12 月

(8) **共鳴2光子光電子分光法による鉛フタロシアニン薄膜/グラファイト界面の非占有準位観測**

渋田 昌弘*, 山本 亮太, 山本 健太, 山田 剛司, 宮久保 圭祐, 宗像 利明

2008 年度 関西薄膜・表面物理セミナー, 大阪, 2008 年 11 月

(9) **2光子光電子分光法による鉛フタロシアニン(PbPc)薄膜/HOPG 薄膜の電子励起状態の観測**

渋田 昌弘*, 山本 勇, 山本 亮太, 山田 剛司, 宮久保 圭祐, 宗像 利明

日本物理学会 2008 年秋期年会, 23aXA-3, 盛岡, 2008 年 9 月

(10) **Cu(111)表面におけるナフタレン分子の吸着構造と電子状態**

山田 剛司*, 野中 聡洋, 渋田 昌弘, 宮久保 圭祐, 宗像 利明

第 24 回化学反応討論会, 2P23, 北大, 2008 年 7 月

(11) **2光子光電子分光によるフタロシアニン超薄膜の非占有準位測定**

山本 亮太*, 渋田 昌弘, 山本 健太, 山田 剛司, 宮久保 圭祐, 宗像利明

第 3 回有機デバイス院生セミナー, 名大, 2008 年 6 月

(12) **ナフタレン吸着表面の2光子光電子分光**

渋田 昌弘*, 中西 昂介, 村上 健, 山田 剛司, 宮久保 圭祐, 宗像 利明

関西薄膜・表面物理セミナー, 大阪, 2007 年 11 月

(13) **2 光子光電子分光法によるナフタレン/Cu(111)表面の電子状態の観測**

渋田 昌弘*, 宮久保 圭介, 宗像 利明

第 86 回日本化学会年会, 2E5-16, 船橋, 2006 年 3 月

Poster presentations

(14) **2光子光電子分光法と低速電子線回折によるナフタレン/Cu(111)表面の電子状態と吸着構造の研究**

阿弥 曜平*, 高野 康弘, 渋田 昌弘, 宮久保 圭祐, 山田 剛司, 宗像 利明

分子科学討論会 2009, 2P068, 名大, 2009 年 9 月

(15) **HOPG 表面におけるナフタレン分子の吸着構造と電子状態**

高野 康弘*, 渋田 昌弘, 磯部 美緒, 山田 剛司, 宮久保 圭祐, 宗像 利明

分子科学討論会 2009, 1P073, 名大, 2009 年 9 月

(16) **2光子光電子分光法と低速電子線回折によるナフタレン/銅(111)表面の電子状態と吸着構造**

阿弥 曜平*, 高野 康弘, 渋田 昌弘, 宮久保 圭祐, 山田 剛司, 宗像 利明

第4回有機デバイス院生研究会, P4, 阪大, 2009 年 6 月

(17) **有機薄膜界面における電子励起ダイナミクス**

山本 健太*, 渋田 昌弘, 宮久保 圭祐, 山田 剛司, 宗像 利明

第4回有機デバイス院生研究会, P3, 阪大, 2009 年 6 月

(18) **Adsorption Structures and Electronic Structures of Naphthalene on Cu(111) Studied by Two-photon Photoemission Spectroscopy and Low Energy Electron Diffraction**

Y. Ami*, Y. Takano, **M. Shibuta**, K. Miyakubo, T. Yamada, T. Munakata

第 25 回化学反応討論会, 2P21, 大宮, 2009 年 6 月

(19) **鉛フタロシアニン/HOPG 薄膜の高分解能 2 光子光電子分光法**

山本 健太*, 渋田 昌弘, 山本 亮太, 宮久保 圭祐, 山田 剛司, 宗像 利明

第2回分子科学会, 2P083, 福岡, 2008 年 9 月

(20) **顕微2光子光電子分光法による銅フタロシアニン薄膜の非占有準位観測**

山本 亮太*, 渋田 昌弘, 山本 健太, 宮久保 圭祐, 山田 剛司, 宗像 利明

第2回分子科学会, 2P082, 福岡, 2008 年 9 月

(21) **2 光子光電子分光法による Cu(111)および HOPG 上ナフタレンの非占有準位測定**

渋田 昌弘*, 村上 健, 山田 剛司, 宮久保 圭祐, 宗像 利明

有機デバイス院生研究会セミナー, P2, 東大, 2007 年 6 月

(22) **2 光子光電子分光法によるナフタレン/Cu(111)の非占有準位測定**

渋田 昌弘*, 宮久保 圭祐, 宗像 利明

分子構造総合討論会 2006, 2P129, 静岡, 2006 年 9 月

Acknowledgement

Many people have supported me during my Ph. D work which could not have been completed successfully without their supports.

Firstly, I would like to especially thank to my supervisor, Professor Toshiaki Munakata of Osaka University who gave me a chance to study science. In my Ph. D work, he has told me all techniques for 2PPE experiments and writing manuscripts.

I also thank to, Dr. Keisuke Miyakubo (lecturer at Osaka University), Dr. Takashi Yamada, (assistant professor at Osaka University), and Dr. Isamu Yamamoto (Institute for molecular science) for many beneficial discussions.

I would like to acknowledge Professor Ulrich Höfer of Phillips University Marburg, Germany. He kindly accepted me in his laboratory during my period of study abroad with very nice members of his laboratory.

I appreciate secretaries at Osaka University, Mrs. Jyunko Morioka, Mrs. Akiko Konoki, and all office staffs in the data room for chemistry at Osaka University for handling many office works.

I am grateful to my all colleagues in the laboratory of surface science at Osaka University for supporting my Ph. D work and enjoying my campus life. The memories will last for a lifetime.

Finally, I would like to express my thanks to dear my parents, and dear all my friends for heartfelt encouragement.

February, 2010

渋田昌弘